NASA-CR-194242

FINAL REPORT FOR NASA GRANT NAG-1-477

by

Warren W. Buck and Khin M. Maung
Department of Physics
Hampton University
Hampton, VA 23668

This is the final report describing the research performed under the NASA Grant number NAG-1-477 at Hampton University during the years 1984-92. During the grant period, four M.S theses, NASA technical reports, and papers in refereed journals were published. Most of the research work performed under this grant were concerned with strong interaction processes ranging from kaon-nucleon interaction to proton-nucleus scattering calculations. Research performed under this grant can in general be categorized in to three groups: (1) Parametrization of fundamental interactions (2) Development of formal theory, and (3) calculations based upon the first two.

Parametrizations of certain fundamental interactions, such as kaon-nucleon interaction, for example, were necessary because kaon-nucleon scattering amplitude was needed to perform kaon-nucleus scattering calculations. Of cause it was possible to calculate kaon-nucleon amplitudes from the first principle, but it was unnecessary for the purpose of the project. Similar work was also done for example for anti-protons and anti-nuclei. Formal developments to some extent were also pursued so that consistent calculations can be done.

Note that all research projects supported under this grant NAG-1-477 were done with the aim that the results and knowledge obtained from these projects will be used in the shielding calculations of long space missions.

The following is the list of awards, papers in refereed journals and NASA technical memos/papers published during the duration of the grant, NAG-1-477. The rest of this report consists of a collection of these papers. Since the NASA technical papers, memos and students' M.S theses are very lengthy, we include only the cover pages of these.

Awards (W. W. Buck):

The first *Outstanding Service Award* from the User's Group of The Continuous Electron Beam Accelerator Facility (CEBAF) 1986

Honorary Superior Accomplishment Award **from NASA/Langley Research Center for "significant contributions in radiation physics enabling practical shield designs for manned space missions, and for authorship of the Space Systems Division Best Paper for 1990-1991."**

Outstanding Publication within the Space Directorate **at NASA/LaRC (1992)**

Non-NASA Funded Projects leveraged by NAG-1-477:

HUGS at CEBAF. U.S. Department of Energy,
The Nuclear Physics Group, The National Science Foundation
The National Conference of Black Physicists, The National Science Foundation

Publications under NAG-1-477:

"Possible Complementary Cosmic Ray Systems: Nuclei and Antinuclei", W.W. Buck, J.W. Wilson, J.W. Norbury, NASA Technical Paper 2741(1987)

"Theoretical Antideuteron-Nucleus Cross Sections" W.W. Buck, J.W. Norbury, L.W. Townsend, J.W. Wilson, **Phys. Rev. C33, 234 (1986)**

"On the Biological Hazard of Galatic Antinuclei" J.W. Wilson, W.W. Buck, L.W. Townsend, **Health Physics, Vol. 50, No. 5 (May 1986), 666**

"The NN Interaction as a Composite System" . W.W. Buck, CEBAF RPAC (1986) p6-4

"Atomic Traffic Cops Love High-Speed Collisions" W.W. Buck, Daily Press Newspaper (Hampton Roads,Virginia) Commentary Section, p., October 20,1985

"Structure Functions for Electron-Nucleon Coincidence", Soon C. Park and W.W. Buck, CEBAF RPAC (1986), p8-24

"Hampton University Graduate Studies (HUGS) at CEBAF Proceedings", CEBAF Publication (1986), Editor, W.W. Buck

"Nuclear Forces in a Dirac Harmonic Oscillator Quark Model", W.W. Buck, F. Gross, W-Y.P. Hwang, L.S. Kisslingler, F. Wang, CEBAF RPAC (1987) p527

"Electroproduction of Antiprotons", W.W. Buck, CEBAF RPAC (1987)

"2nd Annual HUGS at CEBAF Proceedings", CEBAF Publication (1987), W.W. Buck, Editor

"BRYNTRN: A Baryon Transport Computer Code: Computational Procedures and Data Base" J.W. Wilson, L.W. Townsend, S.Y. Chun, W.W. Buck, F. Khan, F. Cucinotta, NASA TM 4037 (June 1988)

"Nucleon-Nucleus Interaction Data Base: Total Nuclear and Absorption Cross Sections", J.W. Wilson, L.W. Townsend, W.W. Buck, S.Y. Chun, B.S. Hong, S.L. Lamkin, NASA TM 4053 (August 1988)

"Relativistic Antinucleon-Nucleon Interaction: A New Level Ordering", W.W. Buck, **Workshop on Relativistic Nuclear Many-Body Physics Proceedings**, World Scientific Publishers, Editors B.C. Clark, R. Perry, J. Vary (June 1988)

"The Third Annual HUGS at CEBAF Proceedings" CEBAF publication, W. W. Buck, editor in chief (1988)

"Eikonal Solutions to Optical Model Coupled-Channel Equations", F. Cucinotta, G. S. Khandelwal, K. M. Maung, L. W. Townsend, J. W. Wilson. NASA Technical Paper number 2830. (1988)

"High Energy Nucleon Data Bases", J. W. Wilson, S. Y. Chun, W. W. Buck, L. W. Townsend, **Health Physics, Vol 55, pp817-819, 1988**

"BRYNTRN: A Baryon Transport Model"J. W. Wilson, L. W. Townsend, J. E. Nealy, S. Y. Chun, B. S. Hong, W. W. Buck, S. L. Lamkin, B. D. Ganapol, F. Khan, and F. A. Cucionatta, NASA TP 2887 (March 1989) - **NASA/LaRC Space Systems Division Best Paper for 1990-1991**

"Isospin Flip as a Relativistic Effect: NNbar Interactions", W.W. Buck, CEBAF preprint 89-023, HU preprint 89-1

"Kaon-Nucleus Scattering", B. Hong, K.M.Maung, J.W.Wilson, W.W.Buck, NASA Technical paper #2920 (July, 1989)

"Nuclear-Fragmentation Studies for Microelectronic Applications", D.M.Ngo, J.W.Wilson, W.W.Buck, T.N.Fogarty, NASA Technical Memorandum #4143(Nov. 1989)

"The Fourth Annual HUGS at CEBAF Proceedings", HU/CEBAF publication, W. W. Buck editor in chief(1989)

" Meson Exchange and the Relativistic Multiple Scattering Fromalism", F. Gross and K. M Maung. Phys. Lett. Vol 229 188(1989).

"Pseudoscalar pi-N coupling and relativistic proton-nucleus scattering", F. GRoss, K. M. Maung, J. A. Tjon, L. W. Townsend and S. J. Wallace. Phys. Rev C Vol 40, R10(1989).

"Progress in Proton Transport Code Development: Microelectronic Application", Duc Ngo, W. W. Buck, T. N. Fogarty, and J. W. Wilson, p371, NASA/HBCU Space Science and Engineering Research Forum Proceedings, March 22-23, 1989, Y, D. Saunders, Y. B. Freeman, M. C. George Editors.

"Kaon-Nucleus Scattering Calculations", B. Hong, W. W. Buck, K. M. Maung, J. W. Wilson, and L. W. Townsend, p146, NASA/HBCU Space Science and Engineering Research Forum Proceedings, March 22-23, 1989, Y, D. Saunders, Y. B. Freeman, M. C. George Editors.

"Covariant Multiple Scattering Series for Elastic Projectile-target Scattering" K. M. Maung and F. Gross. Phys. Rev. C Vol 42, 1681(1990).

"Relativistic proton-nucleus scattering and one-boson exchange models", K. M . Maung, F. Gross, J. A. Tjon, L. W. Townsend and S. J. Wallace. Phys. Rev. C VOl 43 1378(1991).

"Theoretical angular distributions from coherent subthreshold pion production" P. A. Deutchman and K. M. Maung. Phys. Rev. C. Vol, 41 R423 (1990).

"A Nuclear Fragmentation Energy Deposition Model", Duc Ngo, J. W. Wilson, T. N. Fogarty, W. W. Buck, **Transactions on Nuclear Science,Vol38, no. 1, February 1991.**

"Confining Potential in Momentum Space", J. W. Norbuty, D.E. Kahana and K. M. Maung, Can. Jou. Phys. Vol 70, 86 (1992)

✓

Seminars and Conference Talks under NAG-1-477:

"Optical Potential Calculations of Antideuteron Absorptive Cross Sections", Presented by W.W. Buck,with J.W. Norbury, L.W. Townsend, J.M. Wilson, Fall1985 Meeting of the APS Division of Nuclear Physics, Pacific Grove, CA

"Antimatter-New Frontier in Science", Battelle Pacific Northwest Labs (March 14, 1986), **Invited**

"A Search for Galactic Anti-ion Cosmic Rays", 1st NASA-HBCU Forum, Atlanta, GA (April 20-22, 1986),**Invited**

"In Search of Anti Iron", Florida International University, Miami, FLA (1987), **Invited**

"Relativistic Isopin Exposure", The University of Kentucky, Lexington, KY (May 1988), **Invited**

"Nuclear Physics at Hampton University", Virginia State University, Petersburg, VA (May 1988), **Invited**

"Relativistic Antinucleon-Nucleon Interaction: A New Level Ordering", Workshop on Relativistic Nuclear Many-Body Physics, Columbus, OH (June 1988), **Invited**

"Antimatter Predictions from an Optical Model", The Ohio State University, Columbus, OH (August 1988),**Invited**

"Relativistic Antinucleon-Nucleon Interaction: A New Level Ordering", Fall Meeting of the APS Division of Nuclear Physics, Santa Fe, NM (October 1988)

"Some Aspects of Antimatter Annihilation", University of Grenoble, France (March 1989), **Invited**

"Some Aspects of Antinucleon&Antinucleus Interactions", joint seminar @ Univ. of Pittsburgh and Carnegie-Melon Univ., Oct 5, 1989 **Invited**

"HUGS at CEBAF", talk presented at the AAPT Chesapeake Section Fall 1989 Meeting, VA Beach, VA, Oct 21,1989

Session Chairman, Fall Meeting Southeast Section of the APS, Tuscaloosa, ALA, Nov. 9, 1989

"Nuclear Physics at Hampton University", Morehouse University, Atlanta, GA, Nov. 14, 1989, **Invited**

"Physics: Science or Art", 1990 Stone Symposium on Sociology of

Subjectivity, St. Petersburg Beach, FLA Jan. 25-28, 1990, **Invited**

"Relativistic Dynamics: NNbar and qqbar", University of Illinois, Champaign, Ill, March 26, 1990, **Invited**

"A Covariant Quark Model of the Pion", Argonne National Laboratory, Argonne,Ill, Oct 16,1990, **Invited**

"A Covariant Quark Model of the Pion", Carnegie-Mellon University Pittsburgh, PA., March, 1991, **Invited**

Acknowledgement

We would like to thank the High Energy Science Branch of the NASA Langley Research Center for giving us the opportunity to perform research under this grant. We would especially like to thank F. Cucinotta, L. W. Townsend and J. W. Wilson. We would also like to thank our collaborators from other institutions, especially , P. A. Deutchman (Univ. of Idaho), F. Gross (William and Mary), D. E. Kahana (Kest State Univ.), J. W. Norbury (Univ. Wisconsin/Lacrosse), J. A. Tjon (Utrecht) and S. J. Wallace (Univ. of Maryland).

NASA Technical Memorandum 4053

Nucleon-Nucleus Interaction Data Base: Total Nuclear and Absorption Cross Sections

J. W. Wilson and L. W. Townsend
Langley Research Center
Hampton, Virginia

W. W. Buck, S. Y. Chun, and B. S. Hong
Hampton University
Hampton, Virginia

S. L. Lamkin
Planning Research Corporation
Hampton, Virginia

National Aeronautics
and Space Administration

Scientific and Technical
Information Division

1988

NASA Technical Paper 2920

1989

Kaon-Nucleus Scattering

Byungsik Hong and
Khin Maung Maung
Hampton University
Hampton, Virginia

John W. Wilson
Langley Research Center
Hampton, Virginia

Warren W. Buck
Hampton University
Hampton, Virginia

NASA
National Aeronautics and
Space Administration
Office of Management
Scientific and Technical
Information Division

NASA
Technical
Paper
2830

1988

Eikonal Solutions to Optical Model Coupled-Channel Equations

Francis A. Cucinotta,
Govind S. Khandelwal,
and Khin M. Maung
Old Dominion University
Norfolk, Virginia

Lawrence W. Townsend
and John W. Wilson
Langley Research Center
Hampton, Virginia

National Aeronautics
and Space Administration

Scientific and Technical
Information Division

CHARGED PARTICLE TRANSPORT IN ONE DIMENSION

A Thesis

presented to

the Graduate College

Hampton University

In Partial Fulfillment

of the Requirements for the Degree of

MASTER OF SCIENCE

---

by

Sang Yull Chun

April 1988

NUMERICAL SOLUTION OF THE SCHRODINGER EQUATION FOR DIFFERENT TYPES OF POTENTIALS

A THESIS

PRESENTED TO

THE GRADUATE COLLEGE

HAMPTON UNIVERSITY

IN PARTIAL FULFILLMENT OF THE

REQUIREMENTS FOR THE DEGREE OF

MASTER OF SCIENCE

BY

SOON C. PARK

APRIL 1987

KAON NUCLEUS SCATTERING CALCULATION USING KERMAN, McMANUS AND THALER MULTIPLE SCATTERING THEORY

A Thesis

Presented to

The Graduate College

Hampton University

In Partial Fulfillment

of the Requirements for the Degree of

Master of Science

By

Euyheon Hwang

May 1991

OPTICAL MODEL FOR KAON-NUCLEUS SCATTERING

A Thesis

Presented to

The Graduate College

Hampton University

In Partial Fulfillment

of the Requirements for the Degree

Master of Science

---

by

Byungsik Hong

April 1989

PHYSICAL REVIEW C VOLUME 42, NUMBER 4 OCTOBER 1990

Covariant multiple scattering series for elastic projectile-target scattering

Khin Maung Maung
Department of Physics, Hampton University, Hampton, Virginia 23668
and NASA Langley Research Center, Hampton, Virginia 23665

Franz Gross
Department of Physics, College of William and Mary, Williamsburg, Virginia 23185
and Continuous Electron Beam Accelerator Facility, Newport News, Virginia 23606

(Received 14 September 1989)

A covariant formulation of the multiple scattering series for the optical potential is presented. We consider the case of a scalar "nucleon" interacting with a spin zero isospin zero A-body target through meson exchange. We show that a covariant equation for the projectile-target t matrix can be obtained that sums the ladder and crossed ladder diagrams efficiently. From this equation, a multiple scattering series for the optical potential is derived, and we show that in the impulse approximation, the two-body t matrix associated with the first-order optical potential is the one in which one particle is kept on mass shell. The meaning of various terms in the multiple scattering series is given and we describe how to construct the first-order optical potential for elastic scattering calculations.

I. INTRODUCTION

It is well known that the relativistic (Dirac equation) calculations give superior results to the nonrelativistic (NR) calculations in the case of p-nucleus elastic scattering and have been widely used in recent calculations.[1,2] The first-order optical potential used in these calculations is the relativistic impulse approximation[1] (RIA) which is a relativistic generalization of the nonrelativistic tp approximation. In the NR theory the elastic scattering of the projectile from the target nucleus is described by an effective interaction (optical potential) which is to be used in the Schrödinger equation, and the scattering observables are then obtained. The optical potential itself can be expressed as an infinite series of scattering terms, single, double, etc., scatterings (hence the name multiple scattering series) in which there are no two successive scatterings from the same target particle. By keeping only the first term of the infinite series of the optical potential we obtain the first-order optical potential. The tp approximation is achieved only after two more approximations, namely the impulse approximation which treats the struck target nucleon as though it were free, and the factorization approximation which assumes that the range of the interaction is small compared to the size of the nucleus. The last approximation is usually applied in order to avoid the complexities of performing the folding integral to obtain the optical potential. The existence of a multiple scattering series for the optical potential (in fact there are several in the literature) provides us with a means to calculate systematic corrections to the first-order results.

In the relativistic p-nucleus scattering calculations the effective one-body equation is taken to be the fixed energy Dirac equation. This choice is intuitively appealing as long as one considers the proton as an elementary fermion, but the actual validity of this assumption is still in question. This type of question will be answered only when one has the nonperturbative aspects of QCD under the same degree of control as in NR theories. Now the question arises as to what effective interaction (optical potential) should be used in the Dirac equation to describe p-nucleus scattering. As mentioned above, in all the relativistic calculations, the optical potential used has been the RIA.[1] The RIA optical potential is obtained by simply folding a relativistic NN amplitude with the nuclear density matrix. Strictly speaking, use of the RIA is an intuitive guess guided by the nonrelativistic multiple scattering formalism, since a relativistic multiple scattering theory (RMST) has not been available.

It is important to realize that without a multiple scattering theory the t matrix associated with the first-order optical potential cannot be unambiguously determined and consequently the characters of the corrections to be made to the first-order optical potential are not well defined. The absence of such a theory prevents us from making systematic corrections, such as Pauli blocking, in a consistent manner. Therefore it is highly desirable to have an RMST. Probably the most appropriate approach might be to apply the methods of field theory to the problem. But the development of the RMST in this direction has been hampered by the problems arising in the treatment of the interacting many-body ground state,[3] description of the residual interaction between the projectile particle and the target constituents, and many other obstacles not encountered in the NR theory.

In this work we take a less formal but more intuitive approach and describe the projectile-nucleus scattering problem in a meson exchange model. A brief account of this work has already been given.[4] In this paper we will develop the ideas reported there in more detail.

From the beginning, we would like to make it clear

that our aim is to derive a multiple scattering theory for the projectile-nucleus scattering in the context of meson exchange. We will not consider the full implication of the formal field theoretical treatment of the interacting many-body problem, which is admittedly very difficult. We develop an approach which permits the standard multiple scattering techniques of NR theory to be applied with slight modification. We ignore the full complications of antisymmetry required by the Pauli principle and also ignore the spin part of the problem. We do not assume any particular form of equation for the projectile-nucleus t matrix, but begin with the most obvious fact that the t matrix is obtained by summing an infinite set of diagrams in which the projectile is interacting with the target particles through meson exchange. Although the approach we take in this work seems much less complicated than the formal field theoretical approach, it has its share of problems, such as the appearance of spurious singularities and the necessity for judicious treatment of the crossed meson diagrams. In this work we show how an RMST can be formulated within the context of meson exchange, unambiguously determine the t matrix associated with the optical potential, and show that under the impulse approximation the t matrix to be used in the first-order optical potential is the solution of a relativistic two-body equation in which one particle is kept on its mass shell.

This paper is arranged as follows. In Sec. II the derivation of a multiple scattering series of the optical potential is reviewed, following the approach of Watson.[3] In Sec. III A it is shown how the crossed meson diagrams should be treated together with the box diagram for the case where the intermediate state target is in the ground state. In Sec. III B the complications that arise in the case of intermediate target excited states are discussed, and it is shown how to handle the box and crossed box diagrams in this case. In Sec. III C a covariant equation for the projectile-target t matrix is presented and it is shown how a multiple scattering series for the optical potential can be derived. The meaning of various terms in the multiple scattering series are discussed, and it is shown that the most appropriate two-body t matrix to be used in the first-order optical potential under the impulse approximation is the one calculated from a covariant equation in which one particle is kept on the mass shell. A general discussion and conclusion follows.

II. NONRELATIVISTIC FORMALISM

In this section the nonrelativistic multiple scattering formalism is reviewed. The approach of Watson[3] is followed, since it is more closely related to our relativistic formalism than the more commonly used Kerman-McManus-Thaler[6] (KMT) method. Since we are interested in deriving a relativistic multiple scattering series for the optical potential, we will bypass the multiple scattering treatment of the t matrix and will concentrate, in the present section, on the multiple scattering analysis[7] of the nonrelativistic optical potential.

We begin with a total Hamiltonian H for the projectile-nucleus system given by

$$H = H_0 + V , \tag{2.1}$$

with

$$H_0 = H_A + h_0 \tag{2.2}$$

and

$$H_A = \sum_{i=1}^{A} h_i + \sum_{i<j} v_{ij} , \tag{2.3}$$

$$V = \sum_{i=1}^{A} v_i . \tag{2.4}$$

Notice that the total Hamiltonian H is separated into two parts, the unperturbed Hamiltonian H_0 and the residual interaction V. It is the separability of H into H_0 and V, which permits the derivation of a multiple scattering formalism. The residual interaction V is taken to be the sum of the two-body interactions between the projectile particle "0" and the target particle "i." The unperturbed Hamiltonian H_0 is written as the sum of the target Hamiltonian H_A and h_0, the kinetic energy operator for the projectile. In NR formalism, the target Hamiltonian is just the kinetic energy operators of the target particles plus the sum of their pair interactions.

The separation of the total Hamiltonian in Eq. (2.1) implies that we have some means in finding the solution to the target Hamiltonian H_A. Therefore in NR theory the complexities of the A-body problem are separated from the rest at the very beginning. Now write the Lippmann-Schwinger equation for the projectile-nucleus t matrix in operator form as

$$T = V + VG_0T \tag{2.5}$$

with

$$G_0 = (E - H_0 + i\eta)^{-1} . \tag{2.6}$$

Here G_0 is the unperturbed Green's function and the $i\eta$ prescription has been used to incorporate the outgoing boundary condition. The many-body nature of Eq. (2.5) is apparent since the propagator G_0 involves the target Hamiltonian H_A.

For elastic scattering problems it is useful to introduce an effective one-body potential (optical potential). The optical potential is defined as the potential that describes the passage of a projectile through the nucleus with the nucleus treated as a passive medium, i.e., the nucleus is treated as though it cannot be excited. To accomplish this, first define a projection operator P which projects onto the ground state of the target and Q which projects onto the excited states of the target including the breakup states. Therefore,

$$P + Q = 1 , \tag{2.7}$$

where

$$P = |\phi_0\rangle\langle\phi_0| , \tag{2.8}$$

and $|\phi_0\rangle$ is the target ground state. Now Eq. (2.5) can be rewritten as

$$T = U + UPG_0PT , \tag{2.9}$$

$$U = V + VQG_0QU \ . \tag{2.10}$$

The U appearing in these equations is the optical potential operator and Eq. (2.9) together with Eq. (2.10) are equivalent to Eq. (2.5).

Since we are dealing with strong interactions, it is impractical to solve Eq. (2.10) for U as it stands. It is at this point that the multiple scattering approach provides us with a big advantage. We may express U as $\sum_{i=1}^{A} U_i$ and rewrite Eq. (2.10) as

$$U_i = v_i + v_iQG_0Q\sum_{j=1}^{A} U_j \ . \tag{2.11}$$

Now define the Watson τ operator as

$$\tau_i = v_i + v_iQG_0Q\tau_i \tag{2.12}$$

and observe that Eq. (2.11) can be written in terms of τ_i

$$U_i = \tau_i + \tau_iQG_0Q\sum_{j\neq i} U_j \ . \tag{2.13}$$

Summing over the index i in the last equation gives the Watson multiple scattering series for the optical potential operator,

$$U = \sum_{i=1}^{A} \tau_i + \sum_{i=1}^{A} \tau_iQG_0Q\sum_{j\neq i} U_j \ . \tag{2.14}$$

Notice that Eq. (2.14) is an infinite series in τ instead of the two-body interactions v as in Eq. (2.10). Each term of Eq. (2.14) can be interpreted as single scattering, double scattering, and so on, hence the name multiple scattering series. By keeping only the first term of the series we obtain the first-order Watson optical potential

$$U^{1st} = \sum_{i=1}^{A} \tau_i \ . \tag{2.15}$$

The operator τ is not the free two-body t matrix because of the many-body propagator in Eq. (2.12), but related to it by

$$\tau = t + t(QG_0Q - g)\tau \ , \tag{2.16}$$

where the free two-body t-matrix is defined as

$$t = v + vgt \ , \tag{2.17}$$

with g the free two-body propagator. For high projectile incident energies one usually approximates τ by t (impulse approximation[7]) and obtains for the first-order Watson impulse approximation optical potential

$$U^{1st}_{im} = \sum_{i=1}^{A} t_i \ . \tag{2.18}$$

We can also rewrite Eq. (2.14) in terms of the free two-body t matrix, t:

$$U = \sum_{i} t_i + \sum_{i} t_i(QG_0Q - g)U_i + \sum_{i\neq j} t_iQG_0QU_j \ . \tag{2.19}$$

As we have mentioned above the first term in Eq. (2.19) gives the first-order impulse approximation optical potential. The second term can be interpreted as the propagator correction term. This term originates from the fact that we have written the optical potential in terms of the free t matrix t instead of τ. For high projectile energies the differences between t and τ become negligible and the impulse approximation should give good results. The last term represents the multiple scattering terms. For NR scattering calculations the t matrix appearing in Eq. (2.19) can be obtained from Eq. (2.17) by employing a choice of v, for example the Reid potential, or by fitting the NN experimental data directly by using an appropriate functional form. After the choice for the t matrix is made, solving Eq. (2.17) together with Eq. (2.9) is just a technicality.

III. RELATIVISTIC FORMALISM

In the last section we reviewed the nonrelativistic multiple scattering formalism and outlined how a multiple scattering series for the optical potential can be obtained. We pointed out that the key feature that enables us to construct a multiple scattering series is the separability of the total Hamiltonian into an unperturbed Hamiltonian describing the free projectile-target system and the residual interaction which is the sum of the two-body interactions between the projectile and the target particles. Unfortunately, there is no analogous procedure in the relativistic case. First of all, one cannot naively write the target Hamiltonian as the sum of the Dirac Hamiltonians plus the sum of two-body interactions, since the Hamiltonian written in this manner does not have a lower bound.[8] In order to treat the projectile-target scattering consistently in a relativistic formalism one needs to resort to a field theoretical approach.

In this work we take a less ambitious route and show that a relativistic multiple scattering series can be formulated in the context of a relativistic meson exchange model. In the following we will consider a scalar "nucleon" interacting with an A-body spin zero isospin zero target where the interaction between the projectile and the target is described by meson exchange. Since we do not assume any particular form of equation for the projectile target t matrix, we will start from the most obvious fact that it can be obtained by summing all possible meson exchange diagrams for the projectile target system. A minimal set of meson exchange diagrams required for any such theory is the set of ladder and crossed ladder diagrams. In the limit when the heavy target becomes infinitely massive, this set reduces to a one-body equation for the lighter particle moving in an instantaneous potential produced by the heavier particle (the one-body limit[9]), and at high energies gives the eikonal approximation to scattering.[9] In this work we seek a theory in which these relativistic ladder and crossed ladder diagrams are summed efficiently.

In Fig. 1 the target is represented by a double line, the dashed lines represent the exchange particle (meson), and the solid line represents the projectile. For the intermediate states the target can be in its ground state, denoted by $n = 0$, or in excited states, $n \neq 0$, which includes the breakup states. The notation is very compact; each diagram in Fig. 1 actually represents a set of diagrams which can be obtained by opening up the bubbles at the meson-

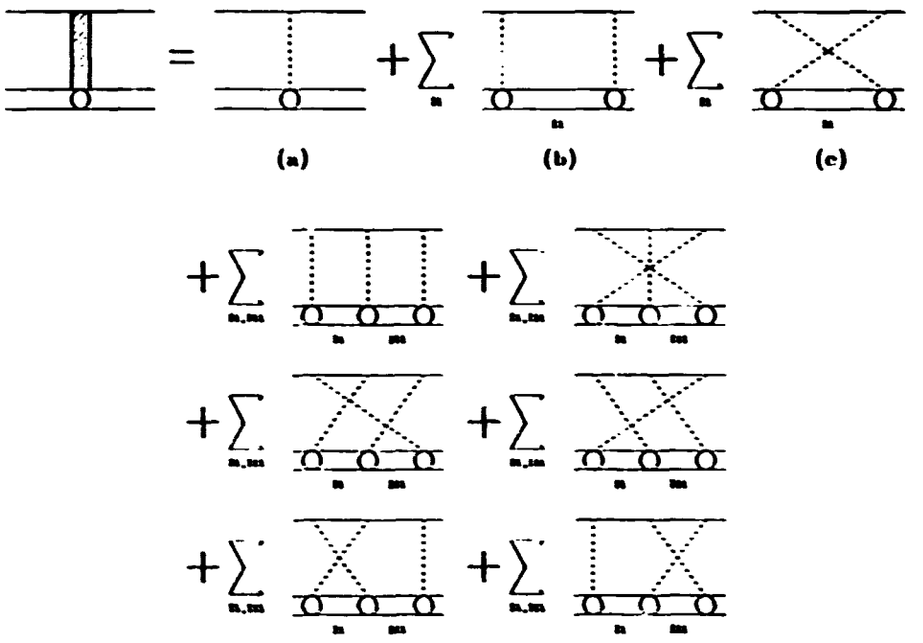

FIG. 1. The projectile-target t matrix is shown as the sum of all meson exchange processes up to the six order diagrams. The single line represents the projectile and the double line represents the target. The dashed lines are the exchanged meson. (a) is the one meson exchange term, (b) is the box, and (c) the crossed box. In the fourth and higher order diagrams, all possible intermediate target states are summed.

target vertices. For example, the set of diagrams contained in the box, Fig. 1(b), and crossed-box, Fig. 1(c), are shown explicitly in Figs. 2 and 3.

In our view, the solution of the relativistic problem in the meson exchange approximation is equivalent to finding an integral equation which sums all of the diagrams shown in Fig. 1. The construction of such an equation confronts us with three problems. The first problem, which does not occur in the nonrelativistic case, is the appearance of the crossed meson diagrams. These and all other irreducible diagrams (i.e., those which cannot be separated into two pieces by a line which intersects only the projectile and the target) will be included in the kernel of the integral equation. The second problem concerns the treatment of excited states. All diagrams, except for the one meson exchange term, include terms in which the target propagates in an excited state. A third problem is that each diagram includes terms in which the projectile may interact with two or more different target particles (multiple scattering). In this section, we will first discuss how the crossed diagrams are handled, and then discuss the complications arising from the occurrence of excited states.

A. Cancellation between the box and crossed-box diagrams

We know from the two-body problem that the ladder sum does not give a good approximation to the true solution of the Bethe-Salpeter equation. There is no reason to believe that it would be otherwise here. In fact, in the

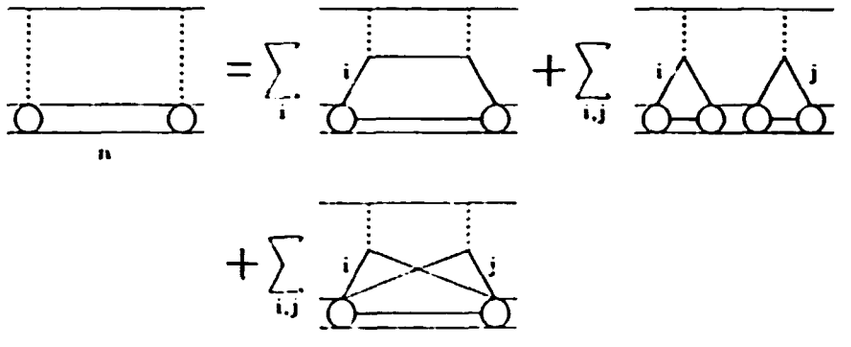

FIG. 2. Figure 1(b) is redrawn by opening up the bubbles at the meson-target vertices. The sum is over the target particles.

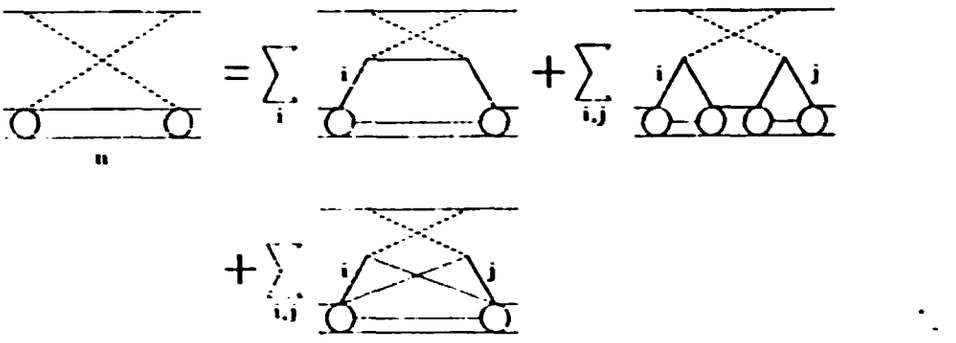

FIG. 3. Figure 1(c) is redrawn by opening up the bubbles at the meson-target vertices. The sum is over the target particles.

two-body problem the box diagram and the crossed-box diagram tend to cancel, showing that it is unjustified to neglect crossed meson diagrams.

In this section we show that the cancellations between the box diagram and the cross-box diagram still occur in the case of projectile nucleus scattering. In order to demonstrate this cancellation, we perform the integration over the relative energy for the intermediate states.

In Fig. 4 the box diagram, Fig. 1(b), and the crossed-box diagram, Fig. 1(c), are redrawn and for the four-momentum variables for each internal particle are labeled. For our purpose now, it is sufficient to consider the target as a structureless particle as shown in Fig. 4. By employing standard Feynman rules the box and crossed-box diagrams of Fig. 4 are given by the following expressions:

$$M^{(a,b)} = \frac{-ig^4}{(2\pi)^4}\int \frac{d^3k'dp_0'[\omega^2-(\epsilon(\mathbf{k})-p_0')^2+i\eta]^{-1}}{[\epsilon^2(\mathbf{k}')-p_0'^2+i\eta][E_a^2(\mathbf{k}')-(W-p_0')^2+i\eta]} \tag{3.1}$$

$$M^{(a,b)} = \frac{-ig^4}{(2\pi)^4}\int \frac{d^3k'dp_0'[\omega^2-(\epsilon(\mathbf{k})-p_0')^2+i\eta]^{-1}}{[\epsilon^2(\mathbf{q})-(2\epsilon(\mathbf{k})-p_0')^2+i\eta][E_a^2(\mathbf{k}')-(W-p_0')^2+i\eta]} \tag{3.2}$$

where the total four momenta in the c.m. is

$$p+P=(W,0)=p'+P'=p''+P'' ,$$

and the three momenta and the on-shell energies are defined as

$$\mathbf{p}=-\mathbf{P}\quad\mathbf{k};\quad\mathbf{q}\quad\mathbf{p}-\mathbf{p}'+\mathbf{p}'';\quad\mathbf{p}'\quad\mathbf{P}''\quad\mathbf{k}' ,$$

$$\omega=[\mu^2+(\mathbf{k}'-\mathbf{k})^2]^{1/2};\quad\epsilon(\mathbf{k})=(m^2+\mathbf{k}^2)^{1/2};\quad E_a(\mathbf{k})=(M_a^2+\mathbf{k}^2)^{1/2} .$$

We assume forward scattering, i.e., $\mathbf{k}=\mathbf{k}''$, so that the meson poles become double poles. The external particles are taken to be on their mass shell.

Figures 5(a) and 5(b) show the locations of the poles (when $|\mathbf{k}|$ and $|\mathbf{k}'|$ are small) for the box diagram and crossed-box diagram, respectively. We will evaluate the box and crossed-box diagrams by using the residue theorem. In the following expressions the superscript on M distinguishes between the box and the crossed-box diagrams, the subscript is for the type of pole under consideration, and the letters U (upper half plane) and L (for lower half plane) are used to remind us how the contour is closed. For example $M^{(a,b)}_{p}(U,n=0)$ means the negative energy projectile pole ($=p$) contribution from the fourth-order box diagram (4.4) for $n=0$, and the integration contour is closed in the upper half plane.

Evaluate the box diagram for $n=0$. Close the contour in the upper half plane and pick up the target positive energy pole, double meson pole, and the projectile negative pole:

$$M^{(a,b)}(U,n=0)=M^{(a,b)}_{t}(U,n=0)+M^{(a,b)}_{2}(U,n=0)+M^{(a,b)}_{p}(U,n=0) ,$$

where we have used the subscript $=$ suggestively for the meson double pole contribution. These contributions are

$$M^{(a,b)}_{t}(U,n=0)\qquad\frac{g^4}{(2\pi)^3}\int\frac{d^3k'[\omega^2-(E_a(\mathbf{k}')-E_a(\mathbf{k}'))^2]^{-2}}{[2E_a(\mathbf{k}')][\epsilon^2(\mathbf{k}')-(\epsilon(\mathbf{k})+E_a(\mathbf{k})-E_a(\mathbf{k}'))^2]^{-1}}$$

$$M^{(a,b)}_{2}(U,n=0)\qquad\frac{g^4}{(2\pi)^3}\int\frac{d^3k'[\quad+\quad B]}{4\omega^3[\epsilon^2(\mathbf{k}')-(\epsilon(\mathbf{k})-\omega)^2]^2[E_a^2(\mathbf{k}')-(E_a(\mathbf{k})+\omega)^2]^2}$$

$$M^{(a,b)}_{p}(U,n=0)\qquad\frac{g^4}{(2\pi)^3}\int\frac{d^3k'}{[\omega^2-(\epsilon(\mathbf{k})+\epsilon(\mathbf{k}'))^2][2\epsilon(\mathbf{k}')][E_a^2(\mathbf{k}')-(W+\epsilon(\mathbf{k}'))^2]}$$

where

$$A=[E_0^2(\mathbf{k}')-(E_0(\mathbf{k})+\omega)^2][[e^2(\mathbf{k}')-(e(\mathbf{k})-\omega)^2]+2\omega(e(\mathbf{k})-\omega)] ,$$

$$B=2\omega(E_0(\mathbf{k})+\omega)[e^2(\mathbf{k}')-(e(\mathbf{k})-\omega)^2] .$$

For the crossed-box diagram we close the contour in the lower half plane for all n and pick up the double meson poles and negative energy projectile and target poles:

$$M^{4B}(L,n)=M_s^{4B}(L,n)+M_p^{4B}(L,n)+M_t^{4B}(L,n) .$$

The individual pole contributions are

$$M_s^{4B}(L,n)=-\frac{g^4}{(2\pi)^3}\int \frac{d^3k'[F+G]}{4\omega^2[e^2(\mathbf{q})-(e(\mathbf{k})-\omega)^2]^2[E_n^2(\mathbf{k}')-(E_0(\mathbf{k})-\omega)^2]^2} ,$$

$$M_p^{4B}(L,n)=-\frac{g^4}{(2\pi)^3}\int \frac{d^3k'}{[\omega^2-(e(\mathbf{k})+e(\mathbf{q}))^2]^2[2e(\mathbf{q})][E_n^2(\mathbf{k}')-(E_0(\mathbf{k})-e(\mathbf{k})-e(\mathbf{q}))^2]} ,$$

$$M_t^{4B}(L,n)=-\frac{g^4}{(2\pi)^3}\int \frac{d^3k'[\omega^2-(E_0(\mathbf{k})+E_n(\mathbf{k}'))^2]^2}{[e^2(\mathbf{q})- \quad -E_0(\mathbf{k})-E_n(\mathbf{k}'))^2][2E_n(\mathbf{k}')]} ,$$

where

$$F=[E_n^2(\mathbf{k}')-(E_0(\mathbf{k})-\omega)^2][[e^2(\mathbf{q})-(e(\mathbf{k})-\omega)^2]+2\omega(e(\mathbf{k})-\omega)] ,$$

$$G=2\omega(E_0(\mathbf{k})-\omega)[e^2(\mathbf{q})-(e(\mathbf{k})-\omega)^2] .$$

At this stage one could show that, at threshold, the dominant contribution of the box diagram for $n=0$ comes from the positive energy target pole and the meson poles give the second largest contribution. For the crossed-box diagram, the meson pole contribution is the dominant one and is nearly equal to the meson pole contribution from the box diagram but with a relative negative sign. Since we are interested in other energies beside

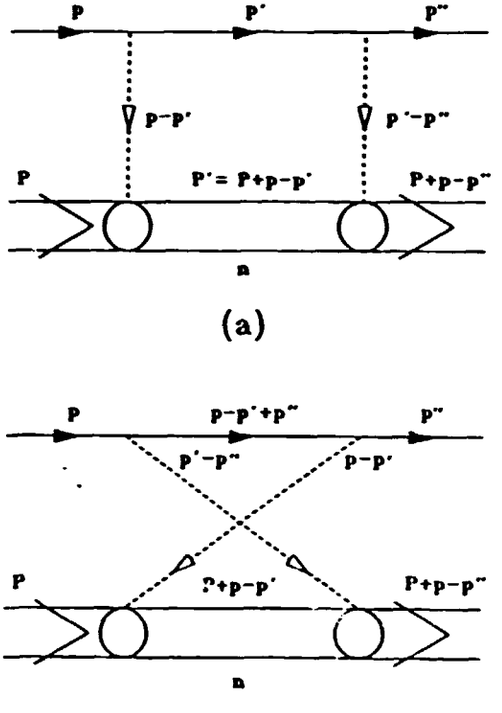

FIG. 4. Figures 1(b) and 1(c) are redrawn with explicit labels for the projectile and the target momenta.

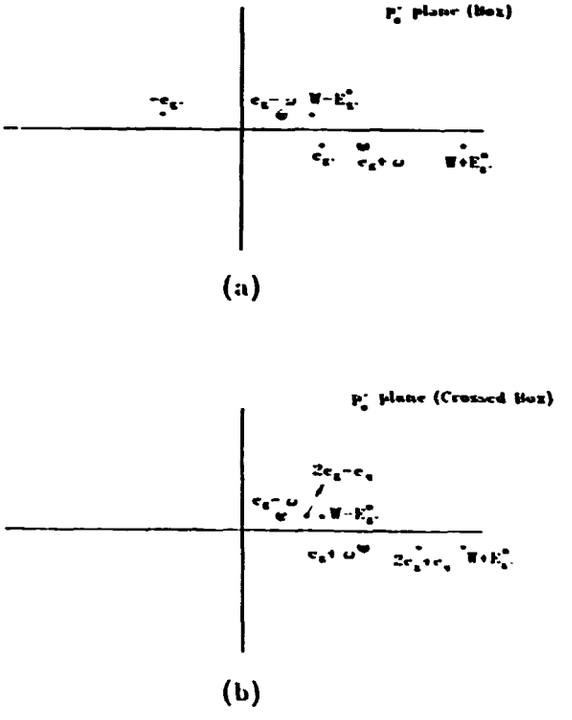

FIG. 5. The pole structures of the box diagram [Fig. 4(a)] and the crossed-box diagram [Fig. 4(b)] are shown in the complex p_n^0 plane. The circled dots represent the double meson poles.

threshold, we evaluate the various pole contributions without any further approximations. The only restriction is forward scattering.

Figure 6 demonstrates the cancellation between the box diagram and the crossed-box diagram. The dashed line is $|(M^{++}_{p}+M^{++}_{z})/M^{++}_{++}|$, the absolute magnitude of the ratio of the sum of negative energy projectile pole and meson pole contribution to the positive energy target pole contribution for $n=0$. The dotted line is the ratio of all the pole contributions from the crossed box to the positive energy target pole of the box diagram. These two lines lie practically on top of each other. Finally, the solid line is $|(M^{++}_{p}+M^{++}_{z}+M^{++}_{B})/M^{++}_{++}|$ which is the ratio of the sum of the full crossed box and negative energy projectile pole plus the meson poles of the box diagram to the positive energy pole of the box diagram. In these calculations, the target mass is taken to be $M_0=16m$, where m is the mass of the projectile particle and the meson mass is taken to be $\mu=m/7$. This figure shows that, when the target is in the ground state ($n=0$), the poles of the box diagram, which remain after the target is put on-shell, and the crossed-box diagram, are each of the order of 10–30% of the leading M^{++}_{++} term, and hence are far from being negligible. However, when the box and crossed box are taken together, an excellent cancellation occurs, as shown by the solid line for the energy range shown. After the cancellation, the positive energy target pole clearly dominates, and whatever is left over is less than 0.3% of this dominant contribution.

If the projectile is put on mass shell, instead of the target, the ratio of the correction from the box and the crossed box to the leading term would be $|(M^{++}_{+}+M^{++}_{z}+M^{++}_{B})/M^{++}_{p}|$, and this is the dot-dashed line shown in Fig. 6. This result shows that the cancellation between the box and crossed-box diagrams is not as complete when the projectile is on-shell, but still quite good. The terms which remain are now between 1–4% of the leading term, an order of magnitude larger than when the target is on-shell.

Figure 7 shows the A dependence of these cancellations. The legend of the curves mean the same as in Fig. 6, but they are shown as functions of the target mass $M_0=Am$, where the binding energy is neglected. The projectile laboratory kinetic energy is fixed at 1 GeV. As can be seen from the solid line, if the target is on-shell the cancellations become better as A increases, and exact cancellation occurs when $A\to\infty$. As shown by the solid line, this is an excellent approximation even for light nuclei. If the projectile is on-shell the cancellation does not improve as $A\to\infty$, shown by the dot-dashed line, reflecting the fact that, in this case, the cancellation depends on the properties of the projectile and not on the target.

The above results suggest that, when the target is in the ground state, it is an excellent approximation to keep only the positive energy target pole for the intermediate states, which is equivalent to keeping the ground state target on its mass shell in all intermediate states. The cancellation is less complete and the approximation less accurate for realistic cases with spin and charge exchange, so that it is desirable, in the general case, to include (at least in principle) these extra terms as higher order corrections to the kernel [they become part of $\bar{U}^{++}$ in Eq. (3.5) as described below].

The alternative approach of putting the projectile on shell has been seen to be less well justified; the additional correction terms are larger and do not decrease as $A\to\infty$. We believe that this analysis provides a satisfactory motivation for using a fixed energy Dirac equation, in which the projectile is off-shell and the target is on-shell, to describe elastic nucleon-nucleus scattering.

B. Treatment of the excited states

In this subsection we will consider how to treat the intermediate target excited states. It would be tempting to

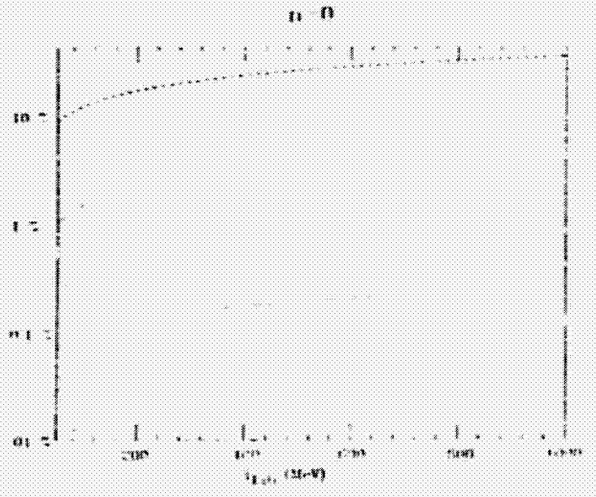

FIG. 6. The cancellations between the box diagram and the crossed-box diagram are shown for $n=0$. The target mass is taken to be $M_0=16m$ where m is the mass of the projectile. See the discussion in the text.

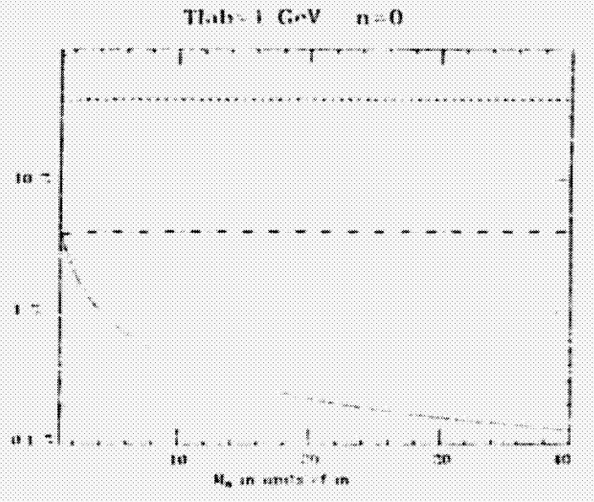

FIG. 7. The target mass dependence of the cancellation is shown for $n=0$. The projectile laboratory kinetic energy is taken to be 1 GeV. See the discussion in the text.

say that the same approximation that we have advocated in the case of $n=0$ should work here also, and that the excited state of the target should be put on mass shell. But for $n\neq 0$, further complications may arise because of the so-called dissolution singularities.[10]

The dissolution singularities are spurious singularities which arise when a highly excited heavy target is put on its mass shell. To see how they come about, consider putting the excited target on its mass shell in the expression for the box diagram, i.e.,

$$[E_n^2(\mathbf{k}')-(W-p_0')^2-i\eta]^{-1}\to 2\pi i\frac{\delta[p_0'-(W-E_n(\mathbf{k}'))]}{2E_n(\mathbf{k}')}\ .$$

The projectile propagator in (3.1) can be factorized into

$$[e^2(\mathbf{k}')-p_0'^2]^{-1}=[e(\mathbf{k}')+(W-E_n(\mathbf{k}'))]^{-1}\times[e(\mathbf{k}')-(W-E_n(\mathbf{k}'))]^{-1}\ .$$

In the last expression we see that there are two singularities, one at $W=e(\mathbf{k}')+E_n(\mathbf{k}')$ which is the usual elastic cut and the other one at $W=E_n(\mathbf{k}')-e(\mathbf{k}')$ which is the dissolution singularity. This second singularity is spurious because it does not occur when the diagram is calculated exactly. (It can be shown that it is cancelled by a similar singularity in the $M_p^{4,4}$ term.) When $n=0$, this singularity occurs at $W=E_0-e$, which is way below threshold and hence not of importance. However, when the intermediate state is highly excited ($n\neq 0$), the singularity can move into the physical region and is a cause for concern. It has been an obstacle in developing an RMST.

To see when this singularity becomes potentially dangerous, study the locations of the poles in the box diagram, Fig. 5(a). By approximating $W\approx M_0+m$ (threshold) and taking $|\mathbf{k}'|$ to be small so that $e(\mathbf{k}')\approx m$ and $E_n(\mathbf{k}')\approx M_n$, we see that the negative energy projectile pole and the positive energy target pole are separated by an amount M_0-M_n+2m in the upper half plane. As M_n increases, the positive energy target pole moves towards the negative energy projectile pole and when the excitation energy of the target reaches $2m$ the poles touch and a singularity arises. In this situation it is clearly not a good approximation to take one of these poles and "neglect" the other. In addition to these spurious singularities in the projectile propagator, there are other spurious singularities arising from the meson propagators when the excited state target is put on its mass shell. For calculational purposes these meson singularities are even worse than the ones from the projectile propagator since they can arise for relatively low excitation energies. At threshold they will appear when the excitation energy reaches the meson mass.

The situation in the lower half plane [Fig. 5(a)] is different. As E_n increases the negative energy target pole moves away from the positive energy projectile pole. To see this explicitly we put the projectile on its mass shell in Eq. (3.1):

$$[e^2(\mathbf{k}')-p_0'^2]^{-1}\to 2\pi i\frac{\delta(p_0'-e(\mathbf{k}'))}{2e(\mathbf{k}')}\ ,$$

and the target propagator is now

$$[E_n^2(\mathbf{k}')-(W-p_0')]^{-1}=[E_n(\mathbf{k}')-(W-e(\mathbf{k}'))]^{-1}\times[E_n(\mathbf{k}')+(W-e(\mathbf{k}'))]^{-1}$$

and exhibits no spurious singularities in the physical region. It can easily be seen that meson propagators do not have any such singularities either.

The above analysis suggests that, when we evaluate the expression (3.1) for $n=0$, we should close the contour in the upper half plane (to obtain the best approximation), but for $n\neq 0$ we should close the contour in the lower half plane to eliminate the problem of spurious singularities.

We now study the accuracy of this prescription by evaluating the box diagram for $n\neq 0$ by closing the contour in the lower half plane. The contributions come from the positive energy projectile pole, double meson pole, and negative energy target pole:

$$M^{4,4}(L,n\neq 0)=M_{1p}^{4,4}(L,n\neq 0)+M_2^{4,4}(L,n\neq 0)+M_{1t}^{4,4}(L,n\neq 0)\ .$$

The contribution from these poles is

$$M_{1p}^{4,4}(L,n\neq 0)=-\frac{g^4}{(2\pi)^3}\int\frac{d^3k'}{[\omega^2-(e(\mathbf{k})-e(\mathbf{k}'))^2]^2[2e(\mathbf{k}')][E_n^2(\mathbf{k}')-(W-e(\mathbf{k}'))^2]}\ ,$$

$$M_{1t}^{4,4}(L,n\neq 0)=-\frac{g^4}{(2\pi)^3}\int\frac{d^3k'}{[\omega^2-(E_0(\mathbf{k})+E_n(\mathbf{k}'))^2]^2[e^2(\mathbf{k}')-(W+E_n(\mathbf{k}'))^2][2E_n(\mathbf{k}')]}\ ,$$

$$M_2^{4,4}(U,n\neq 0)=-\frac{g^4}{(2\pi)^3}\int\frac{d^3k'[C+D]}{4\omega^3[e^2(\mathbf{k}')-(e(\mathbf{k})+\omega)^2]^2[E_n^2(\mathbf{k}')-(E_0(\mathbf{k})-\omega)^2]^2}\ ,$$

where

$$C=[E_n^2(\mathbf{k}')-(E_0(\mathbf{k})-\omega)^2][[e^2(\mathbf{k}')-(e(\mathbf{k})+\omega)^2]-2\omega(e(\mathbf{k})+\omega)]\ ,$$

$$D=2\omega(E_0(\mathbf{k})-\omega)[e^2(\mathbf{k}')-(e(\mathbf{k})+\omega)^2]\ .$$

In Fig. 8 calculations of the $n \neq 0$ cases are shown. The dashed line is the ratio of the sum of the meson poles (box) and target negative energy pole (box) to the positive energy projectile pole (box), i.e., $|(M^{4A}_{-T}+M^{4A}_{\pi})/M^{4A}_{+p}|$. The dotted line shows the ratio of the crossed-box diagram to the positive energy pole of the box diagram. The solid line is $|(M^{4B}+M^{4A}_{-T}+M^{4A}_{\pi})/M^{4A}_{+p}|$ which is the ratio of the sum of the full crossed box and the negative target pole (box) plus meson poles (box) to the positive energy projectile pole. For this calculation the target mass and the meson mass are the same as the $n=0$ case, and the excitation energy of the target is taken to be $\Delta m = m/100$. As in the $n=0$ case, the cancellations between the box and the crossed box still occur to a very large extent, although the cancellation is not as good as in the previous case. It can be seen that, after the cancellation, the leftover terms in the energy range shown are less than 4% of the dominant projectile positive energy pole contribution.

In Fig. 9 the curves mean the same as in Fig. 8, but are shown as the function of target excitation energy with the projectile laboratory kinetic energy fixed at 1 GeV. As before the solid line shows the net result and it is seen that the cancellation becomes better as the excitation energy increases. This is a good signature, since as the excitation energy becomes higher, the one particle knockout term, which is the dominant inelastic contribution at medium energies, will become more important, and it is advantageous to have the cancellations improve as these contributions become larger.

The preceding analysis suggests that for the intermediate target excited states, keeping the positive energy projectile pole of the box diagram provides us with a very good approximation and at the same time avoids the spurious singularities that would arise by putting the excited target on the mass shell.

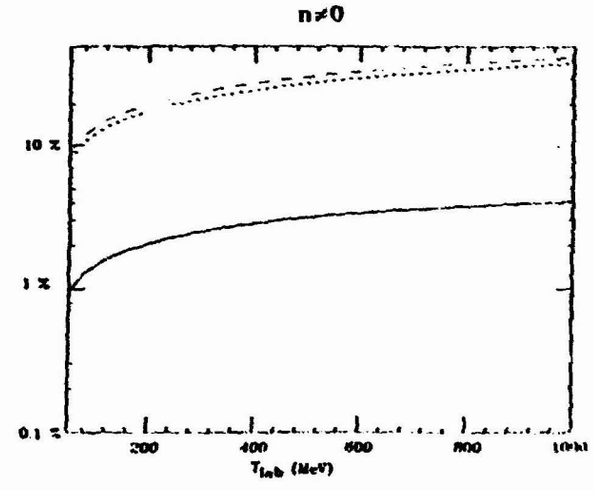

FIG. 8. The cancellations between the box diagram and the crossed-box diagram are shown for $n \neq 0$. M_{π} is the same as Fig. 6 and the excitation energy $\Delta m = m/100$. See the discussion in the text.

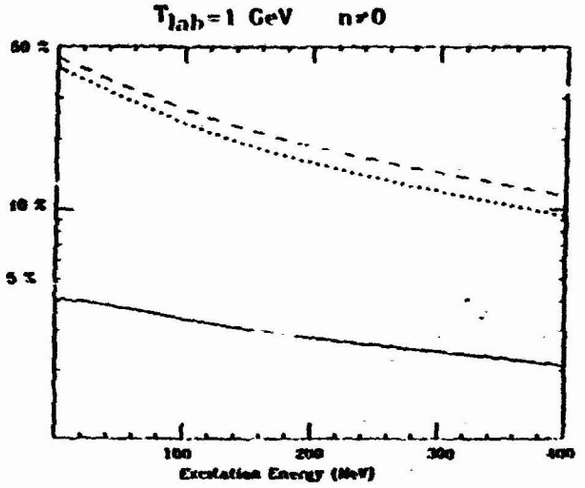

FIG. 9. Cancellations for $n \neq 0$ shown as a function of excitation energy. See the discussion in the text.

C. Multiple scattering series for the optical potential

In the preceding subsections, we have discussed the cancellations between the box and the crossed-box diagrams for both $n=0$ and $n \neq 0$. We have concluded that, because of the excellent cancellations between these diagrams, we should keep the target on the mass shell for $n=0$, and that for $n \neq 0$ we can avoid spurious singularities and still have a very good approximation if the projectile is kept on mass shell. Note that these approximations are obtained by considering the box and crossed box together. If one considered the box diagram only, these approximations would not be as good, as can be seen by the dashed curves of Figs. 6 and 8.

We now follow the suggestion provided by the last two subsections and write an integral equation for the projectile-target t matrix in the following form:

$$\hat{T} = \hat{V} + \hat{V}PG^{I}_{n}\,{}_{n}P\hat{T} + \hat{V}QG^{E}_{n}\,{}_{n}Q\hat{T} \ , \tag{3.3}$$

where $G^{I}_{n}{}_{n}$ is the propagator for the target in its ground state and on its mass shell, $G^{E}_{n}{}_{n}$ is the propagator for the target in its excited states with the projectile on mass shell, and P and Q are target ground state and excited state projection operators, respectively. The three-dimensional propagators appearing in Eq. (3.3) can be written in a manifestly covariant form as

$$G^{I}_{n}{}_{n} = \frac{1}{(2\pi)^3} \int \frac{\delta^3[(W-p'^2)^2 - M_n^2]}{(m^2 - p'^2)} \ ,$$

which in c.m. frame is

$$G^{I}_{n}{}_{n} = \frac{1}{(2\pi)^3} \int \frac{\delta[p'_n - (W - E_n(\mathbf{k}'))]}{2E_n(\mathbf{k}')[e^2(\mathbf{k}') - (W - E_n(\mathbf{k}'))^2]} \ , \tag{3.3a}$$

and

$$G^{E}_{n}{}_{n} = \frac{1}{(2\pi)^3} \int \frac{\delta^3(p'^2 - m^2)}{[M_n^2 - (W - p'^2)^2]} \ ,$$

which in c.m. frame is

$$G^{P}_{n\cdot 0} = -\frac{1}{(2\pi)^3}\frac{M}{2e(k')}\frac{\delta(p'_0 - e(k'))}{[E^{*}_{n}(k') - (W - e(k'))^2]} . \quad (3.3b)$$

Equation (3.3) is the first major result of this paper. It is a three dimensional covariant equation for the projectile-target t matrix. If the multimeson exchange irreducible diagrams (to be described below) are neglected the driving term of this equation, $\hat{V}$, assumes a very simple form. It is the sum of one meson exchanges between the projectile and the target particles. The special feature of this equation is that it has two three-dimensional propagators in which the target is on mass shell when the target is in the ground state and the projectile is on mass shell when the target is in an excited state.

In Eq. (3.3) $\hat{V}$ is the sum of all irreducible meson exchange contributions. In order to derive a multiple scattering series for the optical potential in a fashion similar to NR theory we write

$$\hat{V} = \sum_i \hat{v}_i + \hat{V}'' , \quad (3.4)$$

where the first term is the one meson exchange diagrams summed over the target particle index. The second term $\hat{V}''$ includes the contributions from the irreducible diagrams involving multimeson exchange. To be explicit, the fourth-order contributions to $\hat{V}''$ would be the parts of the box diagram, which do *not* have the target on mass shell when $n = 0$, and the projectile on mass shell when $n \neq 0$, and the crossed-box diagram. These are illustrated in Fig. 10. Higher order diagrams with similar qualifications constitute the rest of $\hat{V}''$. It is now clear that $\hat{V}$ through $\hat{V}''$ can include diagrams in which the projectile particle interacts with more than one target particle through meson exchange. We therefore separate out the processes in which only one target particle is involved and write

$$\hat{V}'' = \sum_i \hat{K}_{ii} + \sum_i \hat{K}_{iii} + \cdots + \sum_i \Lambda_i , \quad (3.5)$$

$$\Lambda_i = \sum_{j\neq i} \hat{K}_{ij} + \sum_{j\neq i,k\neq i} \hat{K}_{ijk} + \cdots , \quad (3.6)$$

where $\hat{K}_{ii}$, $\hat{K}_{iii}$, etc. are the contributions from the multimeson exchange irreducible diagrams in which only one target particle is involved. Λ_i are the multimeson exchange irreducible diagrams with more than one target particle interacting with the projectile. We have demonstrated, to the fourth order, that these terms (i.e., $\hat{K}_{ii}$ and $\hat{K}_{ij}$) are very small compared to $\hat{v}_i$. It was shown in Refs. 12 and 13 that higher order terms such as $\hat{K}_{ijk}$ are also small when the scattering takes place at threshold. We believe that the higher order K's will also be small above threshold.

We note that it is possible to define separate t matrices with deriving terms $\hat{K}_{ij}$, $\hat{K}_{ijk}$, etc., and derive a multiple scattering series. In that approach the resultant multiple scattering series will have a whole set of t matrices. We want to formulate our multiple scattering series in terms of a new t matrix whose kernel is the sum of irreducible diagrams involving only one target particle, i.e., $\hat{v}_i + \hat{K}_{ii} + \cdots$. As pointed out above, the terms $\hat{K}_{ii}$, etc. are small compared to $\hat{v}_i$ but we will include these terms in the kernel of the new t matrix for the sake of completeness. The terms given by Λ_i involve more than one target particle and they will be treated in such a manner that they would appear as higher order corrections in the resultant multiple scattering series.

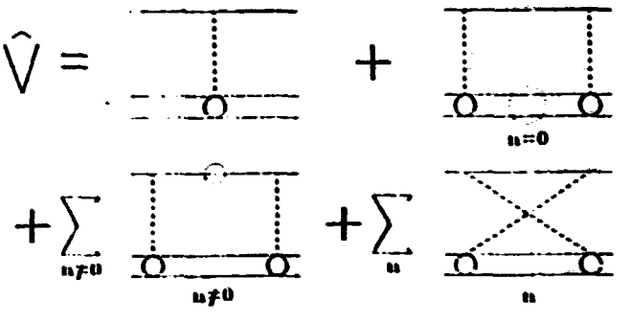

FIG. 10. Diagrams which contribute to $\hat{V}$ are shown to fourth order. The first term is the one meson exchange term. The rest of the diagrams are the irreducible diagrams as defined in the text. The dotted circle on a line indicates that the diagram is to be calculated without the on-shell contribution for the projectile (target). These irreducible diagrams as a whole are defined as $\hat{V}''$ in Eq. (3.4).

In the following we will show how a multiple scattering series for the optical potential that corresponds to Eq. (3.3) can be obtained. By employing the projection operator method, we can rewrite Eq. (3.3) as coupled equations:

$$\hat{T} = \hat{U} + \hat{U}PG^{P}_{n\cdot 0}P\hat{T} = \hat{U} + \hat{T}PG^{P}_{n\cdot 0}P\hat{U} , \quad (3.7a)$$

$$\hat{U} = \hat{V} + \hat{V}QG^{P}_{n\cdot 0}Q\hat{U} = \hat{V} + \hat{U}QG^{P}_{n\cdot 0}Q\hat{V} . \quad (3.7b)$$

Here $\hat{U}$ is our optical potential operator and we seek a multiple scattering series expression for this operator. It should be noted that Eqs. (3.7) are three-dimensional equations. The first one, Eq. (3.7a), is the effective one-body equation for the projectile, and for a fermion projectile it becomes the fixed energy Dirac equation.

Next, as in the NR theory, we write $\hat{U} = \sum_i \hat{U}_i$ and obtain

$$\sum_i \hat{U}_i = \sum_i (\hat{v}_i + \hat{K}_{ii} + \cdots + \Lambda_i) + \sum_{i,j} (\hat{v}_i + \hat{K}_{ii} + \cdots)G^{P}_{n\cdot 0}\hat{U}_j . \quad (3.8)$$

In the above equation, and in the following, the projection operators P and Q are suppressed. It is to be understood that P goes with $G^{P}_{n\cdot 0}$ and Q goes with $G^{Q}_{n\cdot 0}$. Adding and subtracting the quantity $\sum_i (\hat{v}_i + \hat{K}_{ii} + \cdots)\hat{U}_i$ and dropping the sum over i gives

$$\hat{U}_i = (\hat{v}_i + \hat{K}_{ii} + \cdots) + (\hat{v}_i + \hat{K}_{ii} + \cdots)G\hat{U}_i + \sum_{j\neq i} (\hat{v}_i + \hat{K}_{ii} + \cdots)G^{P}_{n\cdot 0}\hat{U}_j + \Lambda_i + \sum_j \Lambda_i G^{P}_{n\cdot 0}\hat{U}_j , \quad (3.9)$$

where we have introduced a new propagator g whose properties are not specified at this stage. Taking the second term on the right-hand side (RHS) of Eq. (3.9) to the left-hand side (LHS) and operating from the left with the inverse of $[1-(\hat{v}_i+\hat{K}_{ii}+\cdots)g]$ gives

$$\hat{U}_i=\bar{t}_i+\sum_j \bar{t}_i(G_{ii,0}^p-g\delta_{i,j})\hat{U}_j+\bar{v}_i\left[1+\sum_j G_{ii,0}^p\hat{U}_j\right],$$

where we have defined $\bar{t}_i$ and $\bar{v}_i$ as

$$\bar{t}_i=(\hat{v}_i+\hat{K}_{ii}+\cdots)+(\hat{v}_i+\hat{K}_{ii}+\cdots)g\bar{t}_i \tag{3.10}$$

and

$$\begin{aligned}\bar{v}_i&=\Lambda_i+(\hat{v}_i+\hat{K}_{ii}+\cdots)g\bar{v}_i\\&=\Lambda_i+(\hat{v}_i+\hat{K}_{ii}+\cdots)g\Lambda_i+\cdots\\&=\Lambda_i+\bar{t}_i g\Lambda_i\ .\end{aligned} \tag{3.11}$$

Resumming over the index i gives

$$\begin{aligned}\hat{U}=&\sum_i\bar{t}_i+\sum_i\bar{t}_i(G_{ii,0}^p-g)\hat{U}_i+\sum_{i\neq j}\bar{t}_iG_{ii,0}^p\hat{U}_j\\&+\sum_i\left[\bar{v}_i\left[1+\sum_j G_{ii,0}^p\hat{U}_j\right]\right].\end{aligned} \tag{3.12}$$

Equation (3.12) is our multiple scattering series for the optical potential, and it is the second major result of this paper. It should be compared with the NR analogue Eq. (2.19).

The first term of this series can be interpreted as the single scattering term for the optical potential and it is given by a t matrix driven by a kernel which is the sum of all irreducible diagrams involving only one target particle. The second term is the propagator correction term which obviously depends on our choice of the propagator g and its NR analog is the second term of Eq. (2.19). The third term on the RHS of (3.12) is the relativistic analog of the third term of Eq. (2.19) and corresponds to multiple scattering corrections and they are directly related to two, three, etc., particle correlations and can be assumed to be small in the first approximation.

The last term includes iterations with the irreducible diagrams which have more than one target particle involved (see the definition of $\bar{v}_i$ and Λ_i) and it does not contribute in the single scattering processes. These terms have also no NR analog and they originate from the multimeson exchange irreducible diagrams. We note that it is also possible to recombine this last term with the third term by separating the pieces according to the number of target particles involved. For example the first contribution to the double scattering would be $\sum_{i,j}\hat{K}_{ij}$. It should be noted that because of the conspiracy among the diagrams, these terms are quite small and will not carry the same weight as the true double scattering term such as $\bar{t}_iG_{ii,0}^p\bar{t}_j$, but they would constitute an interesting correction to the double scattering term.

Keeping the first term only gives a single scattering approximation for the optical potential. The propagator g has not yet been specified. In principle, one could use any convenient t matrix for the $\bar{t}$ operator in Eq. (3.12) as long as we are willing to incorporate the corrections represented by the rest of the terms in Eq. (3.12). In practice one usually keeps only the first term of the series and the judicious choice of g is then essential.

Under normal conditions, the second term gives the largest correction to the single scattering approximation, and we therefore should pay the greatest attention to this term. We would like to choose our propagator g so that this correction is minimal. This can be accomplished by choosing the propagator g as shown in Fig. 11. In this figure, both the heavy $A-1$ cluster and the projectile are kept on their mass shells.[11] In the medium energy range the terms represented by the sum $\sum\bar{t}_iQG_{ii,0}^pQ\bar{t}_i$ are dominated by the one nucleon knockout term and our choice of g described above would exactly cancel these dominant inelastic contributions and ensure that they are exactly accounted for in the t matrix itself given by Eq. (3.10). Restricting the $A-1$ cluster to the mass shell ensures cluster separability of the remaining two-nucleon system.[12]

With this choice of g, Eq. (3.10) for $\bar{t}_i$ in the NN subspace reduces to the one particle on mass shell (spectator) equation previously introduced by one of us.[13] A feature of this equation, discussed in Refs. 8 and 13, is that the multimeson irreducible diagrams $\hat{K}_{ii}$, $\hat{K}_{iii}$, etc., are expected to be small compared to $\hat{v}_i$, and can be neglected. To be specific, after neglecting these terms the $\bar{t}_i$ of Eq. (3.10) becomes

$$\bar{t}_i=\hat{v}_i+\hat{v}_ig\bar{t}_i\ . \tag{3.10a}$$

The projection of $\bar{t}_i$ onto this subspace will be denoted by t_i. The only difference between t_i and the free two-body t matrix is the shift in the total energy of the two-body subspace due to the motion of the free $A-1$ cluster. In analogy with the NR theory, this choice of g can be viewed as the "impulse approximation" choice of g in our theory. The spectator Eq. (3.10a) is shown diagrammatically in Fig. 12.

We conclude that the most appropriate t matrix to be used in the optical potential should be calculated from a covariant three-dimensional equation for two particles in which one particle is kept on its mass shell. This choice will minimize the leading correction to the multiple scattering series Eq. (3.12).

The last step is to carry out the necessary projections

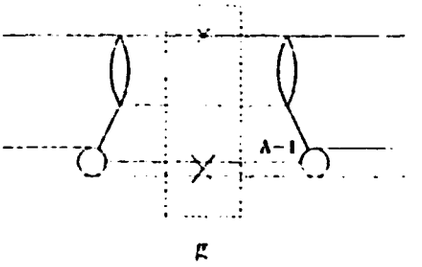

FIG. 11. The optimum choice of the propagator g of Eq. (3.10). The projectile and the $A-1$ cluster are both on the mass shell, indicated by a cross. This choice of g minimizes the leading correction term [the second term of Eq. (3.12)].

FIG. 12. The spectator three particle on-shell equation is shown diagrammatically. The crosses on a line mean that the particle is on the mass shell.

to obtain final equations for elastic scattering in the impulse approximation. The elastic scattering amplitude is $T=PTP$, which satisfies the equation

$$T=U+UG_0^I{}_0T\ . \tag{3.13}$$

where $U=P\hat{U}P$. Equation (3.13) is just the projection of Eq. (3.7a). In the single scattering approximation,

$$\hat{U}=\sum_i \bar{t}_i\ , \tag{3.14}$$

where $U=P\hat{U}P$. Equation (3.13) is just the projection of Eq. (3.7a). In the single scattering approximation,

$$\bar{t}_i=\hat{t}_i+\bar{t}_i g\bar{t}_i\ . \tag{3.10b}$$

Using both (3.10a) and (3.10b) we obtain an alternative equation for $\bar{t}_i$,

$$\bar{t}_i=\hat{t}_i+\hat{t}_i g\bar{t}_i+\hat{t}_i g\bar{t}_i g\bar{t}_i\ . \tag{3.15}$$

If we define $t_i(t_i)$ to be the projection of $\hat{t}_i(\bar{t}_i)$ onto the subspace of states connected to g, the first-order optical potential in the impulse approximation (IA) is finally obtained as

$$U_{\rm IA}^{\rm 1st}=\sum_i P\bar{t}_i P$$
$$=\sum_i (P\hat{t}_i P+P\hat{t}_i g\bar{t}_i P+P\hat{t}_i g\bar{t}_i g\bar{t}_i P)\ , \tag{3.16a}$$

where

$$t_i=v_i+v_i g t_i=v_i+t_i g v_i\ . \tag{3.16b}$$

Note that Eq. (3.16b) is equivalent to the two-body equation with the projectile on-shell, as described above and illustrated in Fig. 12 and (3.15) tells how all four legs of this two-body t matrix are extrapolated off-shell for use in the optical potential. Note that t_i has all four legs off-shell (and includes a delta function in the $A-1$ spectator

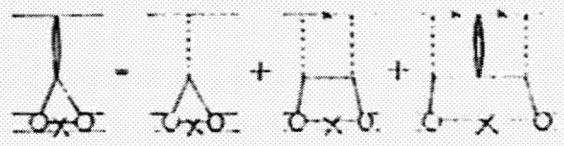

FIG. 13. This figure represents the quadrature equation (3.16a). The fully off-shell t matrix $\hat{t}$ is shown by an open oval. The shaded oval is the spectator t matrix of Eq. (3.10a). The first term on the RHS is the fully off-shell version of one meson exchange contribution used in Eq. (3.9a).

coordinates), but is identical to t_i if one particle is on-shell in the initial and final state (and the delta function in the $A-1$ coordinates is dropped). Furthermore, no further equation must be solved to obtain it; it is obtained directly from t_i by quadrature, Eq. (3.16a). Equation (3.16a) is illustrated in Fig. 13; its fourth-order contribution was already encountered in one of the terms in Fig. 2.

IV. DISCUSSION AND CONCLUSION

The idea that the projectile-target scattering amplitude is given by a relativistic equation where the kernel of the equation is the sum of certain diagrams was previously introduced in Ref. 17. However, these authors did not discuss meson exchange, nor did they derive any details about the multiple scattering series or the appropriate choice of relativistic equation and two-body amplitude.

In this paper we have considered a covariant formalism for projectile-target scattering in the context of meson exchange, and have shown that a multiple scattering series for the optical potential can be derived. We do not claim that we have derived an RMST starting from a field theoretical Lagrangian, but we do claim that we have derived a multiple scattering theory in a covariant manner. Every step of our derivation is manifestly covariant and the end result, the t matrix associated with the impulse approximation optical potential, must also be calculated from a relativistically covariant equation.

In conclusion, we will restate what we have accomplished in this paper. In the context of meson exchange we have derived a covariant equation for the projectile-nucleus t matrix Eq. (3.3). This equation was derived by considering the cancellations between the box and crossed-box diagrams and we have also shown how the spurious singularities can be avoided. We then derived a multiple scattering series for the optical potential and showed, in the impulse approximation, that the t matrix associated with the optical potential is to be calculated from a relativistic three-dimensional equation in which one particle is kept on its mass shell. We also described how the fully off-shell extension of this t matrix Eq. (3.10a) can be calculated from a quadrature, Eq. (3.16a). We emphasize that our development leads to a precise definition of the t matrix to be used in the impulse approximation of the first-order optical potential. This is the principal difference between our result and the RIA as commonly used. The t matrix is to be obtained from a one particle on mass shell equation. Hence intermediate states with both nucleons in negative energy states cannot occur, except at the "end points," as illustrated in Fig. 13. This result is obtained from a careful analysis of meson exchange diagrams, and seems to be the most appropriate for the problem of elastic nucleon-nucleus scattering. Numerical tests support this approach. It has been found that the contributions from channels in which both nucleons are in negative energy states are negligible.[13] The amplitudes calculated from Eq. (3.16b) have been used in an analysis of p-^{40}Ca elastic scattering,[14,15] and excellent agreement with experimental data has been obtained. Differences between ours and that of Ljon and

Wallace[1] were visible, but not large.

Since our first-order impulse approximation optical potential is derived from a multiple scattering theory, it is possible to make systematic corrections to the first-order calculations. We first intend to calculate the four leg off-shell t matrix from the quadrature equation (3.16a) and then evaluate other corrections. For example the double scattering correction term can be calculated in a straightforward manner as in the NR theory. Calculation of two-particle correlation functions, in a relativistically consistent manner, will be an obstacle. In the first approximation, one could treat the excited state target as a nonrelativistic object and neglect the small contributions from the negative energy propagation. In this approximation the second order (double scattering terms) in the expansion of the optical potential can be calculated in a standard manner by employing the t matrix obtained from the spectator equation.

Finally we point out that we have not considered the problem of antisymmetry between the projectile and the target particles, nor the self-consistent treatment of the A-body target state. We have also ignored the complications due to spin. It is very likely that the projectile-target antisymmetry can be closely approximated by the Takeda-Watson[16] prescription used in NR calculations.

ACKNOWLEDGMENTS

It is a pleasure to acknowledge helpful conversations with S. J. Wallace, who first alerted us to the problems of dissolution singularities. We would also like to thank P. C. Tandy and W. Van Orden for discussions on the subject on various occasions. K.M.M. would like to acknowledge the kind hospitality of CEBAF. This work was supported in part by the Department of Energy, through CEBAF, and by NASA Grant No. NAG-1-477.

---

[1]J. R. Shepard, J. A. McNeil, and S. J. Wallace, Phys. Rev. Lett. 50, 1443 (1983); J. A. Tjon and S. J. Wallace, Phys. Rev. C 36, 1085 (1987).

[2]B. C. Clark, S. Hama, R. L. Mercer, L. Ray, and B. D. Serot, Phys. Rev. Lett. 50, 1644 (1983); B. C. Clark, S. Hama, R. L. Mercer, L. Ray, and G. W. Hoffmann, Phys. Rev. C 28, 1421 (1983); L. Ray and G. W. Hoffmann, *ibid.* 31, 538 (1985); M. V. Hynes, A. Picklesimer, P. C. Tandy, and R. M. Thaler, Phys. Rev. Lett. 52, 978 (1984); Phys. Rev. C 31, 1438 (1985).

[3]G. E. Brown and D. G. Ravenhall, Proc. R. Soc. London, Sect. A 208, 552 (1951); J. Sucher, Rep. Prog. Phys. 41, 1781 (1978); Phys. Rev. A 22, 348 (1980).

[4]K. M. Maung and F. Gross, Bull. Am. Phys. Soc. 32, 1029 (1987); F. Gross and K. M. Maung, Phys. Lett. B 229, 188 (1989).

[5]K. M. Watson, Phys. Rev. 89, 575 (1953).

[6]A. K. Kerman, H. McManus, and R. M. Thaler, Ann. Phys. (N.Y.) 8, 511 (1959).

[7]Good accounts on the NR multiple scattering theories can be found in J. M. Eisnberg and D. S. Kolton, *Theory of Meson Interactions with Nuclei* (Wiley Interscience, New York, 1980); P. C. Tandy, in *Relativistic Dynamics and Quark-Nuclear Physics*, edited by M. B. Johnson and A. Picklesimer (Wiley Interscience, New York, 1986).

[8]F. Gross, Phys. Rev. C 26, 2203 (1982).

[9]M. Levy and J. Sucher, Phys. Rev. 186, 1656 (1969); H. D. I. Abarbanel and C. Itzykson, Phys. Rev. Lett. 23, 53 (1969); S. J. Wallace and J. A. McNeil, Phys. Rev. D 16, 3565 (1977).

[10]S. J. Wallace (private communication).

[11]Note that the prescription that the $A-1$ cluster be on mass shell has been given by L. S. Celenza and C. M. Shakin, *Relativistic Nuclear Physics* (World Scientific, Singapore, 1986), p. 194.

[12]F. Gross, Phys. Rev. C 26, 2226 (1982).

[13]F. Gross, Phys. Rev. 186, 1448 (1969).

[14]F. Gross, K. M. Maung, T. Tjon, L. W. Townsend, and S. J. Wallace (unpublished).

[15]F. Gross, K. M. Maung, T. Tjon, L. W. Townsend, and S. J. Wallace, Phys. Rev. C 40, R10 (1989).

[16]G. Takeda and K. M. Watson, Phys. Rev. 97, 1336 (1955).

[17]L. S. Celenza, M. K. Liou, L. C. Liu, and C. M. Shakin, Phys. Rev. C 10, 398 (1974).

RAPID COMMUNICATIONS

PHYSICAL REVIEW C VOLUME 40, NUMBER 1 JULY 1989

Pseudoscalar πN coupling and relativistic proton-nucleus scattering

Franz Gross
Department of Physics, College of William and Mary, Williamsburg, Virginia 23185 and Continuous Electron Beam Accelerator Facility, Newport News, Virginia 23606

Khin Maung Maung
Department of Physics, Old Dominion University, Norfolk, Virginia 23508 and National Aeronautics and Space Administration Langley Research Center, Hampton, Virginia 23665

J. A. Tjon
Institute of Theoretical Physics, University of Utrecht, 3508 TA Utrecht, The Netherlands

L. W. Townsend
National Aeronautics and Space Administration Langley Research Center, Hampton, Virginia 23665

S. J. Wallace
Department of Physics and Astronomy, University of Maryland, College Park, Maryland 20742

(Received 5 August 1988)

Relativistic p-^{40}Ca elastic scattering observables are calculated using relativistic NN amplitudes obtained from the solution of a two-body relativistic equation. Results at 200 MeV are presented for three sets of NN amplitudes, two with pure pseudovector coupling for the pion and one with a 25% admixture of pseudoscalar coupling. Differences between the predictions of these three models provide a measure of the uncertainty in constructing Dirac optical potentials from NN amplitudes.

It is well known that the relativistic impulse approximation (RIA) gives a good description of medium energy p-nucleus scattering observables.[1] In this approach the scattering of the proton is described by a Dirac equation with an optical potential U of the form

$$U_{RIA}^{(\rho_1\rho_1')}(r) = \int d^3r' T^{(\rho_1\rho_2,\rho_1'\rho_2')}(r,r')\rho^{(\rho_2\rho_2')}(r') , \qquad (1)$$

where the ρ superscripts (known as ρ spin) are positive (negative) for nucleons in a positive (negative) energy state. This equation therefore expresses the optical potential as a folding of the NN T matrix describing scattering of two initial nucleons in ρ-spin states (ρ_1,ρ_2) to two final nucleons in ρ-spin states (ρ_1',ρ_2') by a nucleon density distribution ρ which depends on the ρ spin of the initial and the final bound nucleon.

Previous work[2] has clearly established that the success of the RIA depends strongly on the $U^{(+,-)}$ and $U^{(-,+)}$ amplitudes, which in turn depend on knowledge of T-matrix elements in which *at least one* particle in the initial or final state is in the negative energy state. (In this paper these amplitudes will be referred to collectively as "negative ρ-spin amplitudes.") Furthermore, the size of these negative ρ-spin amplitudes at low energy has been found to be very sensitive to the amount of γ^5 coupling used for the pion. It has come to be accepted that pure $\gamma^5\gamma^\mu$ coupling is required to give a satisfactory description of p-nucleus scattering at low energies. In this paper we report results which show that a surprisingly sizable admixture (25%) of γ^5 coupling will still give good agreement with p-^{40}Ca data at 200 MeV, provided the NN T matrix has been obtained from a relativistic meson exchange calculation which fits the observed NN data. This 25% admixture seems to us quite large; in the recent fit to the NN T matrix used in this paper and reported in Ref. 4, no larger value could be found, and Fleischer and Tjon[3] found some time ago that it was impossible to fit NN data with pure (100%) γ^5 coupling.

Before describing our calculation in detail, we briefly review previous work, focusing on results which depend on the form of the off-shell pion coupling. In the original calculations,[1] the values of the negative ρ-spin amplitudes were inferred by expanding T in terms of five Fermi covariants, and fitting these to the on-shell $T^{(++,++)}$ data.[5] It was found that this procedure is ambiguous and sensitive to the choice of the five covariants.[6] For example, using the covariant $\gamma_1^5\gamma_2^5$ [which corresponds to assuming the pion coupling is pseudoscalar (PS)] or $-(\gamma^5 q\cdot\gamma)_1\times(\gamma^5 q\cdot\gamma)_2/4m^2$ [corresponding to the assumption that the pion coupling is pseudovector (PV)] gives identical results in the (++,++) sector, but their extrapolations to the negative ρ-spin sectors are very different, resulting in generally poor fits at low energy (200 MeV) when the $\gamma_1^5\gamma_2^5$ covariant is used. One finds divergent energy dependence of scalar and vector potentials as energy decreases and consequently divergent virtual pair contributions to proton scattering when the $\gamma_1^5\gamma_2^5$ covariant is used. To overcome this problem Tjon and Wallace[7] adopted a meson exchange model of the NN interaction with pure PV coupling for the pion as a basis for predicting all

$T^{(s's,m's)}$ matrix elements in Eq. (1). Use of a dynamical model which describes the NN observables in a qualitative way over the 0–1000 MeV range was thought to be the best way to minimize the ambiguity in prediction of the optical potential. The optical potential based on a complete set of amplitudes (referred to as IA2) produces good agreement with experimental results over a wide range of projectile energies from 200 to 800 MeV.[8] The divergent behavior of the potentials at lower energies is absent in this case.

In this paper, we study the sensitivities of the p-nucleus scattering observables to realistic variations in the amount of γ^5 vs $\gamma^5\gamma^\mu$ coupling of the pion. We continue to demand that our NN T matrix be the solution of a relativistic equation with a meson exchange kernel which has been adjusted to give a quantitatively accurate fit to the NN data. Two new sets of relativistic NN amplitudes are obtained from the solution of the relativistic equation in which one particle is on shell.[9] To ensure that the resulting amplitudes satisfy the Pauli principle, the one-boson exchange (OBE) kernels used in this calculation were explicitly antisymmetrized.[4,10] Hence the four classes of amplitudes $T^{(+-,++)}$, $T^{(-+,++)}$, $T^{(++,+-)}$, and $T^{(++,--)}$ can all be obtained through antisymmetry, or time reversal invariance, from $T^{(+-,++)}$ which we will refer to simply as $T^{(-,+)}$, and the amplitudes $T^{(+-,+-)}$, $T^{(+-,-+)}$, $T^{(-+,+-)}$, and $T^{(-+,-+)}$ can similarly be obtained from $T^{(+-,+-)}$, referred to as $T^{(-,-)}$. The amplitudes $T^{(--,m's)}$ and $T^{(s'm',--)}$ are all taken to be zero. Finally, the πN coupling used in these new solutions is a mixed coupling of the form

$$\lambda\gamma^5+(1-\lambda)\frac{\gamma\cdot q\gamma^5}{2m}.$$

The parameter λ varies the mix of pseudoscalar and pseudovector coupling, and is defined so that the on-shell amplitude is independent of λ. When λ is unity the coupling is purely pseudoscalar and when it is zero the coupling becomes pure pseudovector.

Two OBE models have been found which fit the NN data equally well, but which have significantly different $T^{(+,-)}$ amplitudes.[4] In model 1, only the four mesons π, σ, ω, and ρ are used. This is the minimal number needed to represent the long-, medium-, and short-range nuclear forces, and a very good fit to the positive energy NN amplitudes is obtained when the parameter λ has the value 0.25, which is 25% pseudoscalar and 75% pseudovector (the fit tightly constraints the value of λ). In another OBE model, model 2, the πN coupling is constrained to be pure pseudovector ($\lambda=0$) consistent with pair suppression and chiral symmetry. In order to fit the NN data equally well, two extra mesons, δ and η, must be included. (The δ meson is needed to get the correct splitting between $^1S_0$ and $^3S_1$ central terms, which emerges automatically when $\lambda=0.25$.) These two models allow us to explore the sensitivity to the amount of pseudoscalar coupling one may use and still obtain a good fit to the NN observables. They both differ significantly from the model used by Tjon and Wallace.

The results for the polarized p-^{40}Ca elastic scattering at 200 MeV obtained from the two models are shown in Fig. 1. Calculations are based on the IA2 formalism of Ref. 8, and we used the relativistic ^{40}Ca densities supplied by Horowitz and Serot.[12] Surprisingly, both models give a reasonable description for the p-nucleus observables, and it can be seen that the mixed coupling model gives superior results over the pure pseudovector coupling case. However, since the integral in (1) has only been evaluated in the $t\rho$ approximation (in which the T matrix is evaluated on shell and factored out of the integral) and other effects such as Pauli blocking and vacuum polarization have not been included, it cannot be concluded that the mixed coupling case will continue to give the best results after these effects are taken into account.

We would like to emphasize that the relativistic NN amplitudes used were the results of dynamical calculations based on a relativistic equation, in which all parameters were fixed by the NN data. No further adjustments in any parameter were made in calculating the p-^{40}Ca observables. Calculations have also been performed at 300 and 500 MeV and the predictions agree with the data as well as for the case of 200 MeV.

In order to isolate other possible model dependence arising from negative-energy components of T, we compare models 1 and 2 above with a calculation of Tjon and Wallace[7] in Fig. 2. In this case we standardize the comparisons by replacing the $T^{(++,++)}$ amplitudes in each case by the on-shell amplitudes determined by Arndt *et al.*[13] First note that the two pseudovector models (model 2 and Tjon-Wallace) are in close agreement in spite of the

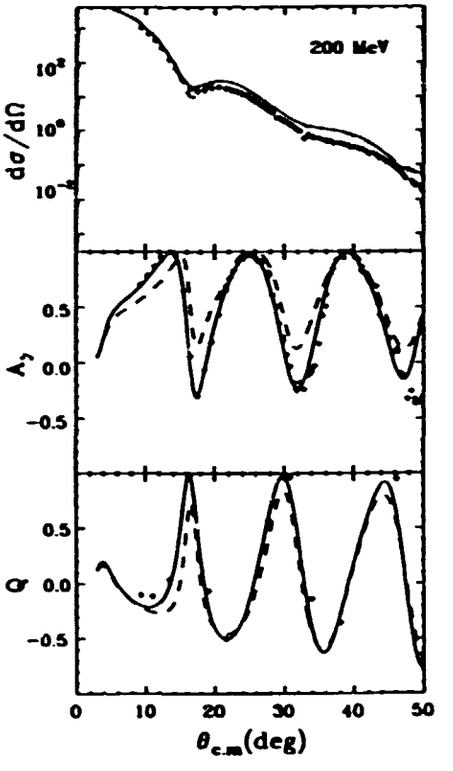

FIG. 1. Predictions for p-^{40}Ca observables for the $\lambda=0.25$ model 1 (solid line) and $\lambda=0$ model 2 (dashed line) described in the text. The stars are data from Ref. 11.

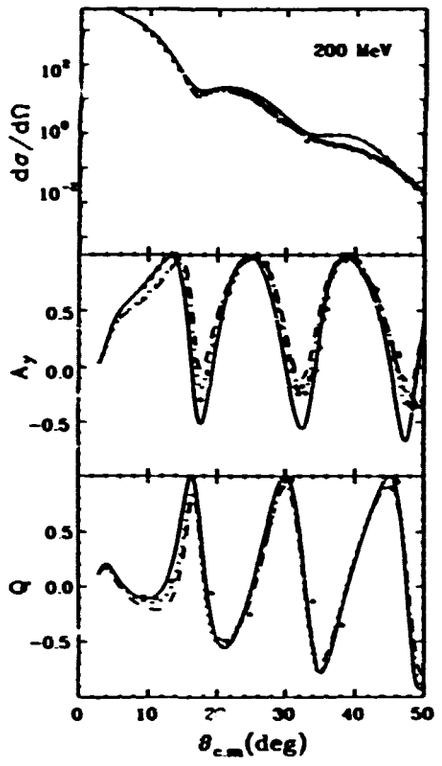

FIG. 2. Results for the p-^{40}Ca observables with theoretical $T^{(++,++)}$ amplitudes replaced by the Arndt amplitudes, and theoretical amplitudes in other ρ-spin sectors left unchanged. Model 1 (solid line), model 2 (dashed line), and the calculation by Tjon and Wallace (dotted line) are shown. The data are as in Fig. 1.

fact that the Tjon-Wallace model uses a Blankenbecler-Sugar reduction of the Bethe-Salpeter equation which includes $(--)$ channels (in which *both* of the initial or final particles have negative ρ spin) in the NN sector, and additional $N\Delta$ channels,[14] both of which were neglected in model 2. We have checked that the differences shown in Fig. 2 are *not* due to the additional $(--)$ channels. Thus the sensitivity of Dirac results to the heavy mesons and the presence or absence of $N\Delta$ and $\Delta\Delta$ channels or the $(--)$ states of the NN channel seems to be minimal. Next, note that the larger differences between models 1 and 2 attributable to the form of pion coupling are substantially unchanged, in this standardized comparison, even though the depth of the oscillation in A_y has increased somewhat for both models. This shows that the p nucleus results are sensitive to fine details in the $T^{(++,++)}$ amplitude, but that the differences between models 1 and 2 cannot be attributed to these sensitivities.

In summary, we have shown that the differences in the predictions of models 1 and 2, both of which fit the on-shell NN data very well, are due to the differences in their admixture of γ^5 coupling, which cannot be uniquely determined by the on-shell data. While this model dependence is significant it is surprisingly small considering the large admixture (25%) of γ^5 coupling required by model 1.

Finally, it is amusing that the simpler model 1, with the exchange of only four mesons and a 25% admixture of γ^5 coupling for the pion, fits the observables as well as it does. This result suggests either that some degree of pair nonsuppression on the Born level may be allowed, or that the σ counter terms required to control the γ^5 part of the pion coupling may already be included as part of the phenomenological σ exchange potential used in the NN models. In view of the success here, it may be worth examining the results of such mixed coupling models, both at lower energies where the sensitivity to πN coupling is larger, and in other reactions, such as electromagnetic processes or processes involving pion production or absorption.

Two of us (F.G. and S.J.W.) gratefully acknowledge the support of the U.S. Department of Energy. One of us (K.M.M.) gratefully acknowledges the support of NASA, Grant No. NCCI-42. K.M.M. and J.A.T. would like to acknowledge the hospitality of the Continuous Electron Beam Accelerator Facility, where this work was discussed and carried out.

[1]J. R. Shepard, J. A. McNeil, and S. J. Wallace, Phys. Rev. Lett. 50, 1443 (1983); B. C. Clark, S. Hama, R. L. Mercer, L. Ray, and B. D. Serot, *ibid.* 50, 1644 (1983); B. C. Clark, S. Hama, R. L. Mercer, L. Ray, and G. W. Hoffmann, Phys. Rev. C 28, 1421 (1983); L. Ray and G. W. Hoffmann, *ibid.* 31, 538 (1985).

[2]M. V. Hynes, A. Picklesimer, P. C. Tandy, and R. M. Thaler, Phys. Rev. Lett. 52, 978 (1984); Phys. Rev. C 31, 1438 (1985).

[3]J. Fleischer and J. A. Tjon, Nucl. Phys. B84, 375 (1975); Phys. Rev. D 15, 2537 (1977).

[4]F. Gross, K. Holinde, and J. W. Van Orden (unpublished).

[5]J. A. McNeil, L. Ray, and S. J. Wallace, Phys. Rev. C 27, 2123 (1983).

[6]D. Adams and M. Bleszynski, Phys. Lett. 136B, 10 (1984); C. Horowitz, Phys. Rev. C 31, 1340 (1985); J. A. Tjon and S. J. Wallace, *ibid.* 32, 267 (1985); Phys. Rev. Lett. 54, 1357 (1985).

[7]J. A. Tjon and S. J. Wallace, Phys. Rev. C 35, 280 (1987).

[8]J. A. Tjon and S. J. Wallace, Phys. Rev. C 36, 1085 (1987); N. Ottenstein, J. A. Tjon, and S. J. Wallace, *ibid.* 38, 2272 (1988); 38, 2289 (1988).

[9]F. Gross, Phys. Rev. 186, 1448 (1969); Phys. Rev. D 10, 223 (1974).

[10]F. Gross, Phys. Rev. C 26, 2226 (1982).

[11]E. J. Stephenson, J. Phys. Soc. Jpn. (Suppl.) 55, 316 (1985); P. Schwandt (private communication).

[12]The relativistic ^{40}Ca wave functions used in this calculation were obtained from C. Horowitz and B. Serot, Nucl. Phys. A368, 503 (1981).

[13]R. A. Arndt, L. D. Roper, R. A. Bryan, R. B. Clark, B. J. VerWest, and P. Signell, Phys. Rev. D 28, 97 (1983).

[14]E. E. van Faassen and J. A. Tjon, Phys. Rev. C 28, 2354 (1983).

PHYSICAL REVIEW C VOLUME 41, NUMBER 2 FEBRUARY 1990

Theoretical angular distributions from coherent subthreshold pion production

P. A. Deutchman*
Physics Department, University of Idaho, Moscow, Idaho 83843

Khin Maung Maung
Physics Department, Hampton University, Hampton, Virginia 23668

(Received 5 June 1989)

For the first time, we have calculated theoretical angular distributions for exclusive π^0 production in C+C collisions at 84 MeV/nucleon using a quantum-coherent, microscopic, many-body formalism. We use a model spin, transition-spin, Δ-isobar-formation interaction that is expanded in angular momentum multipoles and we now have the results from a complete code that includes these multipoles to all orders which couple to shell-model information. Also the first time, we calculate pion contributions coming from both the target and projectile and find that these contributions are important in determining the shape of the theoretical angular distributions. We compare the theoretical calculations to π^0 data and find that our results are similar to the shape of the data at higher pion energies and bear some similarity in trend to the pion bremsstrahlung model. We also find that the shape of the theoretical angular distribution is sensitive to shell-model information.

There continues to be interest in finding a sensitivity to collective or coherent mechanisms in subthreshold heavy-ion pion production.[1,2] This interest is enhanced by the experimental ability to measure neutral pions[3-5] which leads to data that are not complicated by final-state Coulomb effects on the outgoing pions. The present model interaction has been described briefly in previous works[6,7] where pion spectra were calculated over a range of incident energies from subthreshold to relativistic values for ^{16}O on ^{12}C; however, those calculations used only the lowest-order ($k=0$) angular momentum multipole. We have now included all orders and discovered that the multipole expansion is highly convergent in the subthreshold region. For the first time with this model we calculate the angular distributions for coherent π^0 production in C+C collisions at 85 MeV/nucleon at three different energy cuts.

The Lorentz-invariant differential cross section calculated in the *projectile* rest frame for a given target isospin $M(T)$ is given by

$$\frac{d^3\sigma}{d^3p_\pi/E_\pi}=\frac{2\pi}{\hbar v}\frac{E_\pi V^3}{(2\pi\hbar)^6}\frac{d}{dE_F}\int d^3p_{T^*}|C_{FI}|^2, \quad (1)$$

where v is the incident speed of the target as seen in the projectile rest frame, E_π is the total pion energy, and V is the quantization volume which cancels an identical term coming from the second-order amplitude C_{FI}. The total energy of the final state E_F is the sum of energies from the pion, recoil projectile, and excited target of momentum p_{T^*}. Making the high momentum, forward scattering approximation that $p_{T^*}\gg P_{\pi R}$ where $p_{\pi R}$ is the momentum of the recoil projectile plus pion as seen from the projectile rest frame, then $d/dE_F\simeq(E_F/p_{T^*}c^2)d/dp_{T^*}$. Furthermore, the scattering amplitude is assumed to be approximately independent of the target solid angle. These assumptions are consistent with peripheral collisions of low recoil and simplify the integrations over the target momentum p_{T^*}. The sums over all target isospins $M(T)$ of the differential cross section are then taken. The second-order amplitude

$$C_{FI}=\frac{\sum_N\langle F|V_2|N\rangle\langle N|V_1|I\rangle}{E_\pi+M_Nc^2-M_\Delta c^2+i\Gamma_\Delta/2}, \quad (2)$$

where $|I\rangle$ refers to the initial state of target, projectile, and the kinetic energy of the target, $|N\rangle$ is the intermediate state where the target is excited to a $J^\pi=1^+$, $T=1$ spin-, isospin-coherent, isobar-analog, nuclear state, and the projectile is excited to a similar state except that a nucleon has been excited to a $\Delta(3,3)$ isobar of mass $M_\Delta c^2=1232$ MeV and width $\Gamma_\Delta=115$ MeV. The final state $|F\rangle$ contains the pion that decays from the Δ and it is assumed that the projectile returns to its ground state. Also, it is assumed that the decay of the Δ from the projectile does not influence the target after the Δ is created so that the center-of-mass plane waves and the internal target wave functions between the intermediate and final states are orthogonal. A nonrelativistic Breit-Wigner propagator for the Δ resonance is used where the energy dependence of the width[8] has been neglected since we are concerned here mainly with angular distributions.

The matrix elements for Δ formation and decay in Eq. (2) are evaluated using the techniques of second quantization and involves a great deal of Racah algebra. The formation matrix $\langle N|V_1|I\rangle$ which excites a particle-hole state in the target and creates a Δ-hole state in the projectile is reduced by Wick's theorem to matrix elements of an interaction between particle hole and scattering states. In order to do an estimate calculation, a separable model Δ-formation interaction was chosen to be

$$v_1=2v_0g(r)g(\xi_p)g(\xi_t)(S_p\cdot\sigma_t)(T_p\cdot\tau_t)\times\sum_\lambda C_\lambda(\Omega_t)\cdot C_\lambda(\Omega_p), \quad (3)$$

where $g(r)$, $g(\xi_p)$, and $g(\xi_t)$ are Gaussian shapes which are functions of the coordinate magnitudes of the nucleus-nucleus center of mass, projectile nucleon, and target nucleon, respectively. This form was motivated by the work of Gaarde, Kammuri, and Osterfeld,[9] but simplified to take into account target Lorentz contraction. The main features of this model interaction are the spin and isospin flip where the target is excited to a giant resonance as well as the projectile with the added feature that a Δ is created in the projectile through the transition spin and isospin. The scalar product of spherical tensors of rank k allows for an exchange of orbital angular momentum $\hbar k$ between the projectile nucleon and target center of mass. The target nucleons, although spin flipped, are left in their spatial ground state so that the matrix element in the target can be approximated by a Lorentz-contracted form factor. This model represents a compromise where orbital angular momentum changes are neglected in the target single-particle states, but allows for a simple handling of the target Lorentz contraction as described previously.[6] The strength of the interaction is given by v_0 which is initially determined from two-body scattering and the factor 2 has been included since the strength of the $\Delta N\pi$ vertex is approximately twice as large as the $NN\pi$ vertex where quark theory gives $g_{\Delta N\pi}=(6\sqrt{2}/5)g_{NN\pi}$.[10] This model represents a step forward compared to our previous model.[11] The calculation of the Δ-decay matrix element $\langle F|V_2|N\rangle$ has also been described previously.[11]

The nuclear, particle-hole states are spin-orbit coupled to produce the j values of the particle and hole and then coupled to produce the total angular momentum of the nucleus. The isospins of the particle-hole state are also coupled to produce the total isospin of the nucleus. Then, linear combinations of these states with particle-hole coefficients X_{ph} are taken to produce the total nuclear state and each matrix element contains $9j$ symbols after lengthy calculations in angular coupling are done. The particle and hole states are generated from the three-dimensional harmonic oscillator and are described in Ref. 6 except that we now apply the model to ^{12}C on ^{12}C. The sum over intermediate states $|N\rangle$ in Eq. (2) contains sums over particle-hole states for both nuclei as well as a sum over angular momentum multipoles k as given by Eq. (1) in Ref. 6 and described therein. This sum contains a product of terms which is given by

$$\sum_k \int_0^\infty j_k(Kr)g(r)r^2dr \int_0^\infty R^{l_\Delta}_{n_\Delta}(\xi)j_k(k_\pi\xi)R^{l_h}_{n_h}(\xi)\xi^2d\xi \begin{pmatrix} l_\Delta & k & l_h \\ 0 & 0 & 0 \end{pmatrix}^2 P_k(\cos\Theta_{\pi K}), \tag{4}$$

where the first integral is in the Born approximation with respect to the target momentum transfer $\hbar K$, and the second integral comes from the projectile Δ-hole decay matrix element with respect to the outgoing pion momentum $\hbar k_\pi$. The properties of the $3j$ symbol

$$\begin{pmatrix} l_\Delta & k & l_h \\ 0 & 0 & 0 \end{pmatrix}$$

restricts k to even/odd values if $l_\Delta+l_h=$even/odd values and severely truncates the k sum through the triangular condition $|l_\Delta-l_h|\le k\le l_\Delta+l_h$. The pion angular distribution is contained in the Legendre polynomial of order k with respect to the correlation angle $\Theta_{\pi K}$ which is the angle between the pion and target momentum transfer. In previous work,[6] we only hand calculated the differential cross section for the $k=0$ term and only calculated the square of Eq. (4) for $k=0$ plus $k=2$ to determine the relative effect of the higher-order multipole. Presently, we have a complete code which includes all k multipoles and have calculated the differential cross section as a function of the correlation angle. After including higher Δ-hole states, we discovered that the main contributions to the cross section come from the $1p_{1/2,3/2,5/2}$-Δ states and the $1p_{3/2}$-hole state in ^{12}C (Δ) for the $k=0$ and 2 multipole values. For example, when we included the Δ states for the $1d$-$2s$ shell which corresponds to $k=1,3$ and $k=1$, respectively with the $1p_{3/2}$-hole state, we found these contributions to be negligible. This occurs because the overlap between the functions in the first and second integral in Eq. (4) diminishes considerably and the value of the $3j$ symbol

$$\begin{pmatrix} l_\Delta & k & l_h \\ 0 & 0 & 0 \end{pmatrix}$$

drops. It appears that the k sum in Eq. (4) is highly convergent. Also, since we assumed equal weight particle-hole coefficients $X_{ph}(P)$, they become smaller when more shell-model states are included. If these coefficients were calculated in the schematic model,[12] we would find that they are inversely proportional to the particle-hole energy difference which cuts down the contributions from higher shell-model states and justifies our truncation to lowest states. We also included the $1f$ shell and found that these results were also negligible. Therefore, the main contributor to the nonisotropic shape of the differential cross sections comes from P_2 although the actual shape is determined by the relative weighting between P_0 and P_2 in the multipole sum.

For the first time, we compared the results of this model to π^0 angular distributions in ^{12}C+^{12}C collisions at 84 MeV/nucleon transformed to the nucleon-nucleon, center-of-mass system.[13] Since we are considering small momentum transfers in the forward direction, we assume that the correlation angle $\Theta_{\pi K}$ is approximately the pion angle measured from the forward direction Θ_π. For fixed values of the pion kinetic energy and angle $(T_\pi^{\text{c.m.}},\Theta_\pi^{\text{c.m.}})$ in the nucleon-nucleon center of mass, we calculate the relativistically transformed set $(T_\pi^{\text{lf}},\Theta_\pi^{\text{lf}})$ for pions produced by the projectile in its own frame to obtain the Lorentz-invariant differential cross section which is further

transformed to the noninvariant cross section in the center-of-mass system. A similar procedure is applied to contribution coming from the target. These two cross sections are then added so that our results contain the incoherent addition of pions coming from projectile and target; however, the Δ's are produced coherently in each nucleus. The results are shown in Figs. 1–3 for three different energy cuts. Since we are concerned primarily with shape fits, the calculations have been normalized to the data at $\cos\theta_\pi = 0.025$ since that data point has an error bar shown in Fig. 3. We do not expect to fit the data in absolute value since the calculation is exclusive whereas the data is inclusive. It is interesting to note that the theoretical shape improves at the highest-energy bin from 100–150 MeV where the peak-to-valley ratio moves towards the data. This trend is compatible with the conclusions of Braun-Munzinger and Stachel[1] where they point out that the low-energy pions are probably emitted from a local hot spot, whereas the pions produced approximately above 100 MeV cannot be fully understood by thermal models alone and may suggest the presence of a coherent mechanism in the production process. It is also interesting that our normalization factor drops by a factor of 10 from the lowest-energy cut to the highest perhaps indicating a convergence at the higher pion energies. It is also intriguing that for the lowest-energy cut, the results from the bremsstrahlung model compared to similar data[14] shows a convex trend as do our results under the condition of incoherent addition of projectile and target pions, whereas the bremsstrahlung calculations and our results improve at the higher-energy cuts.

In conclusion, for the first time, we include pion contributions coming from the target and projectile and find that these contributions are important in determining the theoretical shape of the π^0 angular distributions. We compare the present model with experimental π^0 angular distributions but do not expect to obtain absolute-value fits to the data because our calculation is exclusive whereas the data to which we compare are inclusive; however, we wanted to find out if the qualitative shape and energy trend of the theory bears some resemblance to existing experimental angular distributions before embarking on the more complicated phase of this calculation which is to include the tensor term. We find that the theoretical shape displays a forward-backward peaking similar to the shape of the data at the higher pion energies. The forward peaking in our model is due to pions coming predominantly from the projectile whereas the target predominantly contributes to the backward peaking as seen in the nucleon-nucleon center-of-mass system. We expect this qualitative result would also obtain when the tensor interaction is included. The calculations is also very sensitive to the shell-model information since the multipole sum is very convergent and not much of a washing out of the shell-model signature occurs. This was not obvious from previous work[6,7] where hard calculations were done and it was not known if a washout of the angular distribution would occur with the inclusion of higher-order multipole values. We again expect a similar result with inclusion of the tensor term and now have a tentative explanation for the forward-backward peaking seen in the data.

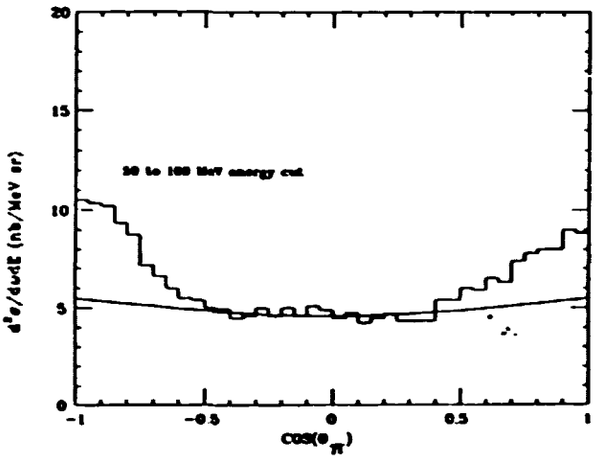

FIG. 2. Same as Fig. 1 except for the 50 to 100 MeV cut.

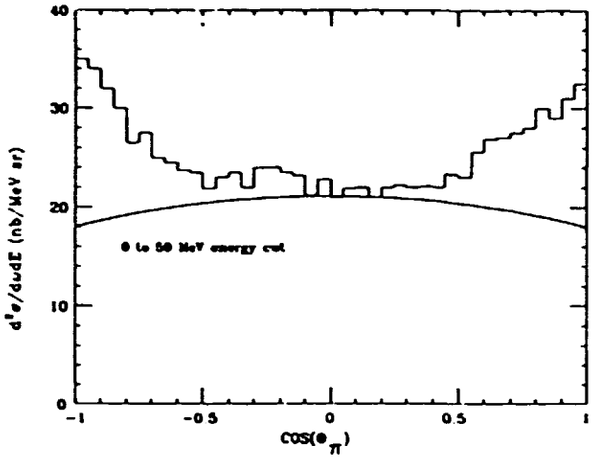

FIG. 1. Theoretical π^0 production compared to the data (Ref. 12) of C+C collisions at 84 MeV/nucleon for the 0 to 50 MeV cut.

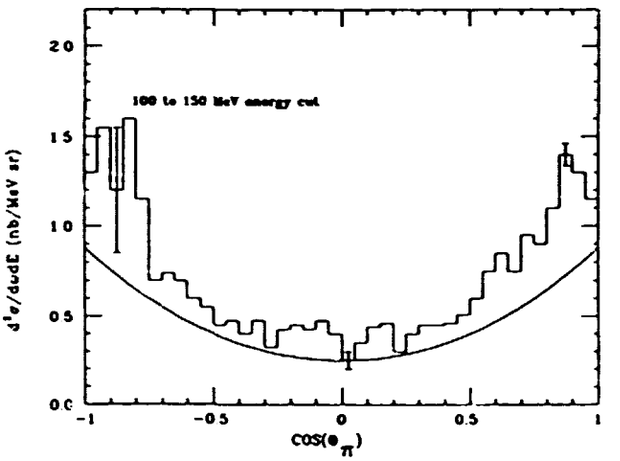

FIG. 3. Same as Fig. 1 except for the 100 to 150 MeV cut.

The model isobar-formation interaction, even though incomplete, leads to a complicated, microscopic, quantum-mechanical, many-body, angular momentum formalism. Our approach was to start with the simpler spin-spin term but include orbital-angular momentum exchanges between projectile and target nucleons as well as the scattering of the relative nucleus-nucleus system and calculate angular distributions to discover the nature of the signature for coherent production. From Ref. 8, in an examination of the momentum transfer dependence q of the central and tensor interactions, it is seen that for low momentum transfers of $q \leq 0.5$ fm^{-1}, the central term dominates over the tensor term. In fact, at $q=0$, the tensor term is zero. At increasing values of q, the central term drops and the tensor term rises until at the critical value of $q \approx 3$ fm^{-1}, the tensor term dominates the cross section because the central term goes to zero. However, for peripheral collisions at subthreshold energies, it is likely that the lowest values of momentum transfer will be favored and that the central term might dominate these reactions. With this work, we are encouraged to include the more complicated tensor interaction and compare the roles of the central to the tensor term. In Ref. 2, where the tensor term was included, only total cross sections have been calculated for the subthreshold process using the impulse Feshbach-Zabek[15] approach. In our work, we are attempting a more fundamental, microscopic, quantum-mechanical approach. We are presently developing a heavy-ion calculation with a more realistic interaction model that includes the tensor term.

The first author (P.A.D.) acknowledges the support of National Science Foundation Grant No. PHY-89-11040.

---

*Present address: School of Physical Sciences, The Flinders University of South Australia, G.P.O. Box 2100, Adelaide, South Australia, Australia 5001.

[1]P. Braun-Munzinger and J. Stachel, Annu. Rev. Nucl. Part. Sci. 37, 97 (1987), and references therein.

[2]C. Guet, M. Soyer, J. Bowlin, and G. E. Brown, Nucl. Phys. A494, 558 (1989).

[3]P. Braun-Munzinger, P. Paul, L. Ricken, J. Stachel, P. H. Zhang, G. R. Young, F. E. Obenshain, and E. Grosse, Phys. Rev. Lett. 52, 255 (1984).

[4]J. Stachel *et al.*, Phys. Rev. C 33, 1420 (1986).

[5]C. Michel, E. Grosse, H. Noll, H. Dabrowski, H. Heckwolf, O. Klepper, W. F. J. Muller, H. Stelzer, C. Brendel, and W. Rosch, Nucl. Instrum. Methods Phys. Res. Sect. A 243, 395 (1986).

[6]P. A. Deutchman, R. L. Buvel, Khin Maung Maung, J. W. Norbury, and L. W. Townsend, Phys. Rev. C 33, 396 (1986).

[7]P. A. Deutchman, Khin Maung Maung, J. W. Norbury, J. O. Rasmussen, and L. W. Townsend, Phys. Rev. C 34, 2377 (1986).

[8]M. Prakash, C. Guet, and G. E. Brown, Nucl. Phys. A 447, 625c (1985).

[9]C. Gaarde, T. Kammuri, and F. Osterfeld, Nucl. Phys. A222, 579 (1974).

[10]G. E. Brown and W. Weise, Phys. Rep. 22, 279 (1975).

[11]J. W. Norbury, P. A. Deutchman, and L. W. Townsend, Nucl. Phys. A433, 691 (1985); P. A. Deutchman, J. W. Norbury, and L. W. Townsend, Nucl. Phys. A454, 733 (1986).

[12]D. J. Rowe, *Nuclear Collective Motion* (Methuen and Co. Ltd., London, 1970), p. 218.

[13]H. Noll *et al.*, Phys. Rev. Lett. 52, 1284 (1984); E. Grosse, Nucl. Phys. A447, 611c (1985).

[14]D. Vasak, W. Greiner, B. Müller, T. Stahl, and M. Uhlig, Nucl. Phys. A428, 291c (1984).

[15]H. Feshbach and M. Zabek, Ann. Phys. (N.Y.) 107, 110 (1977).

PHYSICAL REVIEW C VOLUME 43, NUMBER 3 MARCH 1991

Relativistic proton-nucleus scattering and one-boson-exchange models

Khin Maung Maung
Department of Physics, Hampton University, Hampton, Virginia 23668
and NASA Langley Research Center, Hampton, Virginia 23665

Franz Gross
Department of Physics, College of William and Mary, Williamsburg, Virginia 23185
and Continuous Electron Beam Accelerator Facility, Newport News, Virginia 23606

J. A. Tjon
Institute of Theoretical Physics, University of Utrecht, 3508 TA Utrecht, The Netherlands

L. W. Townsend
NASA Langley Research Center, Hampton, Virginia 23665

S. J. Wallace
Department of Physics and Astronomy, University of Maryland, College Park, Maryland 20742

(Received 15 June 1990)

Relativistic p-^{40}Ca elastic scattering observables are calculated using four sets of relativistic NN amplitudes obtained from different one-boson-exchange (OBE) models. The first two sets are based upon a relativistic equation in which one particle is on mass shell and the other two sets are obtained from a quasipotential reduction of the Bethe-Salpeter equation. Results at 200, 300, and 500 MeV are presented for these amplitudes. Differences between the predictions of these models provide a study of the uncertainty in constructing Dirac optical potentials from OBE-based NN amplitudes.

I. INTRODUCTION

In this work relativistic p-nucleus calculations based on four different sets of NN amplitudes obtained from relativistic meson-exchange models are presented. The comparison of the results based upon these different relativistic NN amplitudes is motivated by the fact that the main ingredient in the success of the Dirac approach to p-nucleus scattering is the virtual $N\bar{N}$ effects[1] which are implicit in the solution of the Dirac equation. For the positive energy component of the wave function we can write

$$(E - E_p - U^{++} - U_{\rm pair})\psi^{++} = 0 ,$$

where

$$U_{\rm pair} = U^{+-}(E + E_p - U^{--})^{-1}U^{-+} .$$

To a good approximation U^{++} is the nonrelativistic potential and it is essentially determined by the NN on-shell data and the density profile of the target nucleus. When one uses meson-exchange models to calculate the relativistic NN amplitudes the pure positive energy amplitudes are fitted to the on-shell data and the amplitudes which belong to the pure relativistic sectors are then determined dynamically. In principle all meson-exchange model calculations should provide the same positive energy amplitudes (since they are fitted to the on-shell data) but the amplitudes in the other sectors would be different depending on the dynamical model used. Therefore the ambiguity in the Dirac optical potential lies in the $U_{\rm pair}$ term, which is determined by amplitudes other than the on-shell one. Since different dynamical models will give different amplitudes, except in the pure positive energy sector, it is important to study these differences and possible effects on the p-nucleus scattering observables which may arise because of these differences.

In previous work,[2] preliminary analyses of relativistic p-^{40}Ca elastic scattering at 200 MeV, using relativistic nucleon-nucleon (NN) amplitudes obtained from the solutions of two-body relativistic equations, were reported. In the present work the calculational methods are described and an extensive array of results for 200, 300, and 500 MeV protons incident upon a ^{40}Ca target are presented. Calculations are preformed with two sets of NN amplitudes obtained from a relativistic wave equation in which one particle is on positive energy mass shell[3] and also with third and fourth sets of NN amplitudes based upon a quasipotential method[4,5] for solving the Bethe-Salpeter equation. The use of the relativistic NN amplitudes obtained from a one particle on-mass shell equation is motivated by a recently formulated covariant multiple scattering theory.[6] In this formalism the authors argued that the NN amplitudes associated with the relativistic impulse approximation optical potential should be the one obtained from a one particle on-mass shell equation.

The outline of the paper is as follows. In Sec. II we present an overview of the optical potential methods used

to compute the elastic scattering observables. A brief discussion of the Tjon and Wallace method[7] for obtaining the invariant NN amplitudes is also included for completeness and further discussions. In Sec. III the meson-exchange models used are described together with the associated relativistic equations and the one-boson-exchange (OBE) parameters are tabulated. In Sec. IV results for elastic scattering observables are presented for all four sets of NN amplitudes. To test these results for possible model dependencies arising from the differing negative energy components of the t matrix, the on-shell amplitudes are replaced by the ones determined by Arndt *et al.*[8] and the resultant scattering observables computed and discussed. Finally, Sec. V summarizes our major results and conclusions.

II. THE DIRAC OPTICAL POTENTIAL

It is well known that the relativistic impulse approximation (RIA) is a useful method for predicting intermediate energy p-nucleus scattering observables.[9] In this approach one begins with the fixed energy Dirac equation

$$[\gamma\cdot p - m - \hat{U}(r)]\psi(r)=0 , \tag{1}$$

where the energy E is $E=(\mathbf{p}^2+m^2)^{1/2}$, p is the on-shell momentum, $\gamma\cdot p=\gamma_\mu p^\mu$, $p^\mu=(E,\mathbf{p})$, and the repeated indices are summed over. The optical potential $\hat{U}$, obtained from the RIA, is written in momentum space as[10]

$$\hat{U}(\mathbf{p}',\mathbf{p})=-\tfrac{1}{4}\mathrm{Tr}_2 \times\left[\int d\mathbf{k}\,\hat{M}(p,k-\tfrac{1}{2}q\to p',k+\tfrac{1}{2}q)\hat{\rho}(\mathbf{k},\mathbf{q})\right] , \tag{2}$$

where $\hat{M}$ is the Feynman NN amplitude and $\hat{\rho}$ is the relativistic nuclear density matrix for the target. In Eq. (2) particle 2 is the target nucleon and the trace is taken over its Dirac indices. Using the factorization approximation Eq. (2) yields

$$\hat{U}(\mathbf{p}',\mathbf{p})=-\tfrac{1}{4}\mathrm{Tr}_2[\hat{M}(p,-\tfrac{1}{2}q\to p',\tfrac{1}{2}q)\hat{\rho}(\mathbf{q})] . \tag{3}$$

Therefore to construct $\hat{U}$ we require $\hat{M}$ and $\hat{\rho}$. For this work involving ^{40}Ca target, the relativistic densities of Horowitz and Serot[11] are used for $\hat{\rho}$. The remaining problem is then to specify $\hat{M}$.

It is customary to separate the full NN amplitudes into a sum of 16 terms each representing a particular ρ-spin sector. They are labeled by indices $(\rho_1'\rho_2'\rho_1\rho_2)$ where each ρ is either $+$ or $-$, and primed (unprimed) quantities denote final (initial) nucleon states. Tjon and Wallace have determined $\hat{M}$ for all 16 ρ-spin sectors by solving the Bethe-Salpeter equation using a quasipotential method[4,5] with pure pseudovector coupling for the pion. In that particular formalism, the invariant NN amplitude is expanded as

$$\hat{F}=-\frac{\hat{M}}{\kappa}=\sum_{\rho_1'\rho_2'\rho_1\rho_2}\Lambda_1^{\rho_1'}\Lambda_2^{\rho_2'}F^{\rho_1'\rho_2'\rho_1\rho_2}\Lambda_1^{\rho_1}\Lambda_2^{\rho_2} , \tag{4}$$

where each ρ is summed over $+$ and $-$, and κ is a kinematic factor [see Eq. (2.10) of Ref. 8]. In Eq. (4) the $F^{\rho_1'\rho_2'\rho_1\rho_2}$ are amplitudes restricted to act only within one ρ-spin sector (hence there are 16 different sets of them) and the Λ's are covariant projection operators given by

$$\Lambda^\rho(\mathbf{p})=\frac{\rho(E_p-\gamma\cdot\mathbf{p})+m}{2m} , \tag{5}$$

where ρ is $+$ or $-$. Details for determining the various ρ-spin sector amplitudes $F^{\rho_1'\rho_2'\rho_1\rho_2}$ are found in Refs. 7 and 10. This complete calculational program is referred to as the IA2 formalism.[10,12]

III. RELATIVISTIC MESON-EXCHANGE MODELS

In this section we briefly describe the relativistic meson-exchange models used in this work. In operator form the relativistic two-body equation can generically be written as

$$M=V+VGM , \tag{6}$$

where M is the invariant amplitude for the two nucleons scattering process, V is the interaction determined by the OBE model, and G is the relativistic two-body propagator. M satisfies the Pauli principle provided that V is suitably antisymmetrized.

The first two OBE model amplitudes[13] used in this work are calculated from a one particle on-mass shell equation and in this case the propagator G in Eq. (6) is the propagator with one particle on the mass shell. Figure 1 depicts Eq. (6) for this case diagrammatically. The open boxes represent the combined OBE terms, properly antisymmetrized, for the mesons used. The horizontal lines represent the nucleons and a cross on a nucleon line indicates that it is on the positive energy mass shell. Explicit antisymmetrization of the OBE kernel insures that the M matrix is correctly antisymmetrized under particle interchange. The first OBE model uses four mesons (π, σ, ρ, and ω). This is the minimal number needed to represent the long, medium, and short range nuclear forces. The πN coupling used is a mixed coupling of the form

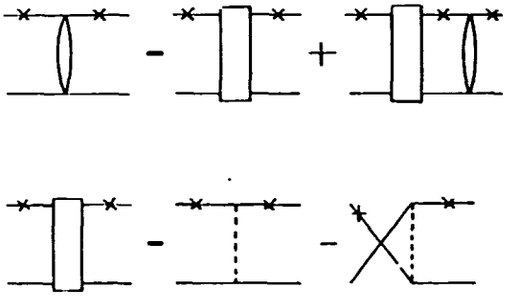

FIG. 1. Diagrammatical representation of one particle on-mass-shell equation. A cross on a nucleon line indicates that the particle is on the positive energy mass shell. Open boxes stand for the antisymmetrized kernel, and vertical dashed lines stand for combined π, σ, ρ, and ω exchange for model 1 and π, σ, ρ, ω, η, and σ_1 exchange for model 2.

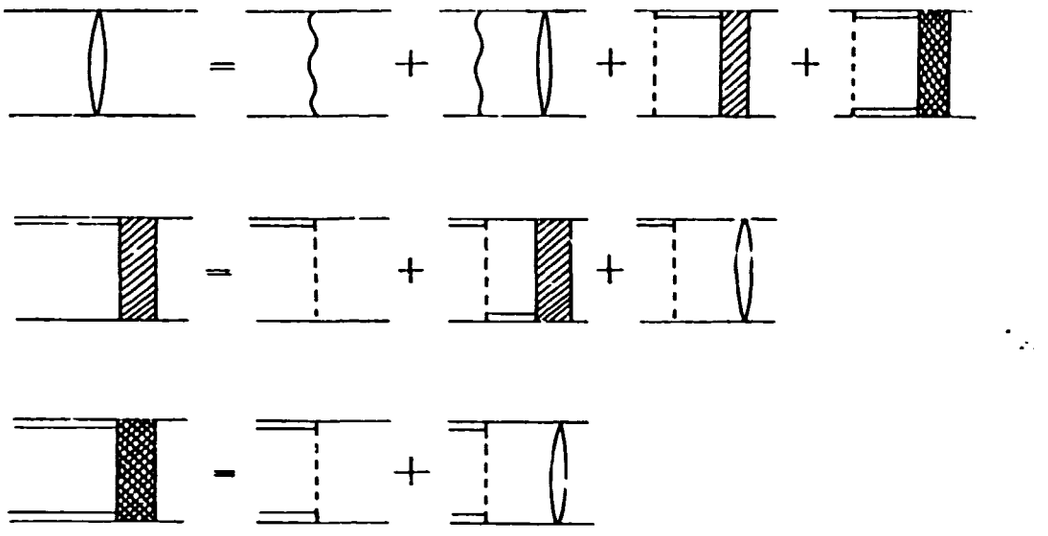

FIG. 2. Diagrammatical representation of Bethe-Salpeter equation for coupled channel $NN+N\Delta+\Delta\Delta$ scattering. The Δ states are indicated by double horizontal lines. The dashed line indicates $\pi+\rho$ exchange; the wiggly line stands for combined π, η, ϵ, δ, ρ, and ω exchange. The single NN channel case can be obtained by leaving out the diagrams with Δ lines.

$$\lambda\gamma^5+(1-\lambda)\frac{\gamma\cdot q\gamma^5}{2m},$$

where the parameter λ varies the mix of the pseudoscalar and pseudovector coupling, and is defined so that the on-shell amplitude is independent of λ. When λ is unity the coupling is purely pseudoscalar and when it is zero the coupling becomes pure pseudovector. Use of this coupling permits us to study the sensitivities of the scattering observables to relative variations in the amount of γ^5 vs $\gamma^5\gamma^\mu$ coupling of the pion. The best value of the mixing parameter λ to fit the data was found to be 0.22 which corresponds to a 22% γ^5 coupling admixture.

In the second model, the πN coupling is constrained to be pure pseudovector ($\lambda=0$) consistent with pair suppression and chiral symmetry. In order to fit the NN data equally well with this constraint, two additional mesons η and σ_1 were added. The σ_1 meson, a phenomenological spin zero isospin 1 meson, is needed to obtain the correct splitting between the $^1S_0$ and $^3S_1$ central potentials when $\lambda=0$. Note that neither of these OBE models contain $N\Delta$ or $\Delta\Delta$ channels but both models are able to fit the NN phase shifts very well up to 300 MeV.

Since in these models (1 and 2) we require that one particle is on the positive energy mass shell ρ-spin amplitudes labeled by $(--,\rho_1\rho_2)$ and $(\rho_1'\rho_2',--)$ are zero by

TABLE I. Meson masses (MeV), cutoff masses (MeV), and coupling constants for OBE models 1 and 2.

	Model 1	Model 2
π $g_\pi^2/4\pi$	13.544 03	13.357 57
m_π	138.0	138.0
λ_π	0.225 57	0.0
σ $g_\sigma^2/4\pi$	5.513 22	5.047 20
m_σ	516.0	514.0
ρ $g_\rho^2/4\pi$	0.382 91	0.586 86
κ_ρ	7.525 25	6.149 20
λ_ρ	1.0	0.752 18
m_ρ	760.0	760.0
ω $g_\omega^2/4\pi$	9.851 06	9.830 54
κ_ω	0.142 59	0.150 50
m_ω	782.8	782.8
σ_1 $g_{\sigma_1}^2/4\pi$		0.325 93
m_{σ_1}		573.0
η $g_\eta^2/4\pi$		6.407 98
m_η		548.8
Λ_N	1610.0	1685.0
Λ_{meson}	2135.0	1830.0

TABLE II. Meson masses (MeV), cutoff masses (MeV), and coupling constants for OBE models 3 and 4.

	Model 3	Model 4
π $g_\pi^2/4\pi$	14.2	14.2
m_π	138.7	138.7
δ $g_\delta^2/4\pi$	0.33	0.33
m_δ	960.0	960.0
η $g_\eta^2/4\pi$	3.09	3.09
m_η	548.0	548.0
ρ $g_\rho^{s^2}/4\pi$	0.43	0.43
m_{ρ_s}	763.0	763.0
ρ $g_\rho^{t^2}/4\pi$	6.8	6.8
m_ρ^t	763.0	763.0
ω $g_\omega^2/4\pi$	11.0	12.0
m_ω	783.0	783.0
ϵ $g_\epsilon^2/4\pi$	7.65	4.7
m_ϵ	570.0	570.0
$f_{\pi\Delta}^2/4\pi$	0.0	0.35
$f_{\rho\Delta}^2/4\pi$	0.0	1.0
Λ_{NN}	1150.0	1150.0
$\Lambda_{N\Delta}$	1070.0	1070.0

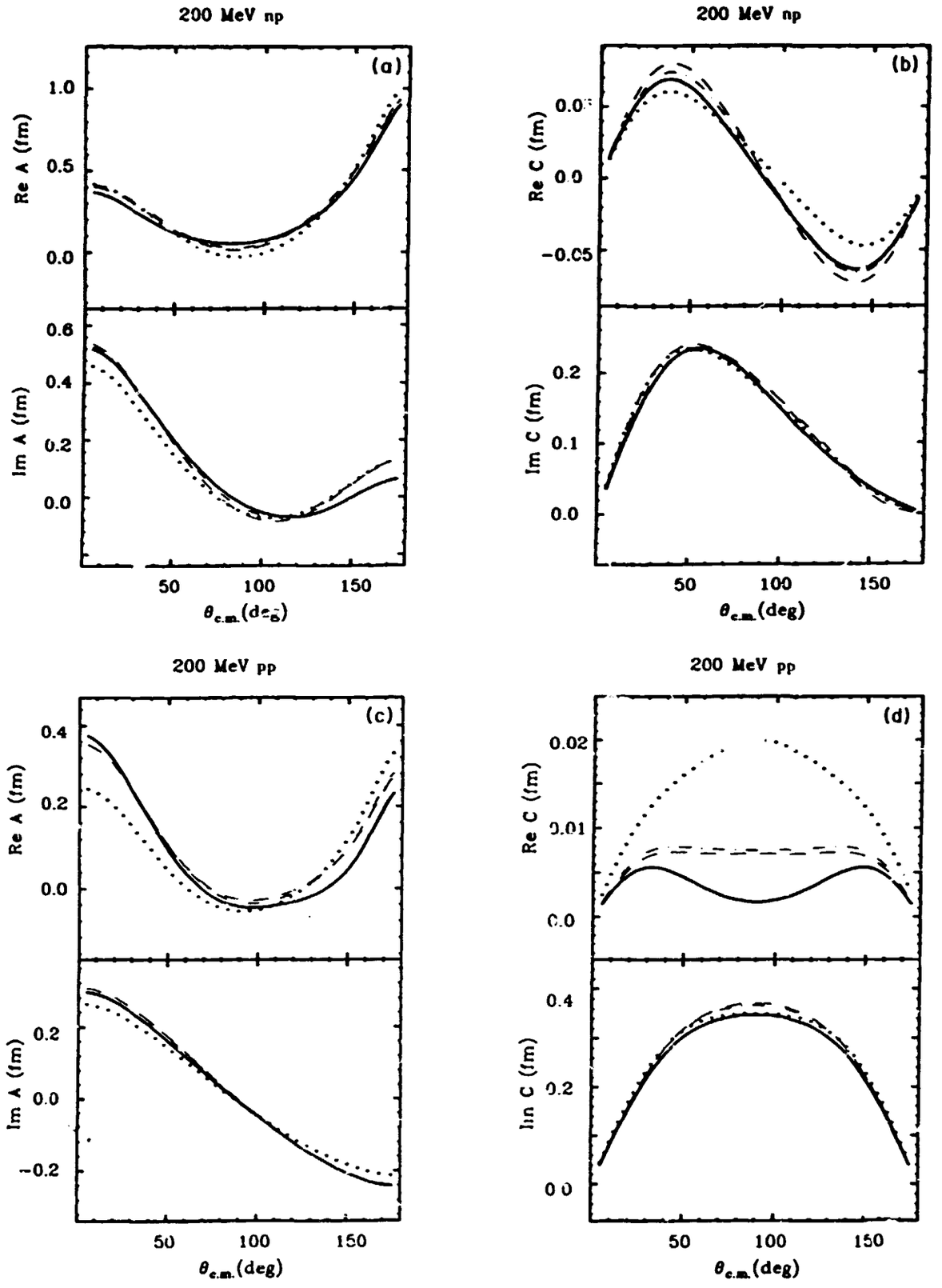

FIG. 3. (a)–(d) The Wolfenstein amplitudes A and C at 200 MeV are presented for models 1, 2, and 3. The mixed coupling case (model 1) is shown by a dashed line, pure pseudovector case (model 2) is shown by a dot-dashed line, and model 3 is shown by a dotted line. For comparison, the empirical Arndt amplitudes are shown by a solid line.

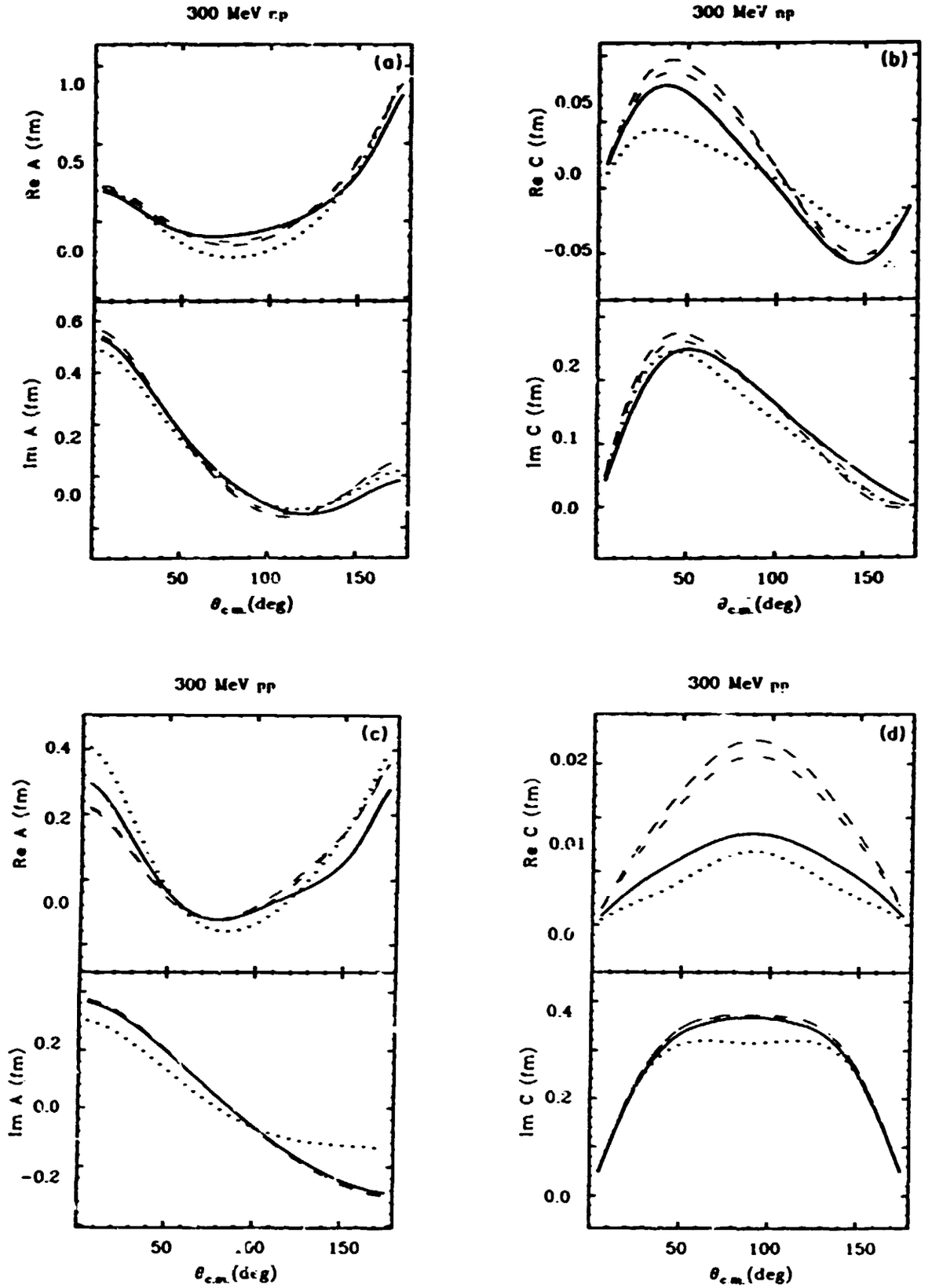

FIG. 4. (a)–(d) The Wolfenstein amplitudes A and C at 300 MeV are presented for models 1, 2, and 4. The mixed coupling case (model 1) is shown by a dashed line, pure pseudovector case (model 2) is shown by a dot-dashed line, and model 4 is shown by a dotted line. For comparison, the empirical Arndt amplitudes are shown by a solid line.

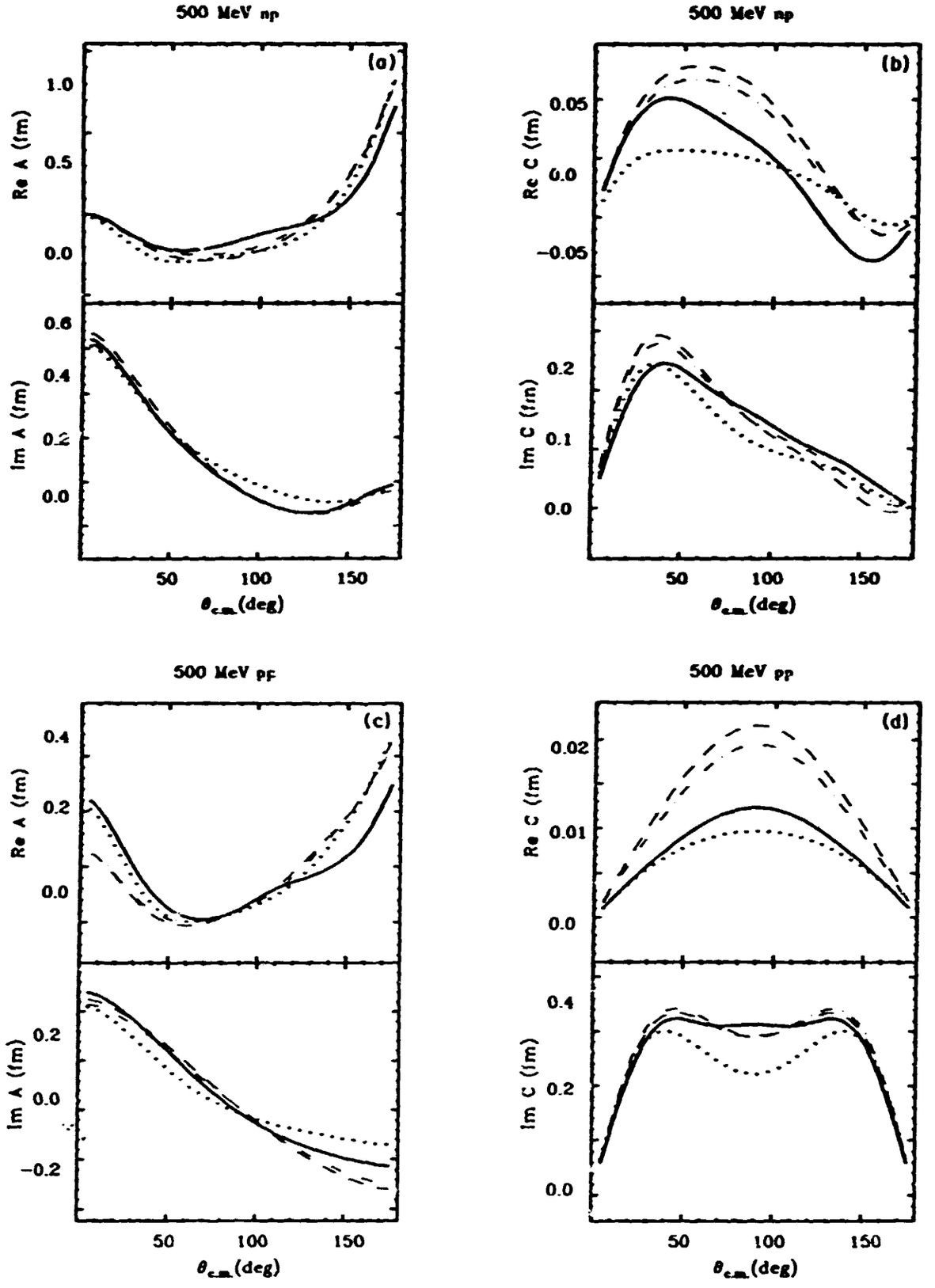

FIG. 5. (a)–(d) The Wolfenstein amplitudes A and C at 500 MeV are presented for models 1, 2, and 4. The mixed coupling case (model 1) is shown by a dashed line, pure pseudovector case (model 2) is shown by a dot-dashed line, and model 4 is shown by a dotted line. For comparison, the empirical Arndt amplitudes are shown by a solid line.

definition. In addition, the $(+-,++)$, $(-+,++)$, $(++,+-)$, and $(++,-+)$ amplitudes, which we will label simply as $(-,+)$, are obtained from the $(+-,++)$ amplitudes using antisymmetry or time reversal properties. Similarly, the amplitudes $(+-,+-)$, $(+-,-+)$, $(-+,+-)$, and $(-+,-+)$, labeled as $(-,-)$, are obtained from $(+-,+-)$ amplitudes.

The third and fourth OBE model amplitudes[4,5] that we employ in this work are calculated from a quasipotential equation based upon the Bethe-Salpeter equation. In this case the propagator G of Eq. (6) is the quasipotential Blankenbecler-Sugar propagator.[4,5] The third model includes only the NN channels.[4] In our calculations, the g_ϵ coupling constant of model 3 has been increased slightly as compared to Ref. 4, in order to improve on the fits of the S-wave phases. It is needed because of the inclusion of the negative energy spinor state channels, which has a repulsive nature in the S-wave channels. In addition to the NN channel the fourth model also includes the $N\Delta$ and $\Delta\Delta$ channels.[5] The scattering equations for these cases are shown diagrammatically in Fig. 2. The equation for the case where there are no $N\Delta$ and $\Delta\Delta$ channels can be obtained by leaving out the diagrams with the Δ lines.

The meson masses, coupling constants, and cutoff masses for these models are given in Tables I and II. To see the goodness of fit to the on-shell NN data, the Wolfenstein A and C amplitudes at 200 MeV are shown in Fig. 3 for the first three OBE models together with the empirical Arndt amplitudes. It is to be noted that while the first two models resulted in reasonably close fits to each other, the third model differs quite visibly from the first two and also from the Arndt amplitudes. This goodness of fit to the on-shell data is also one of the possible ambiguities that can arise in the optical potential when the NN amplitudes obtained from OBE models are used. At 300 and 500 MeV, models 1, 2, and 4 give reasonable fits to the Arndt A and C amplitudes and they are shown in Figs. 4 and 5. The fits of models 1 and 2 are generally less good than at 200 MeV, but it turns out that the fits to the NN amplitudes at 300 and 500 MeV are not as crucial to the success of the p-nucleus prediction

IV. RESULTS

Elastic scattering observables.

The results for p-^{40}Ca elastic scattering observables are presented in this section. Calculations are based on the IA2 formalism of Refs. 7 and 10 and use the relativistic nuclear densities supplied by Horowitz and Serot.[11]

Figures 6–8 display results for elastic scattering observables, obtained with the OBE models discused above, for proton energies 200, 300, and 500 MeV. In all three figures, results from the mixed coupling model[13] are shown by a solid line, results from the pure pseudovector model[13] are shown by a dashed line, and one of the two models of Ref. 4 is shown by a dotted line. In Figs. 6–8 p-nucleus calculations are done by using the theoretical amplitudes. For comparison purposes experimental data from Refs. 14, 15, and 16 are included for 200, 300, and 500 MeV, respectively. At 200 MeV, $N\Delta$ and $\Delta\Delta$ channels are omitted in all three models. At this energy, model 4, which is designed to study the effects of coupling to the Δ states at higher projectile energies, is not used in the calculation. All models give a reasonable description of the scattering observables, although model 3 (Ref. 4: with no $N\Delta$ or $\Delta\Delta$ channels) seems to describe the A_y better in the forward angle region. Note that, although model 3 seems to describe the 200 MeV p-nucleus data, it does not reproduce the Wolfenstein A and C very well as can be seen from Fig. 3. At this stage our conclusion is somewhat uncertain. It would be an interesting study in the future to compare the p-nucleus results of these models with the same quality of fit to the NN on-shell amplitudes. These results also show that the two OBE models of Ref. 13 ($\lambda=0$ and $\lambda=0.22$) give similar results although model 1 ($\lambda=0.22$) seems to describe the experimental data somewhat better.[17]

For 300 and 500 MeV, the dotted lines are the results of model 4, which includes $N\Delta$ and $\Delta\Delta$ channels, while the other two models (1 and 2) remain unchanged. At

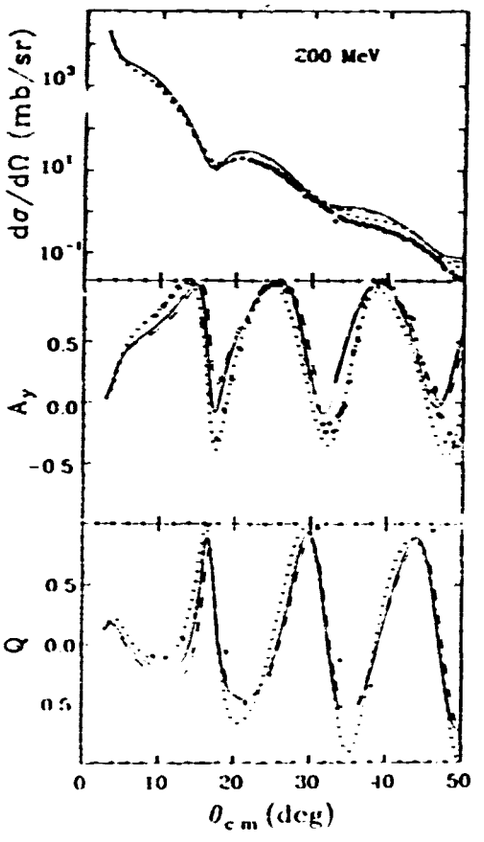

FIG. 6. p-^{40}Ca scattering observables at 200 MeV. Model 1 results are shown by a solid line, model 2 results by a dashed line, and model 3 results by a dotted line. Note that in all three calculations $N\Delta$ and $\Delta\Delta$ channels are omitted. Data are from Ref. 14.

these energies, all three models give reasonably good fits to the on-shell Arndt *NN* amplitudes, although there are some differences. From the 300 and 500 MeV results, it seems that the experimental data do not appear to favor any one of the *NN* amplitudes over the other, although the polarization observables at 500 MeV seem to be somewhat better fit by models 1 and 2 in the region of the first minimum. We also notice that at these energies the differences between the $\lambda=0.22$ (model 1) and $\lambda=0$ (model 2) appear to be very small suggesting that the *p*-nucleus scattering observables are not very sensitive to the relative admixture of γ^5 coupling at these energies.

As mentioned above, the best way to compare the *p*-nucleus results of these different models would be to have the same goodness of fit to the *NN* on-shell data. Since it is impractical to do this at the current stage of development we proceed as follows. In order to separate the effects of the negative energy components from differences which may arise from the goodness of fit, we standardize the comparisons by replacing the $(++,++)$ amplitudes in each model with the on-shell amplitudes determined by Arndt *et al.*[8] The results are displayed in Figs. 9–11. First note that all three models are in reasonably close agreement with the experimental data although the previous agreement with data and model 3 at 200 MeV seems to be destroyed somewhat. This shows that at this energy (200 MeV) *p*-nucleus results are very sensitive to the positive energy sector of the *NN* amplitudes. Standardized calculations based on model 4 at 200 MeV (*N*Δ and ΔΔ states included) have been shown in Ref. 12 to give a very good description of the data.

At 300 and 500 MeV, the mixed coupling model (model 1) and model 4 are in very close agreement in spite of the fact that model 4 uses a Blankenbecler-Sugar reduction of the Bethe-Salpeter equation which includes $(-,-)$ channels (in which both of the initial and final particles have negative *p* spin), and additional *N*Δ channels, both of which are absent in models 1 and 2. Therefore the sensitivity of the results to the presence or absence of *N*Δ and ΔΔ channels or $(-,-)$ states appears to be minimal at best, indicating that the *p*-nucleus theory at high energy (at least up to 500 MeV) is not critically sensitive to the goodness of the fit to the *NN* system. Comparing Figs. 6–8 with Figs. 9–11, we also note that the difference between models 1 and 2, attributable to the form of the pion coupling, are substantially unchanged in the standardized comparison.

For models 1 and 2 at 200 MeV, use of the Arndt amplitudes appears to give a slight improvement in the agreement with the experimental data. In addition the

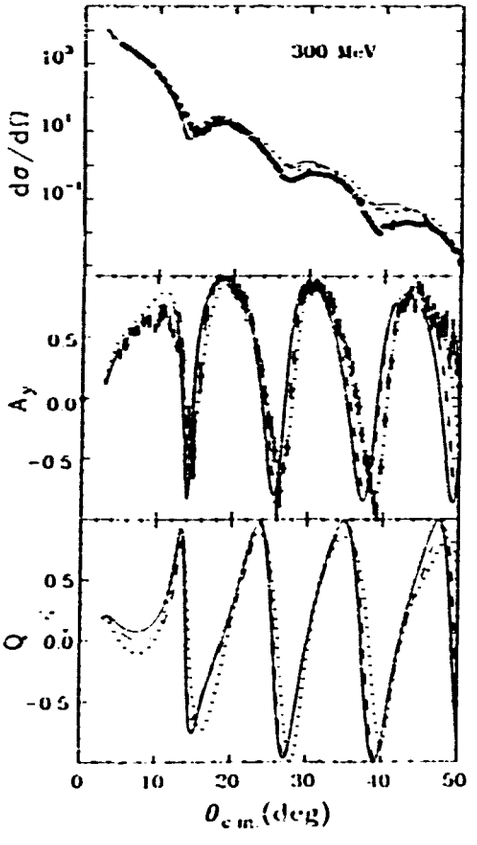

FIG. 7. p-^{40}Ca scattering observables at 300 MeV. Models 1 and 2 results are shown by solid and dashed lines, respectively. Model 4 (which contains *N*Δ and ΔΔ channels) results are shown by a dotted line. Data are from Ref. 15.

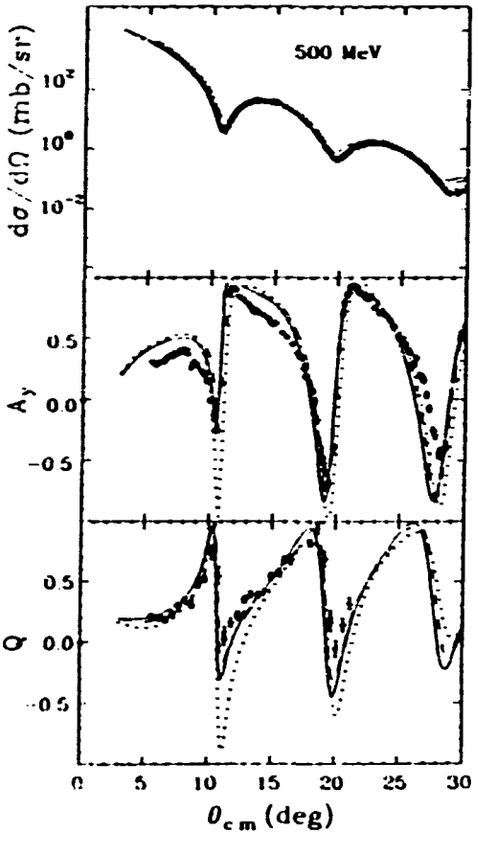

FIG. 8. p-^{40}Ca scattering observables at 500 MeV. The meaning of the curves is the same as in Fig. 5. Data are from Ref. 16.

minima in A_y appear deeper and the minima in Q appear shallower with the use of the Arndt amplitudes thereby demonstrating that the p-nucleus scattering observables are sensitive to the details of the $(++,++)$ amplitudes, at this energy, even though differences between model . and model 2 are not attributable to these sensitivities.

V. SUMMARY AND DISCUSSION

In this work we have presented p-nucleus scattering calculations based on four different sets of relativistic NN amplitudes. The first two sets of amplitudes are obtained from a three dimensional relativistic two-body equation in which one particle is kept on the positive energy mass shell. The difference between these two models is that one uses a pure pseudovector πN coupling and the other uses a mixed coupling (22% pseudoscalar). The results for 200, 300, and 500 MeV proton energies are presented. For all three energies both models include only the NN channels. Comparisons of the results of these two models show that, although both models give reasonable agreement with the experimental data, there are some definite model dependencies. This model dependency seems to lessen at higher proton energies. Since these two models reproduce the on-shell NN data equally well, as shown in Fig. 3, we cannot attribute these differences in p-nucleus observables to the ambiguity in fitting the on-shell data. This statement is also supported by the fact that the differences in p-nucleus results seem relatively unchanged when the Arndt amplitudes are used to standardize comparisons.

The third and fourth set of NN amplitudes are based on the quasipotential reduction of the Bethe-Salpeter equation. The third model includes only the NN channels while the fourth one includes both the $N\Delta$ and $\Delta\Delta$ channels. Both models use pure pseudovector πN coupling. The p-nucleus calculation at 200 MeV was done with amplitudes obtained from model 3 (see Ref. 12 for one based on model 4) and at 300 and 500 MeV model 4 amplitudes were used. Since model 3 does not reproduce the NN on-shell data at 200 MeV very well, there is some ambiguity in comparing its results to models 1 and 2 at this energy. When Arndt amplitudes are used for standardized comparison, the results of models 1 and 2 change in a minimal way while the model 3 results change quite visibly. This observation shows that p-nucleus observables are very sensitive to the positive energy NN amplitudes at this energy. This in turn suggests that in order

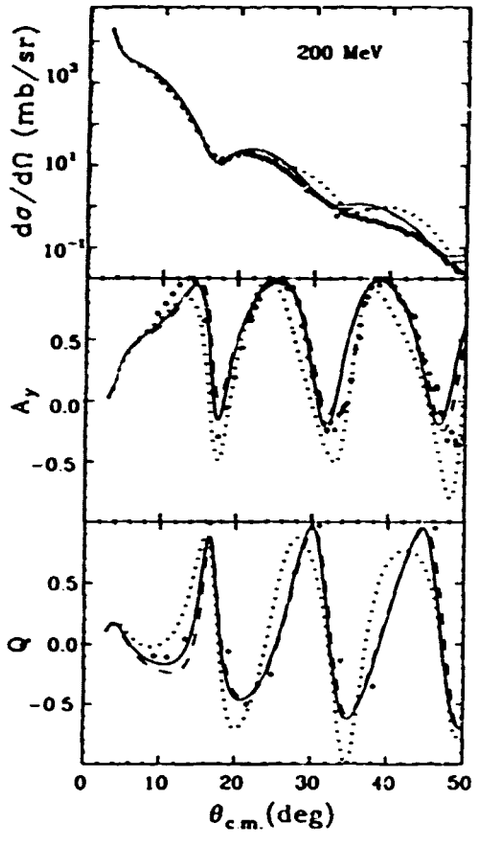

FIG. 9. p-^{40}Ca scattering observables at 200 MeV. The meaning of the curves is the same as in Fig. 4, but the positive energy amplitudes in all three models are standardized to the Arndt amplitudes.

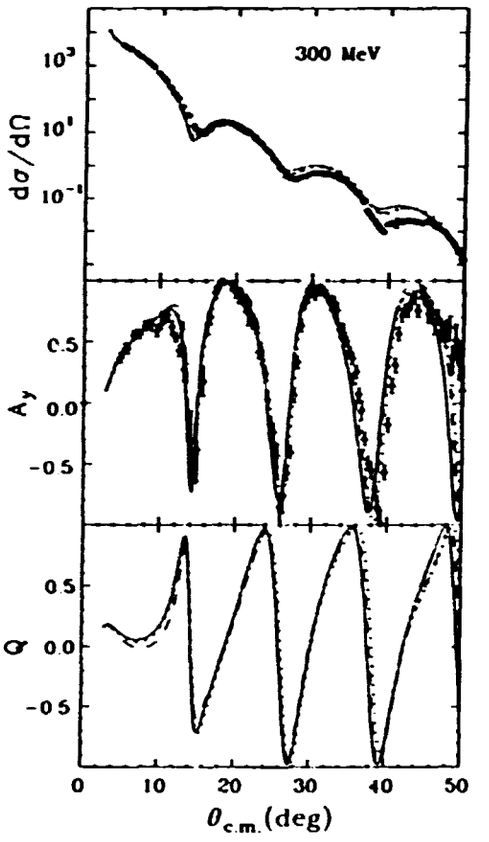

FIG. 10. p-^{40}Ca scattering observables at 300 MeV. The meaning of the curves is the same as in Fig. 5, but the positive energy amplitudes in all three models are standardized to the Arndt amplitudes.

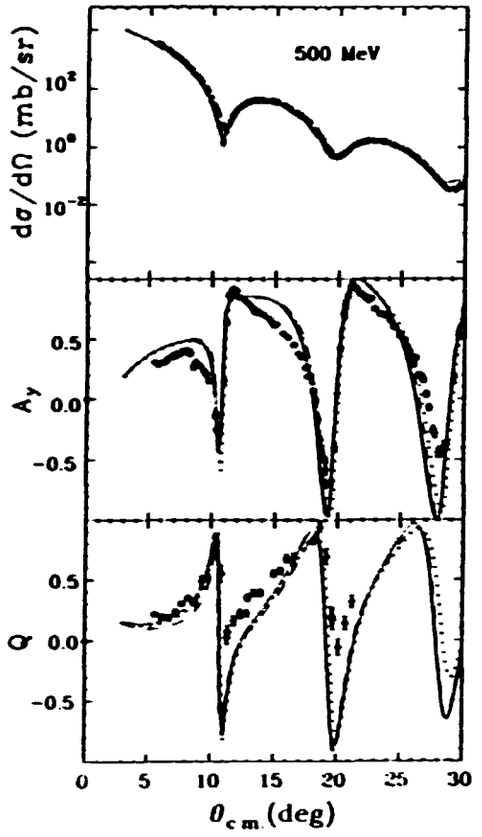

FIG. 11. p-^{40}Ca scattering observables at 500 MeV. The meaning of the curves is the same as in Fig. 6, but the positive energy amplitudes in all three models are standardized to the Arndt amplitudes.

to use relativistic NN amplitudes obtained from OBE models without ambiguity, it is essential to have a good quality fit to the on-shell data. Although this statement is quite obvious and seems unnecessary, it is important to note that p-nucleus scattering is one of the areas in which the pure relativistic amplitudes can be tested and these amplitudes are determined only dynamically (through fitting the on-shell amplitudes) once an OBE model is chosen.

At 300 and 500 MeV, model 4, which includes the delta isobar channels, and models 1 and 2 are compared. They all describe the experimental data very well. In particular, the results for models 1 and 2 are very close and there are no obvious model dependencies. Except for the fact that model 4 seems to give a very deep first minima for A_y and Q at 500 MeV, all three models give very similar predictions for the p-nucleus scattering observables. When the standardized comparison is made, the differences in the models disappear almost totally. These results suggest that at high energies (up to 500 MeV), p-nucleus theory is insensitive to the quality of fit to the NN amplitudes, including the presence or absence of $N\Delta$ and $\Delta\Delta$ channels, and the $(-,-)$ channels in the NN sector. Most of the effects of the Δ's in elastic p-nucleus scattering may be described as giving rise to an attraction in the NN channels at medium range and which are effectively simulated by a stronger epsilon coupling constant in the other model.

In summary, we conclude that OBE models provide an unambiguous way of determining the relativistic NN amplitudes provided that a good quality fit to the on-shell data is achieved. There is a definite model dependency in p-nucleus results depending on the choice of πN coupling but this dependency seems to disappear as the incident proton energy becomes higher. It is well known that the original RIA, which uses the five Fermi covariants, gave unreasonably large scalar and vector components at low energies. This has been attributed to the large pair contributions which result from pseudoscalar πN coupling. Since one of the OBE models (model 1) studied in this work contains 22% pseudoscalar coupling, it seems to suggest that this amount of pseudoscalar admixture is tolerable at this energy. Whether the same amount of admixture is allowable at lower energies and/or is consistent with the nuclear matter results is still an open question at this time. Up to 500 MeV the effects of $N\Delta$ and $\Delta\Delta$ channels in p-nucleus results seem to be minimal and the specific choice of relativistic equation used to determine the relativistic amplitudes does not appear to matter as long as the on-shell NN amplitudes can be reproduced with reasonable accuracy.

ACKNOWLEDGMENTS

K.M.M. and J.A.T. would like to acknowledge the hospitality of the Continuous Electron Beam Accelerator Facility, where this work was discussed and carried out. Two of us (F.G. and S.J.W.) gratefully acknowledge the support of the U.S. Department of Energy. One of us (K.M.M.) gratefully acknowledges the support of NASA, Grant No. NAG-1-477.

[1] M. V. Hynes, A. Picklesimer, P. C. Tandy, and R. M. Thaler, Phys. Rev. Lett. 52, 978 (1984); Phys. Rev. C 31, 1438 (1985).
[2] F. Gross, K. M. Maung, J. A. Tjon, L. W. Townsend, and S. J. Wallace, Phys. Rev. C 40, R10 (1989).
[3] F. Gross, Phys. Rev. 186, 1448 (1969); Phys. Rev. D. 10, 223 (1974).
[4] J. Fleischer and J. A. Tjon, Phys. Rev. D 21, 87 (1980).
[5] E. E. van Faassen and J. A. Tjon, Phys. Rev. C 28, 2354 (1983).
[6] F. Gross and K. M. Maung, Phys. Lett. B 229, 188 (1989); K. M. Maung and F. Gross, Phys. Rev. C 42, 1681 (1990).
[7] J. A. Tjon and S. J. Wallace, Phys. Rev. C 35, 280 (1987).
[8] R. A. Arndt, L. D. Roper, R. A. Bryan, R. B. Clark, B. J. Verwest, and P. Signell, Phys. Rev. D 28, 97 (1983).
[9] J. R. Shepard, J. A. McNeil, and S. J. Wallace, Phys. Rev. Lett. 50, 1443 (1983); B. C. Clark, S. Hama, R. L. Mercer, L. Ray, and B. D. Serot, *ibid.* 50, 1644 (1983); B. C. Clark, S. Hama, R. L. Mercer, L. Ray, and G. W. Hoffmann, Phys. Rev. C 28, 1421 (1983); L. Ray and G. W. Hoffmann, *ibid.* 31, 538 (1985).
[10] J. A. Tjon and S. J. Wallace, Phys. Rev. C 36, 1085 (1987).

[11]C. Horowitz and B. D. Serot, Nucl. Phys. A368, 503 (1981).
[12]N. Ottenstein, J. A. Tjon, and S. J. Wallace, Phys. Rev. C 38, 2272 (1988); 38, 2289 (1988).
[13]F. Gross, J. W. Van Orden, and K. Holinde, Phys. Rev. C 41, R1909 (1990).
[14]E. J. Stephenson, J. Phys. Soc. Jpn. (Suppl.) 55, 316 (1985); E. J. Stephenson, in *Anti-nucleon and Nucleon-Nucleus Interactions*, edited by G. E. Walker, C. D. Goodman, and C. Olmer (Plenum, New York, 1985), p. 299; P. Schwandt (private communication).
[15]D. A. Hutcheon *et al.*, in *Experimental Meson Spectroscopy—1980, Brookhaven*, Proceedings of the Sixth International Conference, edited by S. U. Chung and S. J. Lindenbaum, AIP Conf. Proc. No. 67 (AIP, New York, 1981), p. 454.
[16]G. W. Hoffmann *et al.*, Phys. Rev. Lett. 47, 1436 (1981); A. Rahbar *et al.*, *ibid* 47, 1811 (1981).
[17]In the previous work, Ref. 2, we have concluded that the mixed coupling model, model 1, was superior to model 2 which uses pure pseudovector πN coupling. Recently we have discovered an error in the treatment of the correction for the high partial waves in the p-nucleus calculations with the two OBE models 1 and 2. This error has been corrected in this work and model 1 results still seem to be better than model 2 and the conclusions are not affected although the differences are not as substantial as before.

MESON EXCHANGE AND THE RELATIVISTIC MULTIPLE SCATTERING FORMALISM

Franz GROSS
Department of Physics, College of William and Mary, Williamsburg, VA 23185, USA and Continuous Electron Beam Accelerator Facility, Newport News, VA 23606, USA

and

Khin Maung MAUNG [1]
Department of Physics, Old Dominion University, Norfolk, VA 23508, USA and NASA Langley Research Center, Hampton, VA 23665, USA

Received 22 June 1989

A relativistic multiple scattering theory is formulated in the context of meson exchange. The elastic scattering amplitude for a fermion projectile satisfies a Dirac equation with an optical potential derived from a relativistic multiple scattering series. It is shown that the two-body t-matrix associated with the optical potential is the one with one particle on its mass shell in all intermediate states.

In almost all the relativistic (Dirac) projectile–nucleus scattering calculations done in the past few years, the optical potential used has been the relativistic impulse approximation (RIA) [1] which is the relativistic analogue of the non-relativistic first-order impulse approximation optical potential. The tacit assumption behind the use of RIA, together with the Dirac equation, in which the heavy target is taken to be on its mass shell, is that there exists a multiple scattering series for the optical potential (in which the RIA is an approximation to the first term). However, neither the existence of the relativistic multiple scattering theory (RMST) nor the relation of it to the RIA has been consistently derived. The lack of a RMST not only prevents us from performing a systematic study of the higher-order multiple scattering terms, but also from making other corrections, such as off-shell effects and Pauli blocking, in a consistent manner. Therefore it is highly desirable to have a RMST.

In this work we show that a RMST can be formulated in the context of a relativistic meson exchange model. In the following we will consider a scalar "nucleon" interacting with a spin, isospin zero A-body target through meson exchange. A minimal set of meson exchange diagrams required for any such theory is the set of ladder and crossed ladder diagrams. In the limit when the heavy target becomes infinitely massive, this set reduces to a one-body equation for the lighter particle moving in an instantaneous potential produced by the heavier particle (the one-body limit [2]), and at high energies gives the eikonal approximation to scattering [3]. We will assume that the theory we seek is one in which these relativistic ladder and crossed ladders are summed efficiently.

The contributions to second order in the projectile–meson interaction are box and crossed box diagrams, shown in fig. 1. Since the target is a complex system with (in general) many closely spaced energy levels and continuum states with different combinations of clusters, we assume that all of these states can contribute, at least in principle, to the intermediate states. These states will be labelled by the index n, with $n=0$ referring to the ground state. Included in this sum are states where one, two, and possibly many nucleons are knocked out of the target. The elastic scattering matrix for the two diagrams in fig. 1 is, for spin zero particles,

[1] Present address: Department of Physics, Hampton University, Hampton, VA 23668, USA.

0370-2693/89/$ 03.50 © Elsevier Science Publishers B.V. (North-Holland Physics Publishing Division)

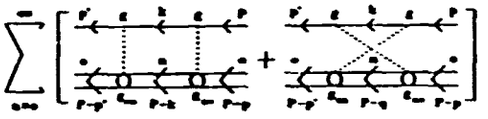

Fig. 1. Feynman diagrams for elastic scattering of a projectile (solid line) from a nucleus (double solid line) in its ground state. These diagrams are second order in the meson (dash line) projectile coupling g, but contain interactions of the A-body target nucleons to all order in g. The index n denotes an arbitrary excited state of the target, with $n=0$ the ground state.

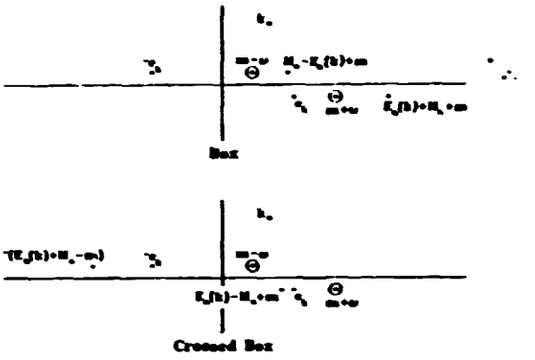

Fig. 2. Singularities of the box and crossed box diagrams in the complex k_0 plane for $W=M_0+m$, and $p=p'=0$. The circle around the meson poles are to indicate that they are double poles when $p=p'$. All the poles move as $|k|$ varies. Cuts coming from the structure of the couplings g_{n0} and g_{on} are not shown.

$$M_{\rm box}=\sum_{n=0}^{\infty} ig^2\int\frac{d^4k\,g_{0n}(P-p',P-k)g_{n0}(P-k,P-p)\Delta(k-p')\Delta(p-k)}{(2\pi)^4(e_k^2-k_0^2-i\epsilon)[E_n^2(k)-(W-k_0)^2-i\epsilon]}, \tag{1}$$

$$M_{\rm cross}=\sum_{n=0}^{\infty} ig^2\int\frac{d^4k\,g_{0n}(P-p',P-q)g_{n0}(P-q,P-p)\Delta(k-P')\Delta(p-k)}{(2\pi)^4(e_k^2-k_0^2-i\epsilon)[E_n^2(q)-(e_p+e_{p'}-W-k_0)^2-i\epsilon]}, \tag{2}$$

where the total four momentum in the center of mass is $P=(W,0)$, $q=p'+p-k$ and the meson propagators are

$$\Delta(k-p)=\frac{1}{\mu^2-(k-p)^2-i\epsilon}=\frac{1}{\omega_{p-k}^2-(k_0-p_0)^2-i\epsilon}. \tag{3}$$

The meson–projectile verticles which couple the ground state to the nth excited state are g_{0n} and g_{n0}, and

$$e_k=(m^2+k^2)^{1/2},\quad E_n(k)=(M_n^2+k^2)^{1/2}, \tag{4}$$

where m is the projectile mass and $M_n=M_0+\Delta_n$ is the mass of the nth excited state of the A nucleon system with excitation energy Δ_n, with $\Delta_0=0$.

The key to our derivation is the analysis of the singularities of the box and the crossed box diagrams in the complex k_0 plane. For this purpose we work at threshold where $p=p'=0$ and $W=M_0+m$. The singularities are shown in fig. 2.

(i) If the k_0 contour for the *box* diagram is closed in the upper half plane, the pole at $M_0-E_0(k)+m$ dominates. This pole corresponds to restricting the target ground state to its positive energy mass shell.

(ii) The next largest contributions to the box diagram, and the leading contributions to the crossed box diagram, come from the meson poles. Furthermore if the k_0 contour for the box diagram and the crossed box diagrams are closed in the upper half plane, these double meson poles at $k_0=m-\omega$ nearly cancel. The sum of these two terms is proportional to

$$\frac{1}{E_n-M_0+\omega}-\frac{1}{M_0-E_n+\omega}\approx\frac{2(M_0-E_n)}{\omega^2-(M_0-E_n)^2}, \tag{5}$$

so that when $n=0$ and $M_0\to\infty$, the pole calculated in (i) above gives the *exact* answer (the negative energy poles are also negligible in this case). If $M_0\neq\infty$, an estimate of the ratio of the meson pole contribution to the

dominant target pole contribution, (i) above, is $\mu^2(m+M_0)/4mM_0^2$.

(iii) For *excited* states of the target nucleus, the pole in the box diagram at $M_0-E_n(k)+m$ may overlap the double meson pole or even the negative energy nucleon pole at $-e_k$. (This happens when $\Delta_n\approx\omega$ or $2m$.) Such overlaps, which seem to be a manifestation of dissolution singularities [4], introduce spurious singularities into the equation. However, all of these spurious singularities are eliminated if the contour is closed in the *lower* half plane. Keeping the pole at $k_0=e_k$ still permits us to separate out the leading term from the box, but in this case the cancellations in (ii) will go like $(m-e_k)/\omega^2$, which does not approach zero as $A\to\infty$. However, this loss of convergence can be accepted since the contributions from excited states are generally smaller anyway.

These observations lead us to write the equation for the projectile target t-matrix in the following operator form:

$$T=V+VG_0^{\mathrm{T}}T+VG_{n\neq 0}^{\mathrm{P}}T, \tag{6}$$

where G_0^{T} is the propagator for the projectile and the target in its ground state, with the *target* on its mass shell, and $G_{n\neq 0}^{\mathrm{P}}$ is the propagator for projectile and excited states of the target, with the *projectile* on the mass shell. In this equation

$$V=\sum_i v^i+V^{\mathrm{nr}}, \tag{7}$$

where v^i are the OBE diagrams describing the interaction of the projectile with the ith nucleon in the target and V^{nr} is the sum of all irreducible terms remaining from the full ladder and crossed ladder sum. Points (i)–(iii) imply that V^{nr} is very small, and if A and m both approach infinity the leading OBE terms are exact [2]. In general eq. (6) sums ladders and crossed ladders exactly if V^{nr} is included.

While eq. (6) is an exact formulation of the problem, it is too complicated to be useful. We need a philosophy for identifying leading contributions which will be summed exactly and others which will be treated perturbatively. The philosophy we use is familiar from non-relativistic multiple scattering theories [5]. The leading effects are assumed to arise from multiple scattering through the intermediate states in which the projectile interacts repeatedly with the same target nucleon. This is important compared to the terms where the projectile is interacting with two or more different target particles since the matrix elements of the latter are proportional to (small) correlation functions involving two or more particles. It is not our intention to improve on these basic assumptions, but rather to describe how they can be implemented in a relativistically covariant manner.

For elastic scattering, a convenient first step is to introduce an effective potential U (the optical potential). In operator form, the t-matrix in terms of the potential U is

$$T=U+UG_0^{\mathrm{T}}T, \tag{8}$$

where the equation for the optical potential follows from eq. (6):

$$U=V+VG_{n\neq 0}^{\mathrm{P}}U=V+UG_{n\neq 0}^{\mathrm{P}}V, \tag{9a}$$

$$U=V+VG_{n\neq 0}^{\mathrm{P}}V+VG_{n\neq 0}^{\mathrm{P}}UG_{n\neq 0}^{\mathrm{P}}V. \tag{9b}$$

Eq. (9a) sums all inelastic contributions; (9b) is convenient for projecting the result onto the elastic subspace needed in eq. (8). For large A, eq. (8) is an effective one-particle equation for the projectile moving in a fixed, instantaneous field generated by the target. If the projectile has spin $\frac{1}{2}$, eq. (8) is a Dirac equation.

To take into account all the leading effects from rescattering from the same nucleon, which controls the strong short range NN interaction, we introduce the multiple scattering series as discussed above. To this end, separate out V^{nr} from V, introduce a new propagator g, such that

$$t^i=v^i+v^ig_it^i, \tag{10}$$

$$\bar{v}^i=V^{\mathrm{nr}}+v^ig_i\bar{v}^i, \tag{11}$$

where $V^n \equiv V/A$. Note that g_i describes the propagation of the ith nucleon in the nucleus, but is otherwise unspecified. With these definitions, eq. (9a) becomes

$$U^i = t^i + \sum_j t^i (G^0_{n_A 0} - g_i \delta_{ij}) U^j + \bar{v}^i \left(1 + G^0_{n_A 0} \sum_j U^j\right), \tag{12a}$$

where

$$U = \sum_i U^i . \tag{12b}$$

Eq. (12) is our final result for the optical potential. It gives the exact result for the sum of all ladders and crossed ladder diagrams, and in the nonrelativistic limit ($m \to 0$), $\bar{v}^i \to 0$.

The propagator g_i should be chosen to minimize the contribution from inelastic channels, so that the second term on the right hand side of eq. (12a) can be treated perturbatively. If these contributions are dominated by one nucleon knockout processes as discussed above and illustrated in fig. 3, choosing g_i to be the propagator with *both* the heavy $A-1$ cluster *and* the projectile on mass shell will *exactly cancel* the dominant inelastic contributions from the second term in eq. (12a) and ensure that they are exactly accounted for in the summation of eq. (10) which produces t^i. Restricting the $A-1$ cluster to its mass shell [81] ensures cluster separability of the remaining two nucleon system [7]. Eq. (10) for t^i then reduces, in the NN subspace, to the one particle on-shell (spectator) equation previously introduced by one of us [8], the only change being the shift in the total energy of the two-body subspace due to the motion of the $A-1$ cluster.

Finally U can be projected onto the elastic subspace using eq. (9b). This leads to an effective two-body t-matrix for the first term on the right hand side of eq. (12a) (denoted by $\hat{t}^i$) which has both nucleons in the initial *and* final states off shell and is obtained by quadrature from the spectator amplitude t

$$\hat{t}^i = \hat{v}^i + \hat{v}^i g_i \hat{v}^i + \hat{v}^i g_i t^i g_i \hat{v}^i . \tag{13}$$

Here $\hat{v}$ is the OBE potential with all four legs off shell (unless one of the legs is projected on-shell by g_i). In applications the first term in eq. (12a) is usually simplified by using the t_ρ approximation and is referred to as the RIA. Our derivation suggests that the full first term of eq. (12a) with g_i defined as in fig. 3 is a more precise definition.

This prescription, with some approximations, is precisely the one recently used to calculate p–^{40}Ca scattering at 200 MeV [9]. This calculation gives very good results, showing that calculations based on the theory presented here can work very well in practice.

In conclusion, we would like to emphasize that, in the context of the meson exchange model, the projectile–nucleus t-matrix does not readily assume the form convenient for multiple scattering analysis. In order to obtain a more manageable kernel and the corresponding t-matrix, we need to consider the explicit cancellations of

[81] Note that the prescription that the $A-1$ cluster be on mass shell has been given in ref. [6].

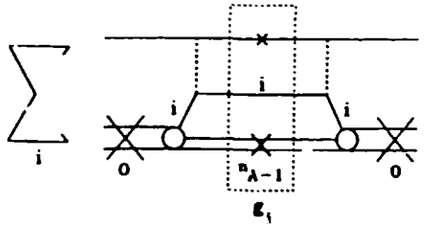

Fig. 3. Diagrammatic representation of second order rescattering of the projectile with the same target nucleon through intermediate states in which one nucleon is knocked out and the remaining $A-1$ system is in some excited state n_{A-1}. Choosing g_i as shown ensures that these leading terms are exactly included in the first term of eq. (12a), and that the other terms are small.

meson poles between the box diagram and the crossed-box diagram. Once the integral equation for the t-matrix is obtained, the optical potential can be derived in a straightforward manner. The optical potential can then be expressed as a multiple scattering series, eq. (12), and in the impulse approximation the t-matrix associated with the optical potential is found to be the one with one particle on its mass shell.

It is a pleasure to acknowledge helpful conversation with S.J. Wallace, who first alerted us to the problems of dissolution singularities. We would also like to thank P.C. Tandy and W. Van Orden for discussions on the subject on various occasions. This work was supported in part by the Department of Energy, through CEBAF, and by NASA grant NCC1-42.

References

[1] J.R. Shepard, J.A. McNeil and S.J. Wallace, Phys. Rev. Lett. 50 (1983) 1443;
B.C. Clark, S. Hama, R.L. Mercer, L. Ray and B.D. Serot, Phys. Rev. Lett. 50 (1983) 1644;
B.C. Clark, S. Hama, R.L. Mercer, L. Ray and G.W. Hoffmann, Phys. Rev. C 28 (1983) 1421;
M.V. Hynes, A. Picklesimer, P.C. Tandy and R.M. Thaler, Phys. Rev. Lett. 52 (1984) 978; Phys. Rev. C 31 (1985) 1438;
L. Ray and G.W. Hoffmann, Phys. Rev. C 31 (1985) 538.
[2] F. Gross, Phys. Rev. C 26 (1982) 2203.
[3] M. Levy and J. Sucher, Phys. Rev. 186 (1969) 1656;
H.D.I. Abarbanel and C. Itzykson, Phys. Rev. Lett. 23 (1969) 53;
S.J. Wallace and J.A. McNeil, Phys. Rev. D 16 (1977) 3565.
[4] G.E. Brown and D.G. Ravenhall, Proc. R. Soc. London, Sect. A 208 (1951) 552;
J. Sucher, Rep. Prog. Phys. 41 (1978) 1781; Phys. Rev. A 22 (1980) 348.
[5] K.M. Watson, Phys. Rev. 89 (1953) 575;
A.K. Kerman, H. McManus and R.M. Thaler, Ann. Phys. 8 (1959) 511.
[6] L.S. Celenza and C.M. Shakin, in: Relativistic nuclear physics, World Scientific Lecture Notes in Physics, Vol. 2 (World Scientific, Singapore, 1986).
[7] F. Gross, Phys. Rev. C 26 (1982) 2226.
[8] F. Gross, Phys. Rev. 186 (1969) 1448.
[9] F. Gross, K.M. Maung, T. Tjon, L.W. Townsend and S.J. Wallace, CEBAF preprint PR-88-010, submitted for publication.

PHYSICAL REVIEW C VOLUME 33, NUMBER 1 JANUARY 198

Theoretical antideuteron-nucleus absorptive cross sections

W. W. Buck
Department of Physics, Hampton University, Hampton, Virginia 23668

J. W. Norbury
Physics Department, Old Dominion University, Norfolk, Virginia 23508

L. W. Townsend and J. W. Wilson
National Aeronautics and Space Administration, Langley Research Center, Hampton, Virginia 23665

(Received 26 July 1985)

Antideuteron-nucleus absorptive cross sections for intermediate to high energies are calculated using an ion-ion optical model. Good agreement with experiment (within 15 percent) is obtained in this same model for $\bar{p}$-nucleus cross sections at laboratory energies up to 15 GeV. We describe a technique for estimating antinucleus-nucleus cross sections from $N\bar{N}$ data and suggest that further cosmic ray studies to search for antideuterons and other antinuclei be undertaken.

The search for antimatter in the form of cosmic ray antinuclei is an intriguing and speculative endeavor. Certainly, with present experimental capabilities, producing particles heavier than antiprotons in the laboratory is difficult at best. Indeed, the question as to whether or not one should even search for antinuclei in cosmic rays has been addressed from several different perspectives. One point of view,[1] for example, argues that theoretical abundances, estimated from empirical observations, of antinuclei with $Z \geq 3$ are negligible. Although the extreme rarity of antinuclei events may reflect nonconservation of baryon number in our universe, the purpose of this paper is not to address these issues but, rather, to provide a calculational procedure for determining whether or not an antinucleus has interacted with a nucleus. To do this we calculate antinucleus-nucleus total and absorptive cross sections utilizing an optical potential model[2,3] of nucleus-nucleus scattering as described below. Numerical results for $\bar{d}$ nucleus are presented to illustrate the predictions. Since experimental data for antinucleus-nucleus collisions are nonexistent, predictions for $\bar{p}$-nucleus cross sections are made, compared to available experimental data, and are found to be in good agreement (within 15 percent). Comprehensive tabulations of the predicted antinucleus-nucleus cross sections are published elsewhere.[4]

For the scattering of composite nuclei, a general multiple-scattering theory (neglecting three-body interactions) has been developed by Wilson.[5] The series reduces to the usual Watson form when the projectile is elementary. Through the use of the impulse and closure approximations, a simple, folded, optical model potential was derived[2] as

$$W(x)=A_P A_T \int d^3z\, \rho_T(z) \times \int d^3y\, \rho_P(x+v+z)\bar{t}(e,y) , \quad (1)$$

where e is the $N\bar{N}$ kinetic energy in the c.m. frame, y is the $N\bar{N}$ relative separation, ρ_T and ρ_P are the target and projectile number density distributions normalized to unity, $\bar{t}(e,y)$ is the energy-dependent constituent-averaged two-nucleon transition amplitude obtained from scattering experiments, and A_P and A_T are the projectile and target atomic numbers, respectively. With no renormalization or parameter adjustments, this optical potential has been previously used in a Wentzel-Kramers-Brillouin (WKB) formulation to obtain excellent agreement with experimental elastic scattering differential, reaction, and total cross section data at energies lower than 25 MeV/nucleon.[6] More often, however, this optical potential approximation is used within the context of an eikonal formalism to predict nucleon-nucleus, deuteron-nucleus, and nucleus absorptive (inelastic) cross sections to within 3% for energies higher than 80 MeV/particle and to within 10% for lower energies.[2,3,7] From eikonal scattering theory, the absorption (reaction) cross section is

$$\sigma_{abs}=2\pi \int_0^\infty [1-\exp[-2\,\mathrm{Im}\chi(b)]]\, b\, db , \quad (2)$$

where the complex phase function is (with $\hbar=1$)

$$\chi(b)=-(2k)^{-1}\int_{-\infty}^{\infty} U(b,z)dz , \quad (3)$$

with k the projectile momentum wave number and b denoting the impact parameter. The reduced potential is then obtained from the optical potential as

$$U(x)=2mA_P A_T(A_P+A_T)^{-1}W(x) , \quad (4)$$

where m is the nucleon mass. Within the eikonal context, this model is similar to the comparable, but alternative, Glauber theory formalism which has been extensively developed by Franco and collaborators.[8] Aside from the improved convergence to the exact multiple-scattering series by the Wilson approximation[5] (due to differences in higher order terms), the Wilson propagator[2] also includes target recoil and terms to order k^2.

In order to apply Eqs. (1)–(4) to antinucleus-nucleus collisions, several assumptions, other than the applicability of the underlying composite-particle multiple-scattering formalism, are necessary. First, we assume that the num-

ber density distribution for an antinucleus is identical to that of its "normal" nucleus counterpart. Hence, aside from the overall sign of the charge distribution, the antinuclei charge distribution parameters and functional forms are assumed to be identical to those of the corresponding nuclear species. We then extract the number densities ρ_A from the corresponding charge densities ρ_C obtained from electron scattering experiments, by assuming that

$$\rho_C(r)=\int \rho_N(r')\rho_A(r+r')d^3r' , \tag{5}$$

where the nucleon charge distribution is taken to be the usual Gaussian form

$$\rho_N(r)=(3/2\pi r_N^2)^{3/2}\exp(-3r^2/2r_N^2) , \tag{6}$$

with a nucleon root mean-square charge radius set equal to the proton value[9] of 0.87 fm.

For elementary projectiles, substitution of (6) into (5) yields a delta function for ρ_A. For nuclei or antinuclei with $A<20$ we use an harmonic oscillator form for ρ_C as

$$\rho_C(r)=\rho_0\left[1+\gamma\left[\frac{r}{a}\right]^2\right]\exp(-r^2/a^2) , \tag{7}$$

where the charge distribution parameters γ and a are listed in Table I. Inserting (6) and (7) into (5) yields

$$\rho_A(r)=(\rho_0\pi^{3/2}/8s^3)[1+(3\gamma/2)-(3\gamma a^2/8s^2)+(\gamma a^2r^2/16s^4)]\exp(-r^2/4s^2) , \tag{8}$$

where

$$s^2=(a^2/4)-(r_N^2/6) . \tag{9}$$

For nuclei or antinuclei with $A\geq 20$ we choose a Woods-Saxon form

$$\rho_C=\rho_0[1+\exp[(r-R)/c]]^{-1} , \tag{10}$$

where R is the half-density radius, and the surface diffuseness c is related to the charge skin thickness t_c through

$$t_c=4.4c . \tag{11}$$

Values for R and t_c are also listed in Table I. Inserting (6) and (10) into (5) yields, after some simplification,[2] a number density ρ_A that is of the Woods-Saxon form with the same R, but different overall normalization ρ_0 and surface thickness. The latter is given (in fm) by

$$t_A=5.08r_N[\ln[(3\beta-1)/(3-\beta)]]^{-1} , \tag{12}$$

where

$$\beta=\exp[2.54r_N/t_c] . \tag{13}$$

In all cases the densities are normalized to unity.

For the antinucleon-nucleon ($N\bar{N}$) transition amplitude, $\bar{t}$, we assume a form

$$\bar{t}(e,y)=\left[\frac{e}{m}\right]^{1/2}\sigma_{\rm tot}(e)[\alpha(e)+i][2\pi B(e)]^{-3/2}\times\exp[-y^2/2B(e)] , \tag{14}$$

which is obtained by taking the Fourier transform of the usual nuclear amplitude.[10] In Eq. (14) $\sigma_{\rm tot}$ is the $N\bar{N}$ total cross section, $\alpha(e)$ is the real-to-imaginary ratio of the forward amplitude, and $B(e)$ is the $N\bar{N}$ slope parameter. With this choice for the two-body amplitude we effectively treat antinucleus-nucleus scattering as a purely complementary system to nucleus-nucleus scattering. Values for $\sigma_{\rm tot}$ are parametrized in terms of the incident particle momentum P by

$$\sigma_{\rm tot}=(61.2\ {\rm mb})+(53.4\ {\rm mb\,GeV}/c)/P-P({\rm mb\,GeV}/c) , \tag{15}$$

which is a modification of the expression given in Ashford *et al.*[11] to extend the cross sections to 15 GeV. Values for the slope parameter, displayed in Fig. 1, were taken from the Paris $N\bar{N}$ potential[12] and from Block and Cahn.[13] Values of the parameter α are not presented for these results since only the imaginary part of the transition amplitude is used to calculate absorption cross sections. Details of the values used for the total cross section estimates are found in Ref. 4.

Predictions for $\bar{p}$-nucleus and $\bar{d}$-nucleus absorption cross sections are displayed in Figs. 2–4. Also plotted in Figs. 2 and 3, for comparison, are data from various experimental measurements.[14–16] Clearly the agreement between theory and experiment is good since the maximum cross section difference for any of these results is less than 15 percent. Typical differences between theory and experiment are 5 percent. Figure 4 displays predicted $\bar{d}$-nucleus absorptive cross sections for the range from 50 MeV/nucleon to 15 GeV/nucleon. These are provided in the event that techniques for producing antideuterons in the laboratory may become available in the future. Simi-

TABLE I. Nuclear charge distribution parameters from electron scattering data.

Nucleus	Distribution[a]	γ (HW) or t (fm)(WS)	a (HW) or R (fm)(WS)
^{2}H	HW	0	1.71
^{4}He	HW	0	1.33
^{7}Li	HW	0.327	1.77
^{9}Be	HW	0.611	1.791
^{11}B	HW	0.811	1.69
^{12}C	HW	1.247	1.649
^{14}N	HW	1.291	1.729
^{16}O	HW	1.544	1.833
^{20}Ne	WS	2.517	2.74
^{27}Al	WS	2.504	3.05
^{40}Ar	WS	2.693	3.47
^{56}Fe	WS	2.611	3.971
^{64}Cu	WS	2.506	4.20
^{80}Br	WS	2.306	4.604
^{109}Ag	WS	2.354	5.139
^{139}La	WS	2.621	5.618
^{208}Pb	WS	2.416	6.624

[a]The harmonic well (HW) distribution is used for $A<20$ and the Woods-Saxon (WS) distribution for $A\geq 20$.

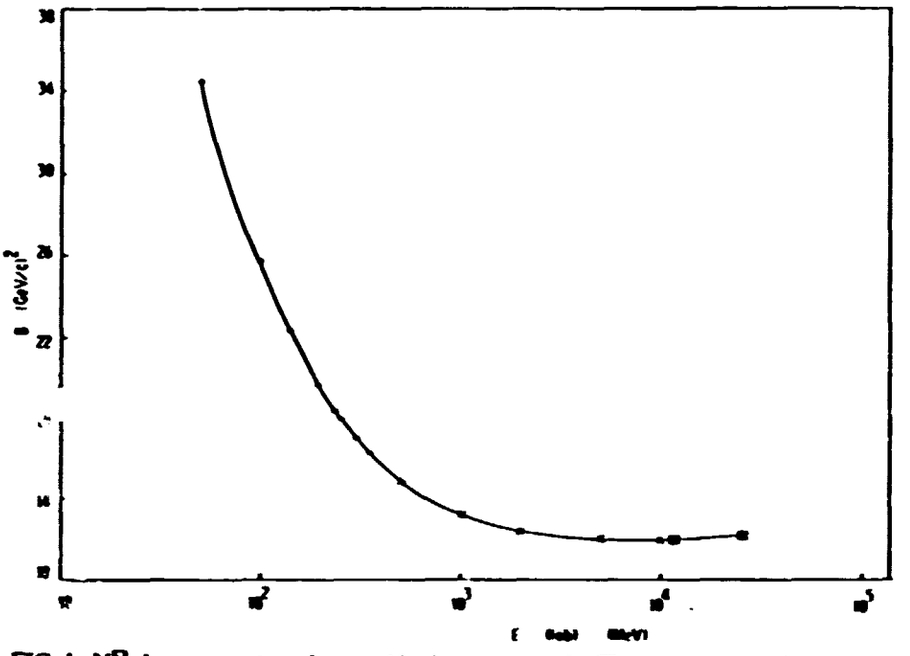

FIG. 1. $N\bar{N}$ slope parameter values used in the present work. The crosses are our interpolation.

larly, the possibility of observing antinuclei in cosmic rays may also contribute to the usefulness of this collision model. Indeed a primary cosmic antitriton event was reported at the 18th International Cosmic Ray Conference.[17] Cross sections for antinucleus-nucleus collisions up to $\bar{F}$e-Pb are tabulated in Ref. 4. For all collision pairs, the cross sections, as in Fig. 4, are smooth curves displaying no complicated structure. For optical model calculations, however, this is not entirely unexpected since it merely reflects the averaging nature of the calculation and the smooth functional dependencies of the input $N\bar{N}$ data.

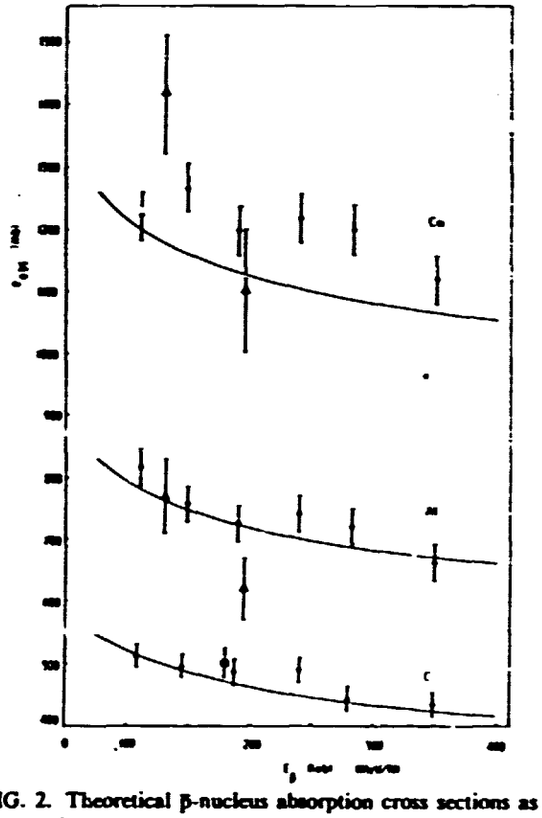

FIG. 2. Theoretical $\bar{p}$-nucleus absorption cross sections as a function of incident kinetic energy. Experimental values were obtained from Refs. 14–16.

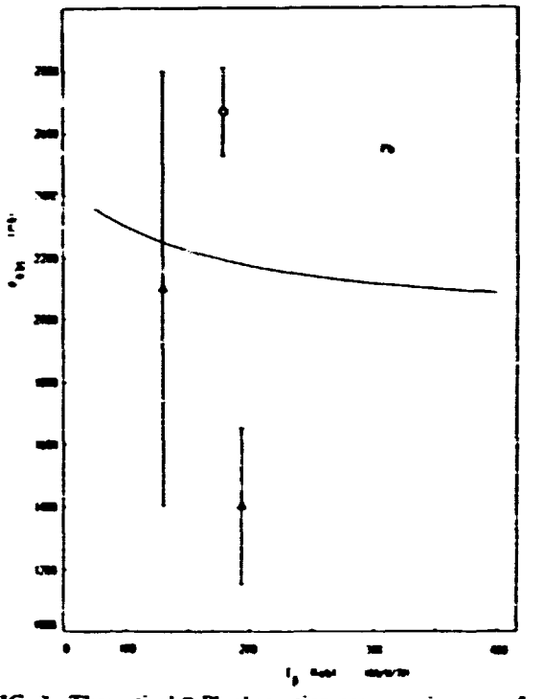

FIG. 3. Theoretical $\bar{p}$-Pb absorption cross sections as a function of incident kinetic energy. Experimental values are taken from Refs. 15 and 16.

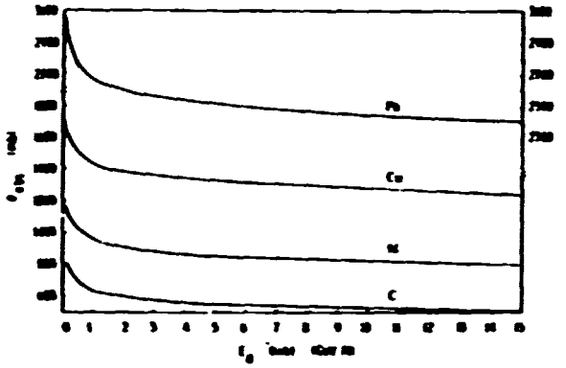

FIG. 4. Theoretical predictions for $\bar{d}$-nucleus absorptive cross sections as a function of incident kinetic energy.

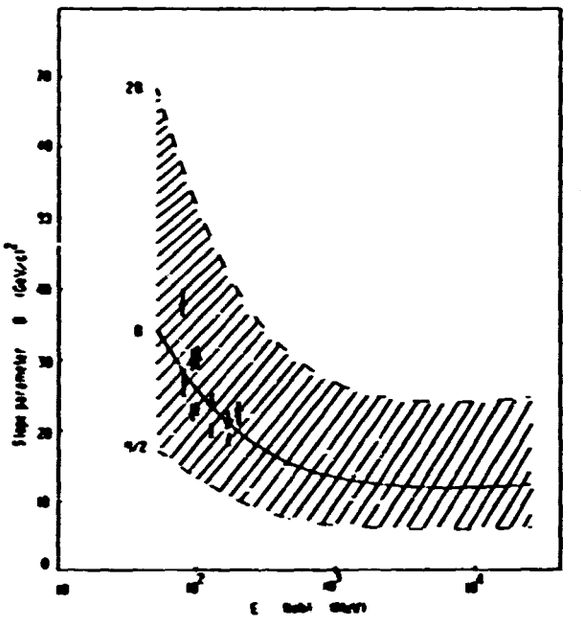

FIG. 5. Range of $N\bar{N}$ slope parameters used in the cross section sensitivity studies. The experimental values are taken from Brookhaven measurements (Ref. 11).

We have also performed an analysis to investigate the sensitivity of our predictions to the magnitude of the slope parameter. This was done by recalculating antiproton- and $\bar{p}$-nucleus cross sections for the cases where the $N\bar{N}$ slope parameters are taken in a rather *ad hoc* fashion as $2B(e)$ and $B(e)/2$. These slope parameter ranges are displayed in Fig. 5 along with the Brookhaven measurements.[11] As anticipated, we found that collisions involving light nuclei are far more sensitive to changes in the slope parameter than collisions involving heavy nuclei, especially at lower energies. For instance, with an assumed slope parameter of $2B$, we find that σ_{abs} at 100 MeV/nucleon, increases by 21% for $\bar{p}$-C (629 mb vs 520 mb), but only by 10% for $\bar{p}$-Pb (2528 mb vs 2303 mb). For $\bar{p}$-Pb at 100 MeV/nucleon, the increase is 6% (5886 mb vs 5542 mb). At 15 Gev/nucleon, the increases for these same collision pairs are 13%, 7%, and 4%, respectively. If the slope parameter is halved (to $0.5B$), we find that σ_{abs} for the same three collision pairs decreases by 13%, 6%, and 4% at 100 MeV/nucleon, and by 9%, 4%, and 3% at 15 GeV/nucleon. Clearly these absorption cross sections are not very sensitive to large changes in the slope parameter.

In summary, we have employed a simple optical model[2] from nucleus-nucleus scattering theory to intermediate energy antinucleus-nucleus collisions. The only new inputs required to complete the calculations are the experimental $N\bar{N}$ elastic scattering parameters (total cross section, elastic slope parameters, and real-to-imaginary ratio of the forward scattering amplitudes). For the energy range considered herein (100 MeV/nucleon to 15 GeV/nucleon), the eikonal formalism is certainly adequate. Although these methods could be extended to even lower energies,[7] other more suitable methods[18] are currently being implemented elsewhere. We have included charge exchange only as it is included in the determination of the Paris $N\bar{N}$ slope parameters. We have not considered pion propagation effects in the target nucleus, two-body correlation functions, and have ignored possibly important spin and isospin excitations of the target.[19] Nevertheless, we find that the model gives rather good agreement with available $\bar{p}$-nucleus data at intermediate energies and expect that the predicted $\bar{d}$-nucleus absorption cross sections are reasonably accurate (certainly within 15 percent). While we realize that the production of enough antideuterons in the laboratory (LEAR for example) to produce a beam is in the distant future, the production of such a beam could open up new areas of research since, for example, high temperatures in nuclear matter, may be achievable[20] with antideuterons of momentum greater than 2 GeV/c. For now, cosmic ray studies appear to offer the best chance for detecting and studying $\bar{d}$ and antinuclei interactions such as the reported antitriton event.[17]

The authors wish to thank Carl Dover, Dan Strottman, Robert Welsh, and Rolf Winter for useful discussions. Support from NASA under Grant Nos. NAG 1-477 (W.W.B.) and NCC 1-42 (J.W.N.) is gratefully acknowledged.

[1]For example, see G. Steigman, Annu. Rev. Astron. Astrophys. 14, 339 (1976); also Annu. Rev. Nucl. Part. Sci. 29, 313 (1979).

[2]J. W. Wilson and L. W. Townsend, Can. J. Phys. 59, 1569 (1981).

[3]L. W. Townsend and J. W. Wilson, NASA Reference Publication No. RP-1134, 1985.

[4]W. W. Buck, J. W. Norbury, L. W. Townsend, and J. W. Wilson, NASA Technical Paper (unpublished); copies of the tables may be obtained from the authors.

[5]J. W. Wilson, Phys. Lett. 52B, 149 (1974).

[6]H. B. Bidasaria, L. W. Townsend, and J. W. Wilson, J. Phys. G 9, L17 (1983).

[7]L. W. Townsend, H. B. Bidasaria, and J. W. Wilson, Can. J. Phys. 61, 867 (1983).

[8]V. Franco and G. K. Varma, Phys. Rev. C 18, 349 (1978), and

references therein.
[9]F. Borkowski, G. G. Simon, V. H. Walther, and R. D. Wendling, Z. Phys. A 275, 29 (1975).
[10]H. Iwasaki *et al.*, Nucl. Phys. A433, 580 (1985).
[11]V. Ashford *et al.*, Phys. Rev. Lett. 54, 518 (1985).
[12]M. Lacombe, B. Loiseau, B. Moussallam, and R. VinhMau, Phys. Lett. 124B, 443 (1983).
[13]M. M. Block and R. N. Cahn, Rev. Mod. Phys. 57, 563 (1985).
[14]K. Nakamura *et al.*, Phys. Rev. Lett. 52, 731 (1984).
[15]D. Garreta *et al.*, Phys. Lett. 149B, 64 (1984).
[16]V. Ashford *et al.*, Phys. Rev. C 31, 663 (1985).
[17]K. M. V. Apparao, N. Durgaprasad, S. A. Stephens, and S. Biswas, in Proceedings of the 18th International Cosmic Ray Conference, Bangalore, India, 1983, Vol. 2, p. 75.
[18]T. Suzuki and H. Narumi, Phys. Lett. 125B, 251 (1983); A. M. Green, W. Stepien-Rudzka, and S. Wycech, Nucl. Phys. A399, 307 (1983); A. M. Green and S. Wycech, *ibid.* A377, 441 (1982).
[19]C. B. Dover *et al.*, Phys. Lett. 143B, 45 (1984); C. B. Dover, M. E. Sainio, and G. E. Walker, Phys. Rev. C 28, 2368 (1983).
[20]D. D. Strottman and W. R. Gibbs, Phys. Lett. 149B, 288 (1984).

CEBAF-PR-89-023
HUPhy-89-1

Isospin Flip as a Relativistic Effect: NN Interactions

W.W. Buck
Department of Physics
Hampton University, Hampton, VA
and
Continuous Electron Beam Accelerator Facility
Newport News, VA 23606

CONTINUOUS
ELECTRON
BEAM
ACCELERATOR
FACILITY

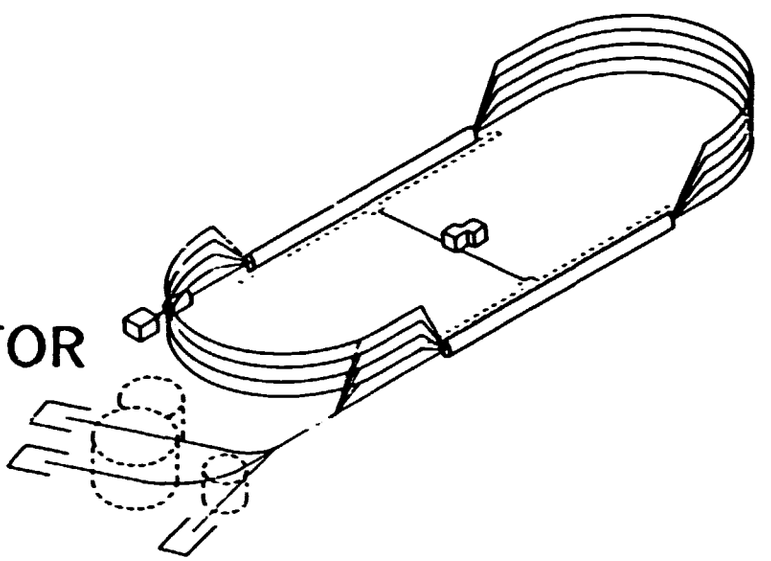

SURA SOUTHEASTERN UNIVERSITIES RESEARCH ASSOCIATION

CEBAF

Newport News, Virginia

Isospin Flip as a Relativistic Effect: $\bar{N}N$ Interactions

W. W. Buck
Department of Physics
Hampton University
and
The Continuous Electron Beam Accelerator Facility
12000 Jefferson Avenue
Newport News, VA 23606

Abstract

Resu s are presented of an analytic relativistic calculation of a OBE nucleon-nucleon (NN) interaction employing the Gross equation. The calculation consists of a non-relativistic reduction that keeps the negative energy states. The result is compared to purely non-relativistic OBEP results and the relativistic effects are separated out. One finds that the resulting relativistic effects are expressable as a power series in $\tau_1 \cdot \tau_2$ that agrees, qualitatively, with NN scattering. Upon G-parity transforming this NN potential, one obtains, qualitatively, a short range $\bar{N}N$ spectroscopy in which the S-states are the lowest states.

In the quest to understand short range nuclear forces, many nuclear theorists have embraced QCD and have made progress toward extracting the roles that quarks play. This approach is further fed by the observation that traditional non-relativistic meson exchange models have difficulty providing any new information on these short range forces. In this paper, new results for the short range interactions are presented that arise from a relativistic view of the N-N interaction that contains negative energy states. Preliminary and partial results were presented earlier.[1] This relativistic approach is not new; it was introduced by Gross in 1974.[2] In this present work, that pioneering work is revisited and expanded upon in such a way as to provide further insight into the nature of the short range forces harboured in the relativistic wave equation. It will be shown that, for the One Boson Exchange Potential considered, the short range contribution can be expressed as a power series in $\tau_1 \cdot \tau_2$, the Nucleon-Nucleon isospin operator. This short range contribution is interpreted as a relativistic effect and is a direct result of coupling to negative energy states. It will further be shown that, as a consequence of this relativistic effect, the G-parity transformation of the elastic NN potential[3] gives rise to a new level ordering prediction, at short ranges, for the Antinucleon-Nucleon ($\bar{N}N$) interaction. The final result of the analytic work presented below is a qualitative description of the (NN and $\bar{N}N$) interactions, as no numerical values for the exchanged mesons' masses or coupling constants are employed. A word of caution is needed, however; the $\bar{N}N$ interaction as presented in this paper is not antisymmetrized. The impact that this may have on the short range NN contributions presented here is uncertain; however, it is assumed that antisymmetrization does not apply to $\bar{N}N$.

The starting point is the Gross equation[2] for the NN system written as:

$$(\bar{\Gamma}C)_{\mu\nu}(\hat{p}) = -\int \frac{d^3k}{(2\pi)^3} V_{\mu\mu',\nu\nu'}(\hat{p},\hat{k},W) G_{\mu'\mu'',\nu'\nu''}(\hat{k},W)(\bar{\Gamma}C)_{\mu''\nu''}(\hat{k}) \qquad (1)$$

where

$$\text{total } 4-\text{momentum} = P = (W,\vec{0}); \qquad W = \text{total rest mass}$$

$$G_{\mu'\mu'',\nu'\nu''}(\vec{k},W) = \frac{[M + \frac{\not{P}}{2} + \not{k}]_{\mu'\mu''}[M + \frac{\not{P}}{2} - \not{k}]_{\nu'\nu''}}{2E_k W(2E_k - W)}$$

$$\hat{k} = (\hat{k}_o,\vec{k}); \hat{p} = (\hat{p}_o,\vec{p}\,)$$

$$\hat{k}_o = E_k - \frac{W}{2}; \hat{p}_o = E_p - \frac{W}{2}$$

$$E_k^2 = M^2 + \vec{k}^{\,2}, M = \text{nucleon mass} \qquad (2)$$

$\bar{\Gamma}$ is the covariant two body vertex function that is state dependent, and C is the charge conjugation matrix. To facilitate making a non-relativistic reduction in order to expose the analytic structure of the interaction, it is useful to write

$$\left[m+\frac{\not{P}}{2}+\not{k}\right]_{\mu'\mu''}=2M\left(\frac{W}{2E_k}\right)u^{(s)}_{\mu'}(\vec{k})\bar{u}^{(s)}_{\mu''}(\vec{k})-2M\left(\frac{2E_k-W}{2E_k}\right)$$
$$\times v^{(s)}_{\mu'}(-\vec{k})\bar{v}^{(s)}_{\mu''}(-\vec{k}) \tag{3}$$

By introducing

$$\psi^+_{rs}(\vec{p})=\frac{M}{[2W(2\pi)^3]^{\frac{1}{2}}}\quad\frac{\bar{u}^{(r)}_{\mu}(\vec{p})\bar{u}^{(-s)}_{\nu}(-\vec{p})\tilde{\Gamma}C)_{\mu\nu}(\vec{p})}{E_p(2E_p-W)} \tag{4a}$$

$$\psi^-_{rs}(\vec{p})=\frac{-M}{[2W(2\pi)^3]^{\frac{1}{2}}}\quad\frac{\bar{u}^{(r)}_{\mu}(\vec{p})\bar{v}^{(-s)}_{\nu}(\vec{p})(\tilde{\Gamma}C)_{\mu\nu}(\vec{p})}{E_pW} \tag{4b}$$

where ψ^+ and ψ^- are the positive and negative energy momentum space wave functions respectively, the following set of coupled equations can be extracted:

$$(2E_p-W)\psi^+_{rs}(\vec{p})=-\int\frac{d^3k}{(2\pi)^3}\left\{V^{++}\psi^+_{r's'}(\vec{k})+V^{+-}\psi^-_{r's'}(\vec{k})\right\} \tag{5}$$

$$-W\psi^-_{rs}(\vec{p})=-\int\frac{d^3k}{(2\pi)^3}\left\{V^{-+}\psi^+_{r's'}(\vec{k})+V^{--}_{r's'}\psi^-_{r's'}(\vec{k})\right\} \tag{6}$$

The V^{++},V^{+-},V^{-+}, and V^{--} are related to the one particle on the mass shell interaction kernels $V_{\mu\mu'\nu\nu'}$ by:

$$V^{++}=\frac{M^2}{E_kE_p}\bar{u}^{(r)}_{\mu}(\vec{p})\bar{u}^{(s)}_{\nu}(-\vec{p})V_{\mu\mu',\nu\nu'}u^{(r')}_{\mu'}(\vec{k})u^{(s')}_{\nu'}(-\vec{k}) \tag{7}$$

$$V^{+-}=\frac{M^2}{E_kE_p}\bar{u}^{(r)}_{\mu}(\vec{p})\bar{u}^{(s)}_{\nu}(-\vec{p})V_{\mu\mu',\nu\nu'}u^{(r)'}(\vec{k})v^{(s')}_{\nu'}(\vec{k}) \tag{8}$$

$$V^{-+}=\frac{M^2}{E_kE_p}\bar{u}^{(r)}_{\mu}(\vec{p})\bar{v}^{(-s)}_{\nu}(\vec{p})V_{\mu\mu',\nu\nu'}u^{(r')}_{\mu'}(\vec{k})u^{(s')}_{\nu'}(-\vec{k}) \tag{9}$$

$$V^{--}=\frac{M^2}{E_kE_p}\bar{u}^{(r)}_{\mu}(\vec{p})\bar{v}^{(-s)}_{\nu}(\vec{p})V_{\mu\mu',\nu\nu'}u^{(r'}_{\mu'}(\vec{k})v^{(-s')}_{\nu'}(\vec{k}) \tag{10}$$

Of course, the non-antisymmetrized $V_{\mu\mu',\nu\nu'}$ represent meson exchanges and, as is customary, these interactions will be approximated by single boson exchanges; namely, π, σ, ρ, and ω. One notes that there is no concern at present for the numerical values of the masses and coupling constants of these bosons. Thus there is no concern that the interaction not reproduce the NN phases, effective ranges, etc. One quite simply wants to compare qualitative features of the relativistic interaction to that of the non-relativistic interaction. This is performed by, essentially, subtracting the non-relativistic interaction from the relativistic interaction presented here. That is, the limit as $r\to 0$ is taken. What remains from this procedure is what one considers the relativistic effect or simply, the interaction difference. To arrive at results that can be treated analytically, a non-

relativistic reduction is performed that keeps the negative energy states. Having stated this, one continues with the calculation.

Employing expansion approximations such as $\frac{(E_p+M)(E_k+M)}{E_kE_p} \approx 4$ and $\frac{(E_p+M)(E_k+M)}{M^2} \approx 4$ with $(E_p+M)^{-1}(E_k+M)^{-1} = \frac{1}{4M^2}(1-\frac{p^2}{4M^2}-\frac{k^2}{4M^2}+-\cdots)$. After quite a bit of algebra, equation 5 is reduced to

$$\left[\frac{p^2}{M}-\frac{p^4}{4M^3}-\epsilon\right]\psi^+_{r_s}(\vec{p}\,) \approx g_\sigma^2 \int \frac{d^3}{(2\pi)^3}\frac{1}{(m_\sigma^2+q^2)}$$
$$\times\left\{1-\frac{1}{4M^2}\left[2i\vec{s}\bullet(2\vec{q}x\vec{k}\,)+2\vec{k}^{\,2}\right]\psi^+_{r's'}(\vec{k}\,)+\frac{\vec{\sigma}_2}{2M}\bullet(2\vec{k}-\vec{q}\,)\psi^-_{r's'}(\vec{k}\,)\right\} \quad (11)$$

for the sigma exchange only. Equation 11 is the result of keeping the lowest order of $\frac{v}{c}$ or $\frac{p}{M}$ compared to the leading term. Equation 11 as well as the other boson exchange contributions can now be Fourier Transformed to configuration space. (Similarly treated is equation 6.) The motivation for going to configuration space is the ease in which non-relativistic and relativistic contributions can be compared. Traditionally, non-relativistic potentials are always presented in position space. Keeping in mind that we seek only qualitative comparisons, we then transform our momentum space reduction into position space.

The resulting configuration space coupled equations are written:

$$-\left(\frac{\nabla^2}{M}+\frac{\nabla^4}{4M^3}+\epsilon\right)\psi^+(\vec{r}\,) = -V^{++}(\vec{r}\,)\psi^+(\vec{r}\,)-V^{+-}(\vec{r}\,)\psi^-(\vec{r}\,) \quad (12)$$

$$-2M\psi^-(\vec{r}\,) = -V^{-+}(\vec{r}\,)\psi^+(\vec{r}\,)-V^{--}(\vec{r}\,)\psi^-(\vec{r}\,) \quad (13)$$

The results of Equation 12 and 13 are not new. Gross presented these equations[2] without the quartic derivative operator.

The potentials V^{++}, V^{+-}, V^{-+}, and V^{--} are:

$$V^{++} = u_c+\sigma_1\bullet\sigma_2 u_{ss}+\hat{S}_{12}u_T+\vec{L}\bullet\vec{S}i_{LS} \quad (14)$$

$$V^{+-} = \frac{i\vec{\sigma}_1\bullet\vec{r}}{r}\;V_1^-+\frac{i\vec{\sigma}_2\bullet\vec{r}}{r}\;V_2^-+\frac{\vec{r}\bullet\vec{\sigma}_1X\vec{\sigma}_2}{2r}\;V_3^-+i\vec{\sigma}_2\bullet\vec{\nabla}v_\ell \quad (15)$$

$$V^{-+} = (V^{+-})^\dagger \quad (16)$$

$$V^{--} = V_o^\sigma\frac{\vec{L}\bullet\vec{S}}{Mr}\;V_1^\sigma+V_o^\omega-\frac{\left(\frac{3}{2}+2k_\omega\right)}{Mr}\;\vec{L}\bullet\vec{S}V_1^\omega$$
$$+\;\tau_1\tau_2\left[\sigma_1\bullet\sigma_2V_o^\pi+\hat{S}_{12}V_2^\pi+V_o^\rho-\frac{\left(\frac{3}{2}+2k_\rho\right)}{Mr}\;\vec{L}\bullet\vec{S}\;V_1^\rho\right]$$
$$+\;\textit{higher order terms} \quad (17)$$

where

$$
\begin{aligned}
u_c &= V_o^\sigma + V_o^\omega + \vec{\tau}_1 \cdot \vec{\tau}_2 V_o^\rho \\
u_{ss} &= \tau_1 \bullet \tau_2 \left[V_o^\pi \frac{m_\rho^2}{6M^2}(1+k_\rho)^2 V_o^\rho \right] + \frac{m_\omega^2}{6M^2}(1+k_\omega)^2 V_o^\omega \\
u_T &= \tau_1 \bullet \tau_2 \left[V_2^\pi - (1+R_p)^2 \right] - (1+k_\omega)^2 V_2^\omega \\
u_{LS} &= -\frac{m_\pi}{Mx} \left[V_1^\sigma + (1.5+2k_\omega) V_1^\omega + \tau_1 \bullet \tau_2 ((1.5+2k_\rho) V_1^\rho \right]
\end{aligned} \tag{18}
$$

and

$$
\begin{aligned}
x &= r m_\pi \\
V_1^- &= -\tau_1 \bullet \tau_2 V_1^\pi \\
V_2^- &= V_1^\sigma - \frac{1}{2} k_\omega V_1^\omega - \tau_1 \bullet \tau_2 \frac{k_\rho}{2} \quad V_1^\rho \\
V_3^- &= -(1+k_\omega) V_1^\omega - \tau_1 \bullet \tau_2 (1+k_\rho) V_1^\rho \\
v_\ell &= \frac{1}{M} \left[V_o^\sigma + V_o^\omega + \tau_1 \bullet \tau_2 V_o^\rho \right] \\
V_o^\sigma(r) &= \frac{-g_\sigma^2}{4\pi} \quad m_\pi \quad \frac{e^{-\alpha x}}{x} \quad ; \quad \text{where} \quad \alpha = \frac{m_\sigma}{m_\pi} \\
V_1^\sigma(r) &= \frac{g_\sigma^2}{4\pi} \quad \frac{m_\pi^2}{2M} \quad \frac{e^{-\alpha x}}{x} \quad \left(\alpha + \frac{1}{x} \right) \\
V_o^\pi(r) &= \frac{g_\pi^2}{4\pi} \quad \frac{m_\pi^3}{12M^2} \quad \frac{e^{-x}}{x} \\
V_1^\pi(r) &= \frac{\lambda g_\pi^2}{4\pi} \quad \frac{m_\pi^2}{2M} \left(1 + \frac{1}{x} \right) \frac{e^{-x}}{x} \\
V_2^\pi(r) &= \frac{g_\pi^2}{4\pi} \quad \frac{m_\pi^3}{12M^2} \left(1 + \frac{3}{x} + \frac{3}{x^2} \right) \frac{e^{-x}}{x} \\
V_o^{\rho,\omega}(r) &= \frac{g_{\rho,\omega}^2}{4\pi} \quad m_\pi \quad \frac{e^{-\rho x, \omega x}}{x} \quad ; \quad \rho = \frac{m_\rho}{m_\pi}; \quad \omega = \frac{m_\omega}{m_\pi} \\
V_1^{\rho,\omega}(r) &= \frac{g_{\rho,\omega}^2}{4\pi} \quad \frac{m_\pi^2}{M} \quad \frac{e^{-\rho' x}}{x} \left(\rho' + \frac{1}{x} \right); \quad \rho' = \rho \text{ or } \omega \\
V_2^{\rho,\omega}(r) &= \frac{g_\rho^2}{4\pi} \quad \frac{m_\pi^3}{12M^2} \quad \frac{e^{-\rho' x}}{x} \left(\rho^2 + \frac{3\rho' x}{x} + \frac{3}{x^2} \right)
\end{aligned} \tag{19}
$$

These relations are well known[2] and one can verify them. The next step is to uncouple Equations 12 and 13 to obtain a single Schroedinger like equation. One finds that

$$
-\left(\frac{\nabla^2}{M} + \varepsilon \right) \psi^+(r) = -(V^{++} - V_R)\, \psi^+(r) \tag{20}
$$

where

$$V_R = \frac{\nabla^4}{4M^3} + V^{+-} \quad \frac{1}{2M\left(1 - \frac{V^{--}}{2M}\right)} \quad V^{-+} \tag{21}$$

This is the non-relativistic reduction to be examined. In all of the work that follows, V^{--} has been neglected. Thus

$$V_R = \frac{\nabla^4}{4M^3} \quad + \frac{|V^{+-}|^2}{2M} \tag{22}$$

One can show, through the employment of spin and angular momentum "aerobics" that equation 20 is equivalent to

$$-\left(\frac{\nabla^2}{M} + \epsilon\right)\Phi = -\left(V_T - \frac{\nabla^4}{4M^3}\right)\Phi \tag{23}$$

where

$$\Phi = \left(1 + \frac{v_l^2}{2}\right) \tag{24}$$

and

$$V_T = V_c + \vec{\sigma}_1 \bullet \vec{\sigma}_2 V_{ss} + \hat{S}_{12} V_{S12} + \vec{L} \bullet \vec{S} V_{LS} + \vec{L} \bullet \vec{D} V_{LD} \tag{25}$$

The V's are the same as those described in reference 2 and are a convoluted arrangement of π, ρ, σ, and ω potentials.

For the next phase of the calculation, one can proceed either from Equation 25 or from the potential found in Equation 21. Proceeding from the former choice, one finds after perf ming some algebra and keeping only the largest contributions as $r \to 0$:

$$\begin{aligned}
V_C &= a_c + b_c \tau_1 \bullet \tau_2 + c_c(\tau_1 \bullet \tau_2)^2 - a_c' - b_c' \tau_1 \bullet \tau_2 - c_c'(\tau_1 \bullet \tau_2)^2 \\
V_{LS} &= -a_{LS} - b_{LS} \tau_1 \bullet \tau_2 - c_{LS}(\tau_1 \bullet \tau_2)^2 \\
V_{S12} &= -a_{S12} - b_{S12} \tau_1 \bullet \tau_2 + c_{S12}(\tau_1 \bullet \tau_2)^2 \\
V_{ss} &= a_{ss} + b_{ss} \tau_1 \bullet \tau_2 + c_{ss} \tau_1 \bullet \tau_2)^2 \\
V_{LD} &= a_{LD} + b_{LD} \tau_1 \bullet \tau_2 + c_{LD}(\tau_1 \bullet \tau_2)^2
\end{aligned} \tag{26}$$

where the a's, b's and c's are positive definite and, to the leading term, are given by

$$\begin{array}{lll}
a_c = \frac{7}{8} F V_o^{\omega^2} & ; \; b_c = \frac{(12+3k_\rho)}{8F} V_o^\rho V_o^\omega & ; \; c_c = (4 + 3k_\rho + 3k_\rho^2)\frac{F}{8} V_o^{\rho^2} \\
a_c' = G V_o^{\omega^3} & ; \; b_c' = 3G V_o^\rho V_o^{\omega^2} & ; \; c_o' = 3G V_o^{\rho^2} V_o^\omega \\
a_{ss} = \frac{F}{3} V_o^{\omega^2} & ; \; b_{ss} = \frac{F}{6}(1 + 3k_\rho) V_o^\rho V_o^\omega & ; \; c_{ss} = \frac{F}{3} V_o^{\rho^2} \\
a_{LD} = 2F V_o^\sigma V_o^\omega & ; \; b_{LD} = F V_o^\omega V_o^\rho & ; \; c_{LD} = \frac{F}{2} V_o^{\rho^2} \\
a_{S12} = \frac{F}{3} V_o^{\omega^2} & ; \; b_{S12} = \frac{F}{6}(1 + 3k_\rho) V_o^\rho V_o^\omega & ; \; c_{S12} = \frac{F}{12}(3 + 2k_\rho) V_o^{\rho^2} \\
a_{LS} = F V_o^{\omega^2} & ; \; b_{LS} = 3F V_c^\omega V_o^\rho & ; \; c_{LS} = \frac{F}{2} V_o^{\rho^2}
\end{array} \tag{27}$$

and

$$F \equiv \frac{m_\pi^2}{M^3 x^2 \left(1+\frac{v_i^2}{2}\right)} \quad ; \quad G = \frac{m^2 x^2 P^2}{4 m_\pi^2} \quad ; \quad D_T = 1 + \frac{v_i^2}{2}$$

$$V_o^B = \frac{g_B^2}{4\pi} \; m_\pi \; \frac{e^{-Bx}}{x} \quad ; \quad B = \sigma, \rho, \omega$$
$$\sigma = \frac{m_\sigma}{m_\pi} \; ; \; \rho = \frac{m_\rho}{m_\pi} \quad ; \quad \omega = \frac{m_\omega}{m_\pi} \qquad (28)$$

One notes that in this limit the pion contributions can be neglected compared to the other terms. To obtain the $\overline{N}N$ potentials for small distances, one G-parity transforms the NN potentials of Equation 26. This effectively changes the sign of the omega coupling constant and, thus, changes the sign of the corresponding coefficients.

The final ingredients that we need before making concluding remarks are the spin matrix elements; all but $\vec{L} \bullet \vec{D}$ can be found elsewhere[3] and the $\vec{L} \bullet \vec{D}$ matrix elements are found in reference 2. For $^{33}P_o$ $\overline{N}N$, one finds $L = -2$, $\hat{S}_{12} = -4$, $\sigma_1 \bullet \sigma_2 = 1$, and $\tau_1 \bullet \tau_2 = 1$. For $^{13}P_o$ $\overline{N}N$, one finds that only $\tau_1 \bullet \tau_2$ changes; $\tau_1 \bullet \tau_2 = -3$. Both of these $\overline{N}N$ ^3P_o states have the same $\vec{L} \bullet \vec{D}$. Making the substitutions into Equation 25 gives the qualitative results that the $^{13}P_o$ potential lies higher than the $^{33}P_o$; a result in agreement with the numerical work of other researchers.[4]. Furthermore, through similar arguments, one finds that the $^{11}S_o$ $\overline{N}N$ lies lower than the $^{13}P_o$ $\overline{N}N$; an unexpected result. Finally, it is clear that all isoscalar $\overline{N}N$ potentials are more repulsive than their isovector counterparts. Hence, $^{11}S_o > {}^{31}S_o$, $^{11}P_1 > {}^{31}P_1$, $^{11}D_2 > {}^{31}D_2$, etc.

These qualitative results should be unaffected by a more complete interaction since it is well known that the omega meson exchange dominates the short range interaction. The omega meson exchange is included explicitly here. More complete interaction models should vary only in their quantitative results such as the amount of energy level shift. It is not clear if the results presented here will affect the $\bar{p}p$ Coulombic states widths. Although, theoretical approaches generally "cut-off" the $\bar{p}p$ interaction inside 1 fm, investigating how the relativistic effects affect Coulombic state widths is worth pursuing.

In conclusion, to obtain analytic results, the Gross equation was examined in a non-relativistic reduction of the NN interaction that keeps the negative energy states. The NN interaction was chosen to be a one boson exchange consisting of π, σ, ρ, and ω. The reduction was then applied to the real part of the $\overline{N}N$ interaction via G-parity. To get a qualitative feeling for what coupling to the negative energy states provides, a short distance limit was taken. One might expect that the difference between relativistic and non-relativistic theoretical descriptions would show up at short distance. This work finds that indeed that is the case; for the $^{11}S_o$ has a real $\overline{N}N$ potential that is more attractive than that of the $^{13}P_o$; a result rather different from reference 3. The fact that this is the case at very short distance for this work or any other work may be worrysome since annihilation was not taken into account. On the other hand, there is no conclusive evidence that annihilation contributes any more than giving the states widths. Furthermore, this "relativistic effect" may start to be evident at ranges as long as 0.4 fm in some channels. An effort is already underway to include annihilation in order to calculate cross sections and other effects. One final note is that the level orderings are directly related to the isospin coherences of Equations 26 and

from a purely non-relativistic viewpoint this can be thought of as a result, in part, of adding the contribution of a Z graph.[5]

I wish to thank Franz Gross, Carl Dover, J.-M. Richard, and Rolf Winter for valuable conversations and CEBAF for its continuing hospitality. This work is supported in part by .ional Science Foundation grant RII-8704038 and NASA grant NAG-1-447.

References

(1) W.W. Buck, Proceedings of the Workshop on Relativistic Nuclear Many-Body Physics, 1988, edited by B.C. Clark, R. Perry, and J. Vary, World Scientific Publishers.
(2) F. Gross, Phys. Rev. D 10, 223 (1974).
(3) W.W. Buck, C.B. Dover, J.M. Richard, Ann. Phys. 121, 47 (1979).
(4) E. Borie and F. Gross, Few Body Conference Proceedings (1980); J.A. Tjon, Phys. Rev. D18, 2565 (1978).
(5) G.E. Brown, private communication

Confining potential in momentum space

JOHN W. NORBURY
Department of Physics, Rider College, Lawrenceville, NJ 08648, U.S.A.
DAVID E. KAHANA
Continuous Electron Beam Accelerator Facility, Newport News, VA 23606, U.S.A.
AND
KHIN MAUNG MAUNG
Department of Physics, Hampton University, Hampton, VA 23668, U.S.A. and NASA Langley Research Center, Hampton, VA 23665, U.S.A.

Received September 4, 1991

A method is presented for the solution in momentum space of the bound-state problem with a linear potential in r space. The potential is unbounded at large r leading to a singularity at small q. The singularity is integrable, when regulated by exponentially screening the r-space potential, and is removed by a subtraction technique. The limit of zero screening is taken analytically, and the numerical solution of the subtracted integral equation gives eigenvalues and wave functions in good agreement with position space calculations.

On présente une méthode pour la résolution dans l'espace des impulsions du problème des états liés, avec un potentiel linéaire dans l'espace r. Ce potentiel n'étant pas borné pour les grandes valeurs de r, on a une singularité pour les faibles valeurs de q. Ce potentiel est intégrable et peut être enlevé par une technique de soustraction, si on ajoute un écran exponentiel au potentiel dans l'espace r. La limite d'écran zéro est prise analytiquement, et la solution numérique de l'équation intégrale soustraite donne des valeurs propres et des fonctions d'onde qui sont en bon accord avec les calculs effectués dans l'espace des positions. La méthode peut facilement être généralisée pour des potentiels variant selon une loi de puissance arbitraire.
[Traduit par la rédaction]

Can. J. Phys. 70, 86 (1992)

Lattice gauge calculations (1) for static (heavy) quarks support the notion that the interquark potential in quantum chromodynamics (QCD) behaves as $V(r) \sim \lambda r$ for large r. Indeed, the linear potential has long been used in phenomenological nonrelativistic quark models of baryons and mesons (2, 3). Meson spectroscopy in particular is successfully described by a linear potential at large r, modified by spin- and colour-dependent Coulomb forces at small r. Most calculations with the linear potential are carried out in coordinate space. This is the simplest procedure for heavy-quark systems, which can perhaps be considered as nonrelativistic; however for light-quark systems it would be desirable to have a relativistic treatment. Bound-state equations in relativistic systems (4) are generally much easier to solve in momentum space, and thus we are led to consider, as a starting point for the relativistic case, the Schrödinger equation for two scalar particles interacting by a linear potential. The methods developed will generalize relatively straightforwardly to relativistic treatments.

To summarize: here, we treat the Schrödinger equation for a linear r-space potential. The method is for the most part straightforward, the only difficulty arising from the singularity of the kernel at the origin of momentum space. Previous treatments (5) have usually been approximate in the sense that the singularity was handled by screening the r-space potential:

$$[1] \quad V(r) \sim \lambda r\, e^{-\eta r}$$

What has perhaps not been generally appreciated is that the limit $\eta \to 0$ can be taken analytically. Previous treatments keep the parameter η finite, leading to some uncertainty as to the nature of the calculated eigenvalues and wave functions. In this connection, recall that the screened linear potential does not, strictly speaking, possess true bound states, instead it has scattering resonances, which for low energy approximate the bound states of the unscreened potential. We will extract the limit of zero screening analytically, using a subtraction technique. The resulting subtracted integral equation is relatively easy to handle numerically. An alternative procedure, not employing any subtraction, and leading to a different integrodifferential equation is presented in ref. 6. Our approach is easy to implement and generalizes without difficulty to higher partial waves. The Schrödinger equation for the lth partial wave is (with the inhomogeneous term already omitted, as it will not contribute to the bound states in the limit of zero screening)

$$[2] \quad \frac{p^2}{2\mu}\phi_l(p) + \int V_l(p,p')\,\phi_l(p')\,p'^2\,dp' = E\phi_l(p)$$

Here $\mu = m_1 m_2/(m_1 + m_2)$ is the reduced mass and V_l given by

$$[3] \quad V_l(p,p') = \frac{\lambda}{\pi}\left[\frac{Q_l(y)}{(pp')^2} + \eta^2\frac{Q_l'(y)}{(pp')^3}\right]$$

is the lth partial-wave component of the Fourier transform of [1]:

$$[4] \quad \hat{V}(p,p') = -\frac{\lambda}{2\pi^2}\left[\frac{2}{[(p'-p)^2+\eta^2]^2} - \frac{8\eta^2}{[(p'-p)^2+\eta^2]^3}\right]$$

The variable y is given by:

$$[5] \quad y = \frac{p^2 + p'^2 + \eta^2}{2pp'}$$

$Q'_l(y)$ and $Q''_l(y)$ are the first and second derivatives (with respect to y) of the Legendre function of the second kind. To illustrate the method we specialize to s-waves, where we find by contour integration

$$[6] \quad \int V_l(p,p')p'^2\,dp' = \frac{\lambda}{\pi}\int dp'\left[Q'_0(y) + \frac{\eta^2}{pp'}Q''_0(y)\right]$$

$$= \frac{\lambda}{\pi}\left[-\frac{\pi p^2}{\eta} + \frac{\pi p^2}{\eta}\right] = 0$$

Note that when $\eta = 0$, $Q'_0(y)$ and $Q''_0(y)$ have double and quadruple poles, respectively, at $p' = p$, so that their integrals do not exist separately. Nevertheless, the two terms added together produce a function with an integrable singularity. This is illustrated in Fig. 1, which shows the kernel as a function of p' for fixed p. One observes that there is a central maximum at $p' = p$ with height scaling as $1/\eta^2$, flanked by two minima at $p' \sim p \pm 2\eta$ whose heights also scale with $1/\eta^2$. The integral vanishes [6] and this allows us to rewrite the Schrödinger equation in subtracted form

$$[7] \quad \frac{p^2}{2\mu}\phi_0(p) + \frac{\lambda}{\pi}\int\left[\frac{Q'_0(y)}{(pp')^2} + \eta^2\frac{Q''_0(y)}{(pp')^3}\right]$$

$$\times\,[\phi_0(p') - \phi_0(p)]p'^2\,dp' = E\phi_0(p)$$

The limit $\eta \to 0$ now exists, and may be extracted by splitting the region of integration to isolate the singularity. We write

$$[8] \quad \int dp'\left[Q'_0(y) + \frac{\eta^2}{pp'}Q''_0(y)\right][\phi_0(p') - \phi_0(p)]$$

$$= \int_0^{p-4\eta} + \int_{p-4\eta}^{p+4\eta} + \int_{p+4\eta}^{\infty}$$

$$= A + B + C$$

The limits $p \pm 4\eta$ are chosen so that all three extrema of the kernel lie in the middle region B. The explicit forms of the Legendre functions are

$$Q'_0(y) = \frac{1}{1-y^2}$$

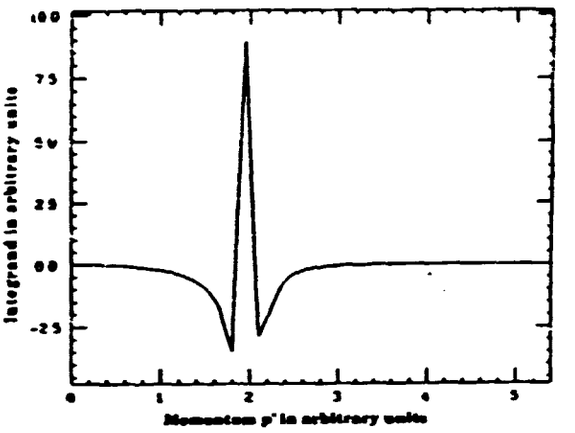

FIG. 1. The singularity structure of the kernel is shown for finite $\eta = 0.075$ with fixed $p = 2$.

$$= pp'\left[\frac{-1}{(p'-p)^2+\eta^2} + \frac{1}{(p'+p)^2+\eta^2}\right]$$

and

$$\frac{\eta^2}{pp'}Q''_0(y) = \eta^2(p^2 + p'^2 + \eta^2)$$

$$\times\left[\frac{-1}{(p'-p)^2+\eta^2} + \frac{1}{(p'+p)^2+\eta^2}\right]^2$$

It is clear that for $p' \neq p$, as is the case in the integrals A and C, the limit $\eta \to 0$ is innocuous, and may be taken immediately, indeed one has

$$[9] \quad \lim_{\eta\to 0}[A + C]$$

$$= P\int_0^{\infty} dp'\left[\frac{-4p^2p'^2}{(p'^2-p^2)^2}\right][\phi_0(p') - \phi_0(p)]$$

where P denotes as usual, the Cauchy principal value of the integral, which has been made well defined by the subtraction. The term B must be handled with care, however, since $p' = p$ inside the region of integration. Assuming $\phi(p')$ is analytic in the neighborhood of p, and making an obvious change of variable we find

$$[10] \quad \lim_{\eta\to 0} B = \lim_{\eta\to 0}\int_{4\eta}^{4\eta} dx\left\{\left[p(p+x)\left[\frac{-1}{x^2+\eta^2} + \frac{1}{(x+2p)^2+\eta^2}\right]\left[x\phi' + \frac{x^2}{2}\phi'' + \ldots\right]\right]\right.$$

$$\left. + \left[\eta^2[(x+p)^2 + p^2 + \eta^2]\left[\frac{-1}{x^2+\eta^2} + \frac{1}{(x+2p)^2+\eta^2}\right]^2\left[x\phi' + \frac{x^2}{2}\phi'' + \ldots\right]\right]\right\} = \lim_{\eta\to 0} B1 + \lim_{\eta\to 0} B2$$

Scaling out 4η then results in

$$[11] \quad \lim_{\eta\to 0} B1 = \lim_{\eta\to 0}\int_{-1}^{1}(4\eta)\,dy\,\frac{p}{4\eta}\left(\frac{p}{4\eta} + y\right)\left(\frac{-16}{1+16y^2}\right)\left[(4\eta)y\phi' + \frac{(4\eta)^2y^2}{2}\phi'' + \ldots\right]$$

$$= |p^2\phi'(p)|\int_{-1}^{1} dy\left(\frac{-16y}{1+16y^2}\right) = 0$$

TABLE 1. Energy eigenvalues in GeV for $l = 0$, $m_1 = m_2 = 1.5$ GeV, and $\lambda = 5$ GeV^2

	N						
	8	10	12	14	16	18	Exact
E_1	5.973	5.972	5.972	5.972	5.972	5.972	5.971
E_2	10.468	10.444	10.443	10.443	10.443	10.443	10.441
E_3	14.389	14.114	14.111	14.104	14.104	14.104	14.101
E_4	18.646	17.452	17.378	17.341	17.335	17.335	17.335
E_5	23.402	21.125	20.997	20.351	20.294	20.293	20.291
E_6	27.206	25.683	23.480	23.281	23.072	23.054	23.046
E_7	33.032	31.269	27.274	26.059	25.842	25.648	25.646
E_8	44.374	36.224	32.113	29.032	28.789	27.947	28.119
E_9		40.519	38.146	33.051	31.561	30.194	30.488
E_{10}		51.774	45.309	38.067	34.428	33.340	32.769
E_{11}			49.940	44.286	38.517	36.489	34.972
E_{12}			58.588	51.893	43.615	37.309	37.109

The contribution of the second term in $B1$ clearly vanishes since it is not singular at $p' = p$, the analysis of $B2$ is similar, and we conclude that B tends to zero. Therefore the limiting form of the equation is

$$[12]\quad \frac{p^2}{2\mu}\phi_n(p) - \frac{\lambda}{\pi p^2}I' \int_0^\infty dp' \left[\frac{4p^2p'^2}{(p'^2 - p^2)^2}\right][\phi_n(p') - \phi_n(p)] = E\phi_n(p)$$

We now discuss the numerical solution of [12], which is not yet a completely trivial matter, since care must be taken to obtain the Cauchy principal value. In this respect there is a difference between the linear potential and the Coulomb potential, the latter giving rise to a logarithmic singularity. For the Coulomb potential, the method used in the literature (7) is to write the Coulomb analog of [12] directly, for example, using Gaussian quadrature, as a matrix equation. Since the singularity is only logarithmic this method is successful for the Coulomb potential. Here, such an approach is not feasible. Instead, we expand ϕ_n in a suitable set of basis functions

$$[13]\quad \phi_n(p) = \sum_m^N C_m g_m(p)$$

Inserting this expansion in [12], multiplying by $p^2 g_m(p)$ and integrating over p, we obtain

$$[14]\quad \sum_m C_m\left\{\int \frac{p^4}{2\mu} g_m(p)g_n(p)\,dp + \frac{\lambda}{\pi}\int\left[\frac{4p^2p'^2}{(p'^2 - p^2)^2}\right] g_m(p)[g_n(p') - g_n(p)]\,dp'\,dp = E\sum_m C_m \int p^2 g_m(p)g_n(p)\,dp\right.$$

which is just the matrix equation

$$[15]\quad \sum_m A_{nm}C_m = E\sum_m G_{nm}C_m$$

The double integral over p and p' is performed by changing to variables $(p' + p)$ and $(p' - p)$. The singularity is in the integral over $(p' - p)$, so this is carried out first using Gaussian quadrature with an even number of points. This type of integration yields the Cauchy principal value automatically (8). A convenient set of functions $g(p)$ is

$$[16]\quad g_n(p) = \frac{1}{(n^2/N)^2 + p^4}$$

where N is the maximum number of functions used in expansion [13]. Figure 2 is a 3D plot of the kernel of [14], showing clearly the cancellation that leads to the principal value. Using the above method, we have calculated both eigenvalues and eigenvectors. In Table 1 the first 12 eigenvalues are listed. We used $m_1 = m_2 = 1.5$ GeV and the string tension $\lambda = 5$ GeV^2. One can see that the lower eigenvalues converge nicely as the number of functions is increased. We compare these with the eigenvalues obtained from a coordinate space calculation (integrating the equation out from $r = 0$ and in from large r, and matching the logarithmic derivatives at the classical turning point), in Table 1. The calculated eigenfunctions also agree with the coordinate space calculation.

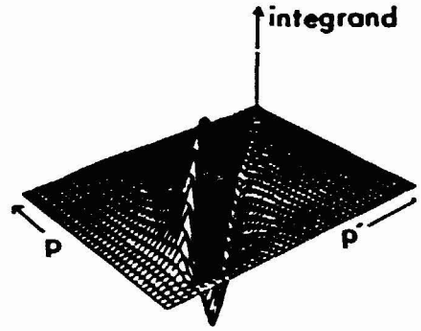

FIG. 2. A three-dimensional figure of the subtracted, regulated integrand; $\eta = 0.075$. The cancellation that produces the Cauchy principle value is evident.

In conclusion, we have treated the problem of two nonrelativistic, scalar particles interacting via a linear potential in momentum space. The relevant Schrödinger equation has a singular kernel. We have shown how after regulating the singularity by exponentially screening the r-space potential, the severity of the singularity can be reduced by a suitable subtraction, and the limit of zero screening extracted analytically. To the best of our knowledge, this point has not been generally understood in the literature. The limiting form of the equation has been treated numerically, and the results are in good agreement with more straightforward coordinate space calculations. Relativistic equations involving linear potentials involve similar singularities, so that the methods developed here will be applicable. We intend to study the relativistic quark–antiquark problem in the future. The method presented here can be generalized to higher partial waves without undue difficulty.

Acknowledgements

We are extremely grateful to Franz Gross for his generous contribution of essential ideas during all stages of this work. We would also like to thank Warren Buck and J.W.N. would like to thank Frank Cucinotta and Barry Ganapol for useful conversations. K.M.M. and J.W.N. would like to thank the Continuous Electron Beam Accelerator Facility for its hospitality. This work was supported in part by the Department of Energy through Continuous Electron Beam Accelerator Facility (D.E.K.), and by NASA grants NAG-1-1134 (J.W.N.) and NAG-1-477 (K.M.M.).

1. J. D. Stack, Phys. Rev. D: Part. Fields, 27, 412 (1983); A. Hasenfratz and P. Hasenfratz, Ann. Rev. Nucl. Part. Sci. 35, 559 (1985).
2. E. Eichten, K. Gottfried, T. Kinoshita, K. D. Lane, and T. M. Yan, Phys. Rev. D: Part. Fields, 17, 3090 (1978); 21, 203 (1980).
3. S. Godfrey and N. Isgur, Phys. Rev. D: Part. Fields, 32, 189 (1985).
4. W. W. Buck and F. Gross, Phys. Rev. C: Nucl. Phys. 20, 2361 (1979); F. Gross, Phys. Rev. 165, 1448 (1969); H. Crater and P. Van Alstine, Phys. Rev. D: Part. Fields 37, 1982 (1988).
5. A. B. Henriques, B. H. Kellett, and R. G. Moorhouse, Phys. Lett. 64B, 85 (1976).
6. J. R. Spence and J. P. Vary, Phys. Rev. D: Part. Fields 35, 2191 (1987).
7. Y. R. Kwon and F. Tabakin, Phys. Rev. C: Nucl. Phys. 18, 932 (1978); R. H. Landau 27, 2191 (1983).
8. I. H. Sloan, J. Comput. Phys. 3, 332 (1968).